



REPUBLIC OF IRAQ

MINISTRY OF HIGHER EDUCATION AND SCIENTIFIC
RESEARCH

AL-FURAT AL-AWSAT TECHNICAL UNIVERSITY

ENGINEERING TECHNICAL COLLEGE – NAJAF

**An Experimental and Numerical Study to Improve the
Performance of Cylindrical Solar Distiller with
Hemispherical Dome Using Fins**

A THESIS SUBMITTED TO THE DEPARTMENT OF MECHANICAL
ENGINEERING TECHNIQUES OF POWER IN PARTIAL
FULFILLMENT OF THE REQUIREMENTS FOR MASTER OF
THERMAL TECHNOLOGIES DEGREE IN MECHANICAL
ENGINEERING TECHNIQUES OF POWER (M.TECH.)

By

Shahazanan Falah Nassif

Supervised by

Prof. Dr. Dhafer Manea Hachim

Asst. Prof. Dr. Wisam A. Abd Al-wahid

2024

Declaration

hereby to declare that the work in this thesis is my own and has not been submitted to other organizations or for acquiring any other degree

Signature:

Name: Shahazanan Falah Nassif

Date: / / 2024

بِسْمِ اللَّهِ الرَّحْمَنِ الرَّحِيمِ

﴿يَرْفَعِ اللَّهُ الَّذِينَ ءَامَنُوا مِنْكُمْ وَالَّذِينَ أُوتُوا

الْعِلْمَ دَرَجَاتٍ وَاللَّهُ بِمَا تَعْمَلُونَ خَبِيرٌ﴾

صدق الله العلي العظيم

سورة المجادلة اية ﴿١١﴾

ACKNOWLEDGMENTS

I would like to express my gratitude to God Allah, the Great Creator,

I would like to express my deep thanks and appreciation to my supervisor, **Professor Dr. Dhafer Manea Hachim**, and **Assistant Professor Dr. Wisam A. Abd Al-wahid** for their assistance and continuous guidance throughout the preparation and writing of my dissertation.

I would also like to extend my sincere gratitude and appreciation to the College of Engineering Technology / Najaf and the Department of Mechanical Engineering, represented by the honorable head of the department, **Professor Dr. Adel Abdel Aziz**, and all the respected members and professors of the department for all the advice they provided me throughout the study period.

Shahazanan Falah Nassif

2024

Supervisor Certification

We certify that this thesis entitled “**An Experimental and Numerical Study to Improve the Performance of Cylindrical Solar Distiller with Hemispherical Dome Using Fins.**” which is being submitted by **Shahazanan Falah Nassif** was prepared under our supervision at the Department of Mechanical Engineering Techniques of Power, College of Technical Engineering-Najaf, AL-Furat Al-Awsat Technical University, as partial fulfillment of the requirements for the degree of Master of Techniques in Thermal Engineering.

Signature:

Name: Prof. Dr. Dhafer Manea Hachim

(Supervisor)

Date: / / 2024

Signature:

Name: Asst. Prof. Dr. Wisam A. Abd Al-wahid

(Co-Supervisor)

Date: / / 2024

In view of the available recommendation, we forward this thesis for debate by the examining committee.

Signature:

Name: Prof. Dr. Adel A. Eidan

Head of mechanical Eng. Tech. of Power Dept.

Date: / / 2024

Committee Report

We certify that we have read this thesis titled “**An Experimental and Numerical Study to Improve the Performance of Cylindrical Solar Distiller with Hemispherical Dome Using Fins**” which is being submitted by **Shahazanan Falah Nassif** and as Examining Committee, examined the student in its contents. In our opinion, the thesis is adequate for the award of the degree of Master of Techniques in Thermal Engineering.

Signature:

Prof. Dr. Hassanain Ghani Hameed

(Chairman)

Date: / / 2024

Signature:

Asst. Prof.Dr. Qahtan Abdul Zahra Faleh

(Member)

Date: / / 2024

Signature:

Asst. Prof.Dr. Mohammed Saad Abbas

(Member)

Date: / / 2024

Signature:

Prof. Dr. Dhafer Manea Hachim

(Supervisor)

Date: / / 2024

Signature:

Asst. Prof. Dr. Wisam A. Abd Al-wahid

(Co-Supervisor)

Date: / / 2024

Approval of the Engineering Technical College- Najaf

Signature:

Name: Prof. Dr. Hassanain Ghani Hameed

Dean of Engineering Technical College- Najaf

Date: / / 2024

ABSTRACT

Solar desalination systems are regarded as sustainable methodologies employed in the desalination process of non-potable water sources. The increase in the demand for potable water in recent years can be attributed to the multitude of pollutants that adversely affect natural water bodies. The of this investigation includes two principal components. The initial component involves the numerical simulation of the proposed model (which incorporates the utilization of fins within the cylindrical solar still featuring a hemispherical dome), focusing on the analysis of the fins' lengths employed (4 mm, 6 mm, and 8 mm), alongside the assessment of the number of fins utilized (4 fins and 5 fins). The secondary component aims to determine the optimal dimensions for the fins based on the outcomes derived from the numerical simulation, followed by practical testing in the climatic conditions of Iraq, specifically in the city of Najaf (31.590°N and 44.190°E). The numerical data indicated that cumulative productivity fluctuates in accordance with the month of the year in relation to the condensation area. An increase of the condensate area by 70%, 281%, and 492% in July, at drum heights of 50, 200, and 350 mm respectively, results in productivity enhancements of 14%, 12%, and 10%. The incorporation of fins significantly enhances the throughput of the distiller by up to 64.7% in comparison to the configuration devoid of fins, with the optimal modified hemispherical cylindrical solar still configuration exhibiting a fin length of 8 mm, N_f 5, and L_w 50 mm. The maximum rate of error between the simulation outcomes and those of preceding studies ranges from approximately 4.62% to 11%. The experimental results indicate that including fins into the CSSHD consistently produces enhanced productivity across the whole period of the experiment. The maximum daily productivity reached was 3.7 kg/m² in March.

Contents

Declaration.....	II
Acknowledgements.....	IV
Supervisor Certification.....	V
Committee Report.....	VI
Contents.....	VIII
List of Figure.....	X
List of Table.....	XV
Nomenclature.....	XV
Greek Symbols.....	XVII
Subscripts.....	XVII
Chapter One.....	1
Introduction.....	1
1.1 General.....	1
1.2 Solar Desalination.....	2
1.2.1 Advantage solar still.....	3
1.2.2 Disadvantage solar still.....	3
1.3 Solar Still.....	3
1.3.1 passive.....	3
1.3.2 Active.....	4
1.4 Kinds of passive solar stills.....	5
1.4.1 Single basin single slope solar still.....	5
1.4.2 Single basin double slope solar still.....	6
1.4.3 Tubur solar still.....	6
1.4.4 Single basin triangular solar still.....	6
1.4.5 Hemispherical solar still.....	7
1.4.6. Cylindrical solar still with a hemispherical dome (CSSHD).....	7
1.5. Research Background.....	8
1.6. Problem Statement.....	8
1.7. Objective of present work.....	9
Chapter Two.....	10
Literature Review.....	10
2.1 Introduction.....	10

2.2 Experimental Studies	10
2.3 Theoretical Studies.....	40
2.4 Theoretical and Experimental Studies.....	43
2.3. Summary of Literature Survey.....	45
Chapter Three.....	49
Numerical Simulation	49
3.1 Introduction.....	49
3.2 Proposed Model Geometry	49
3.3 Proposed Modeling and numerical simulation	52
3.3.1 Assumptions for Modeling	52
3.3.2 Governing Equations	52
3.3.3 Modules Boundary and Initial Conditions.....	55
3.4 CFD Time-Dependent Solver.....	56
3.5 Meshing and Grid Dependence Test	58
3.6 Validation of the Current Model.....	59
Chapter Four	62
Experimental Work.....	62
4.1.Introduction.....	62
4.2.Design and Construction of (CSSHD).....	64
4.2.1 Basin	62
4.2.2 Glass Cover (CSSHD)	64
4.2.3. Solid Telfon Base.....	66
4.2.4 Sealant.....	66
Piping ports	67
4.3 Measurements Devices of (CSSHD)	67
4.3.1 Data Logging Equipment.....	68
4.3.2 Solar Power Meter	68
4.3.3 Wind speed measurement	69
4.3.4 Digital Scale.....	70
4.4 Experimental procedure.....	71
Chapter Five.....	74
Results And Discussions.....	74
5.1. Introduction.....	74

5.2. Numerical Results	74
5.2.1. Study the effect of weather conditions	74
5.2.2. Study the effect of number fins used	77
5.2.3. Study the effect of height of fins	85
5.2.4. Study the effect of height of cylinder	91
5.3. Temperature, Concentration Contours and Streamlines.....	100
5.4. Experimental Results	104
5.4.1. Weather Condition	104
5.4.2. Comparison between CSSHD with fins and CSSHD without fins	105
5.4. Comparing Numerical and experimental Results.....	113
5.5 Cost calculation.....	114
Chapter Six.....	116
Conclusion and Recommendations.....	116
6.1. Introduction.....	116
6.2. The Conclusion	116
6.3. Recommendation	117
References.....	118
.....	الخلاصة

List of Figures

Figure 1.1 :Classification of system for solar stills.....	4
Figure 1.2 :single basin single slope solar still	5
Figure 1.3 :Single basin double slope solar still	5
Figure 1.4 :Tubular solar still.....	6
Figure 1.5 :Photo for diagram of single basin triangular solar still.	6
Figure 1.6: Diagram of schematics the hemispheric solar system	6
Figure 1.7 :Diagram of schematics the CSSHD	7
Figure 2.1 :Photo of the present test rig.....	11
Figure 2.2 :(a) Representative sketch of present work solar still, (b) measurements of still, and (c)photograph of used still for height of 10 cm.	10
Figure 2.3 : View of the basin of hemispherical distillers with black gravels.....	13
Figure 2.4: Photographic view of the basin with and without fins for three hemispherical distillers.....	14

Figure 2.5 :CSSHD and conventional single slope solar still used in present work.....	15
Figure 2.6 : Photograph of experimental setup.....	16
Figure 2.7 : Photograph of experimental setup.....	17
Figure 2.8: A photograph of the position of the iron fins inside the distilled basin as the distance between them changes (0, 1, 2, 3, 4, and 5 cm).....	18
Figure 2.9: (a) Graphical representation of the different configurations.....	20
Figure 2.9: (b) Experimental setup	20
Figure 2.10: (a)detailed experimental setup of the hemispheric solar distilleries.	21
Figure 2.10: (b) Photograph depicting a basin with rock salt balls arranged at varying intervals of 3.0, 4.0, 5.0, and 6.0 cm.	21
Figure 2.11: Photographic view of MHSD-DFASTR&SC and THSD.....	22
Figure 2.12 :Photo of EHCF position inside distilled basin with the change of the distance between them (0, 2, 3, and 4 cm) in order	23
Figure 2.13 : Photographs of the experimental setups: (a) Floating Hemispherical Solar Still (FHSS); (b) Reference Passive Solar Still (RPSS); (c) Outdoor experiments of FHSS next to RPSS.....	24
Figure 2.14 : Photograph of the experimental set-up with the PCM-loaded	25
Figure 2.15: Photograph of three units of the experimental HSS	26
Figure 2.16 :Photo of the basin configuration of the four hemispherical distillers	27
Figure 2.17:(a)Schematic of corrugated stepped dish solar distiller (Cr SD SD)(b) Photo of tested dish solar still (DSD).....	28
Figure 2.18 :(a) River rocks used in experiments(b) Experimental setup used in the work.....	29
Figure 2.19: (a) Photographic view of different corrugated absorbers Flat plate.(b) Square corrugate bsorber (c)Semi –circular corrugate absorber (d)Triangular corrugate. absorber	30
Figure 2.20: Experimental setup photograph.....	31
Figure 2.21 :(a) Basin with phosphate grannulate.(b) Basin with zinc metal sheet and phosphate grannulate.(c) Basin with copper metal sheet and phosphategrannulate.(d) Micrograph of Phosphate pellets.	32
Figure 2.22: (a) A photograph of the hemispherical solar still basin without and withaluminum waste(b) A schematic of two hemispherical distillers (RHSS and HSS-Awls)	33
Figure 2.23: Marble pieces at different colors used in the experiment.....	34
Figure 2.24: A photograp of experimental stage.....	35
Figure 2.25 : (a) Pictorial view of the designed absorber basins in each distiller.....	36

Figure 2.25 :(b) Conventional hemispheric solar basin distillatory. (a1) Schematized diagram; (b1) Pictorial view.	37
Figure 2.26 : Basin photo of the three hemispherical distillers (THSD, HSD-SSCSSW, and HSD-CSCSSW).....	37
Figure 2.27: Photograph of the experimental test rig.	38
Figure 28 :The experiment set up (a) photograph, (b) the schematic	39
Figure 29: The cylindrical solar still is depicted in a cross-sectional view showing various heat losses and gains	40
Figure 2.30: Photographic view of the proposed hemispherical solar stills	42
Figure 3.1: The diagram presented depicts cylindrical solar still with a hemispherical dome, (a) without fins in basin, and, (b) with fins in basin, (c) Dimensions of the solar stillFigure.....	50
Figure 3.2: The flow chart to show the simulation process of present work.....	57
Figure 3.3:(a) Grid created at the CSSHD with different numbers of elements(b) mesh generation	58
Figure 3.4: Comparison of hourly productivity with experimental work of [34].....	59
Figure 3.5: Comparison of hourly water temperature with experimental work of [34].....	60
Figure 3.6:Comparison of cumulative productivity with experimental work of [16].....	61
Figure 4.1: Experimental rig.....	63
Figure 4.2 : schematic of experimental rig	63
Figure 4.3: Photographic view of the basin with fins hemispherical distillers.....	64
Figure 4.4: Photographic view of solar still glass.....	65
Figure 4.5: Photograph displaying the sealant used in a solar still.....	66
Figure 4.6: Photograph depicting CSSHD pipe ports.....	67
Figure 4.7: Data logger and k-type thermocouple	68
Figure 4.8 :Solar Radiation	69
Figure 4.9: Wind speed measurement.....	70
Figure 4.10: Digital Scale	71
Figure 4.11: The flow chart Process for the experimental work.....	74
Figure 5.1: Weather Conditions of 15-January 2024	75
Figure 5.2: Weather Conditions of 15-March 2024	75
Figure 5.3: Weather Conditions of 15-July 2024	76
Figure 5.4: Weather Conditions of 15-October 2024.....	76
Figure 5.5: Variations of water temperature for CSSHD at $H_f=8$ mm, $L_w=350$ mm (a) N_f $= 4$ (b) $N_f=5$	77

Figure 5.6: Variations of basin temperature for CSSHD at $H_f=8$ mm, $L_w=350$ mm (a) $N_f=4$ (b) $N_f=5$	78
Figure 5.7: Variations of Basin Temperature for CSSHD $L_w=350$ mm at $N_f=0$, $N_f=4$ and $N_f=5$ for July.....	78
Figure 5.8: Variations of Inner Glass temperature for CSSHD at $H_f=8$ mm, $L_w=350$ mm (a) $N_f=4$ (b) $N_f=5$	79
Figure 5.9: Variations of Out Glass temperature for CSSHD at $H_f=8$ mm, $L_w=350$ mm (a) $N_f=4$ (b) $N_f=5$	79
Figure 5.10: Total Cumulative Productivity for CSSHD at $H_f=8$ mm, $L_w=350$ mm	80
Figure 5.11: Variations of Efficiency for CSSHD at $H_f=8$ mm, $L_w=350$ mm (a) $N_f=4$ (b) $N_f=5$	81
Figure 5.12: Variations of Total accumulated energy rate for CSSHD at $H_f=8$ mm , $L_w=350$ mm (a) $N_f=4$ (b) $N_f=5$	82
Figure 5.13: Variations of Average moisture air velocity for CSSHD at $H_f=8$ mm, $L_w=350$ mm (a) $N_f=4$ (b) $N_f=5$	83
Figure 5.14: Change in Hourly Productivity for CSSHD at $H_f=8$ mm, $L_w=350$ mm (a) $N_f=4$ (b) $N_f=5$	83
Figure 5.15: The effect of fin shadow during January and July.....	84
Figure 5.16: Average source heat flux over time during winter and July.....	85
Figure 5.17: Variations of water temperature for CSSHD at $N_f=5$, $L_w=350$ mm (a) $H_f=4$ mm (b) $H_f=6$ mm.....	86
Figure 5.18: Variations of basin temperature for CSSHD at $N_f=5$, $L_w=350$ mm (a) $H_f=4$ mm (b) $H_f=6$ mm.....	86
Figure 5.19: Variations of Inner Glass temperature for CSSHD at $N_f=5$, $L_w=350$ mm (a) $H_f=4$ mm (b) $H_f=6$ mm	87
Figure 5.20: Variations of Out Glass temperature for CSSHD at $N_f=5$, $L_w=350$ mm (a) $H_f=4$ mm (b) $H_f=6$ mm.....	87
Figure 5.21: Total Cumulative Productivity for CSSHD at $N_f=5$, $L_w=350$ mm.....	88
Figure 5.22: Total Cumulative Productivity for CSSHD January at $N_f=5$, $L_w=350$ mm.....	89
Figure 5.23: Variations of Efficiency for CSSHD at $N_f=5$, $L_w=350$ mm (a) $H_f=4$ mm (b) $H_f=6$ mm	90
Figure 5.24: Variations of Total accumulated energy rate for CSSHD at $N_f=5$, $L_w=350$ mm (a) $H_f=4$ mm (b) $H_f=6$ mm.....	90

Figure 5.25: Variations Average moisture air velocity for CSSHD at $N_f=5$, $L_w=350$ mm (a) $H_f=4$ mm (b) $H_f=6$ mm	91
Figure 5.26: Change in Hourly Productivity for CSSHD at $N_f=5$, $L_w=350$ mm (a) $H_f=4$ mm (b) $H_f=6$ mm.....	92
Figure :5.27: Variations of water temperature for CSSHD at $N_f=5$, $H_f=8$ mm (a) $L_w=0$ mm (b) $L_w=50$ mm (c) $L_w=200$ mm	93
Figure 5.28: Variations of basin temperature for CSSHD at $N_f=5$, $H_f=8$ mm (a) $L_w=0$ mm (b) $L_w=50$ mm (c) $L_w=200$ mm	93
Figure 5.29: Variations of Inner Glass temperature for CSSHD at $N_f=5$, $H_f=8$ mm (a) $L_w=0$ mm (b) $L_w=50$ mm (c) $L_w=200$ mm	94
Figure 5.30: Variations of Out Glass temperature for CSSHD at $N_f=5$, $H_f=8$ mm (a) $L_w=0$ mm (b) $L_w=50$ mm (c) $L_w=200$ mm	94
Figure 5.31: Total Cumulative Productivity for CSSHD at $N_f=5$, $H_f=8$ mm.....	95
Figure 5.32: Variations of Efficiency for CSSHD at $N_f=5$, $H_f=8$ mm (a) $L_w=0$ mm (b) $L_w=50$ mm (c) $L_w=200$ mm	96
Figure 5.33: Variations of Total accumulated energy rate for CSSHD at $N_f=5$, H_f (a) $L_w=0$ mm (b) $L_w=50$ mm (c) $L_w=200$ mm	97
Figure 5.34: Variations of Average moisture air velocity for CSSHD at $N_f=5$, $H_f=8$ mm (a) $L_w=0$ mm (b) $L_w=50$ mm (c) $L_w=200$ mm.....	98
Figure 5.35: V Change in Hourly Productivity for CSSHD at $N_f=5$, $H_f=8$ mm (a) $L_w=0$ mm (b) $L_w=50$ mm (c) $L_w=200$ mm	99
Figure 5.36: Variation of the temperature contours during a day 15-January, 15-March, 15-July, and 15-October.....	101
Figure 5.37: Presents the water vapor concentration during a day 15-January, 15-March, 15-July, and 15-October.....	102
Figure 5.38: Streamlines and velocity field during a day 15-January, 15-March, 15-July, and 15-October.....	103
Figure 5.39: Variation of solar radiation ambient temperature and wind speed with respect to time 4-3-2024.....	106
Figure 5.40: Variation of solar radiation, ambient temperature and wind speed with respect to time 5-3-2024.	106
Figure 5.41 :Variation of solar radiation, ambient temperature and wind speed with respect to time 6-3-2024.	107

Figure 5.42: Variation of solar radiation, ambient temperature and wind speed with respect to time 10-3-2024.	107
Figure 5.43 :Variation of solar radiation, ambient temperature and wind speed with respect to time 11-3-2024.....	108
Figure 5.44: Variations of temperature for two solar still a-with fins b- without fins , at day (4-3-2024).....	109
Figure 5.45 :Variations of temperature for two solar still a-with fins b- without fins , at day (5-3-2024).....	109
Figure 5.46: Variations of temperature for two solar still a-with fins b- without fins , at day (6-3-2024).....	110
Figure 5.47: Variations of temperature for two solar still a-with fins b- without fins , at day (10-3-2024).....	110
Figure 5.48 :Variations of temperature for two solar still a-with fins b- without fins , at day (11-3-2024).....	111
Figure 5.49: Comparison of experimental results between two solar stills at five days a-with fins b- without fins.....	112
Figure 5.50: Displays the different levels of Total productivity, comparing the use of fins and without fins.....	112
Figure 5.51: Validation Experimental Work with Numerical	112

List of Table

Table 2.1: Summarizes literature studies	44
Table 3.1: The parameters that effect of area of condensation and area of basin	51
Table 3.2: Boundary Conditions	55
Table 3.3: Initial conditions	56
Table 3.4: The parameters of design used for validation setup of hemispherical solar still	60
Table 3.5: The parameters of design used for validation setup of CHSSD [16]	61
Table 4.1: Thermal properties of basin.....	64
Table 4.2: Thermal properties of glass cover.....	65
Table 5.1: Fixed cost estimation for present still.....	114
Table 5.2: Type and the total cost	114

Nomenclature

Symbols	Definition	Units
D_{AB}	Mass diffusivity of vapor	m^2/s
K	Thermal conductivity	$W/m.k$
G	Gravitational acceleration (9.807)	m/s^2
R_w	Heat source water	W
R_b	Heat source basin	W
H_{evap}	Heat of vaporization	J/kg
h_r	Radiative heat transfer coefficient	$W/m^2 .K$
h_{ins}	High of insulation	m
I	Solar radiation intensity	W/m^2
T_{amb}	Ambient temperature	K
T_b	Basin liner temperature	K
T_{gi}	Inner glass temperature	K
T_{go}	Outer glass temperature	K
T_{sky}	Sky temperature	K
T_w	Water surface temperature	K
t_g	Glass thickness	m
t_w	High of water	m
M_v	Molar mass of vapor	kg/mol
P	Fluid pressure	Pa
Q	Heat source	W
Q_c	Convective heat transfer	W
Q_{co}	Conductive heat transfer	W
Q_{cd}	Condensation heat transfer	W
Q_{rw_gin}	Radiation from water surface to inner glass	W
Q_{rgin-w}	Radiation from inner glass to water surface	W
$Q_{cgout-amb}$	Convection to ambient	W
q	Heat flux by conduction	W/m^2
q_o	Heat source	W/m^3
k_g	Thermal conductivity of glass	$W/m^2. K$
H_{evap}	Heat of vaporization	J/kg
R_w	Heat source water	W
R_b	Heat source basin	W
G	Total solar radiation	W/m^2
t_{ins}	Thickness of insulation	m
h_{ins}	High of insulation	m
k_{ins}	Thermal conductivity of insulation	$W/m^2. K$
C_w	Concentration on water surface	mol/m^3
P	partial pressure	N/m^2
N_f	Number of fins	-
H_f	High of fins	m
R_b	Solar energy absorbed by the back sheet layer of the panel	W
R_{fg}	Solar energy absorbed by front glass layer of the panel	W
T	Temperature	C°
T	Time	s
u	Velocity vector, fluid velocity	m/s

P_h	hourly Productivity	kg/h
lw_{av}	average latent heat of evaporation of water	J/kg
A_b	Area of Basin of still	m ²
G(t)	hourly solar radiation	W/m ²
P_{cum}	cumulative productivity	kg
Greek Symbols		
a_w	Water absorptivity	
a_g	Glass absorptivity	
p	Density	kg/m ³
a_b	Basin absorptivity	-
σ	Stefan–Boltzmann constant (5.669 × 10 ⁻⁸)	W/m.k ⁴
v	Kinematic viscosity	m ² /s
M	Fluid dynamic viscosity	N.s/ m ²
k	Permeability	m ²
η	Efficiency	
Subscripts		
Symbols	Definition	
amb	Ambient	
Ou	outlet	
ref	Reference conditions	
In	Inlet	
ins	Insulation	
evap	Evaporation	
Abbreviation		
Symbol	Description	
CSSHD	Cylindrical solar still with a hemispherical dome	
RMSD	Root mean square percent deviation	
PCM	Phase change material	
BDF	Backward Differentiation Formula	
MHSS-RM	Modified Hemispherical Distiller with Reflective Mirror	
MHSS-IF5	MHSS-IF5 Modified Hemispherical Solar Still with Iron fine 5 cm	
MHSS-IF7	MHSS-IF7 Modified Hemispherical Solar Still with Iron fine7 cm	
TCC-RM	Truncated circular cone-shaped reflector mirrors	
SHD	SHD Simple Hemispherical Distiller	
SHD-BF	Simple Hemispherical Distiller with Black Flax	
SHD-YF	Simple Hemispherical Distiller with Yellow Flax	
HSD-EHCF-PCM	Hemispherical Solar Distiller with Extended Hollow Cylindrical Fins Incorporating Phase Change,	
HSD-SSCSSW	Hemispherical solar distillers containing spiral-shaped coils of scrubber steel wire	
HSD-CSCSSW	Hemispherical solar distillers cake-shaped coils of scrubber steel wire	

Chapter One

Introduction

1.1 General Introduction

Water is an essential component for human survival, along with food and air. Many people are experiencing a scarcity of safe drinking water in arid and isolated areas. However, if these areas were abundant in solar energy, the situation may be improved. The solar still is a crucial device for minimizing water scarcity. Individuals relied on rivers, lakes, and subterranean reservoirs for their household freshwater needs, as well as for agricultural and industrial output. Furthermore, the majority of desalination facilities utilize fossil fuels as their primary energy source. The conventional techniques for desalination include reverse osmosis and electro dialysis, which can be greatly reduced by providing fresh drinking water to mitigate the effects of various human diseases.

Nevertheless, the utilization of water from these sources may not always be accessible or preferable due to the presence of excessive salts and pollutants. Approximately 1.1 billion individuals lack accessible access to potable water. Due to the elevated salinity levels, numerous individuals must refrain from consuming water sourced from a well or a lake. As a result of consuming contaminated water, certain individuals are unable to tolerate the potential hazards associated with utilizing saline water for their daily needs. Consequently, they contract cholera and then seek medical treatment at a hospital, [1]. The majority of literature on solar energy focuses on the construction of a significant solar still facility in Chile in the 1870s by Swedish engineer Carlos Wilson. This facility might be regarded as the inaugural industrial installation for harnessing solar energy.

In the 1950s, in the state of California, the objective was to further enhance the efficiency of producing 4000 m³ of distilled water on a daily basis.

After ten years, all engineers specializing in solar energy unanimously concluded that the construction of major solar distillation plants is excessively costly and cannot effectively rival conventional fuel-based alternatives. Consequently, focus shifted towards compact solar distillation plants. In 1960s and mid-1970s, there was a total of 38 facilities located in 14 different countries around the world. These factories produced varying amounts of distilled water each day, with outputs ranging from a few hundred to thirty thousand liters. Researchers from different countries have presented numerous static designs with the objective of achieving maximum production at little expense.[2]

1.2 Solar Desalination

In conventional sun desalination, a basin is filled with saline water and covered with a surface that allows solar radiation to pass through. The steam undergoes condensation, changing into water. which then accumulates on the surface and is collected in a container. The cost distribution of solar distillation differs significantly from those of other distillation methods. The primary expense is in the initial capital outlay. Nevertheless, the operational cost of the gadget is remarkably low, and the energy required for its functioning is either negligible or completely free. Due to the sun's energy being completely accessible without charge, this device can operate with a "zero cost" energy source. The primary factor influencing the initial cost of a solar desalination facility is the cost of land, which is determined by the quantity of area needed for the project. The price of solar device is a crucial determinant of the project's overall cost.[2]

1.2.1 Advantages of Solar Stills

- An inexpensive and compact method for delivering purified water to households or small communities.
- Essential simplicity in its physical structure.
- The device may be operated without the requirement for any moving parts such as pumps or motors.
- The utilization of solar energy is environmentally favorable as it relies solely on renewable and non-polluting sources.
- Service and maintenance can be performed without the need for a professional operator.
- Local fabrication allows for the possibility of repair.

1.2.2. Disadvantages of Solar Stills

- The outcome varies based on the prevailing environmental conditions.
- Insufficient production rate of drinkable water.
- Low efficiency operation.

1.3 Solar Stills

It is still possible to split solar still into two major forms as shown in Fig (1.1).

1.3.1 Passive: This is a conventional solar still system that relies only on solar energy as the primary source of thermal energy. It can also be combined with thermal energy from the sun or used for direct solar desalination. The solar energy is utilized to heat the water and generate the distillation process. This method is primarily suitable for small production systems such as solar stills, in regions where the demand for fresh water is below 200 m³/day. This limited output rate is explained by the low working temperature and pressure of the steam.[3]

1.3.2 Active: In the active method, additional thermal energy is combined with passive solar energy to accelerate evaporation. This additional thermal energy can be sourced from various industrial plants, such as power plants, solar collectors, or any available waste thermal energy. Electric pumps, valves, and controllers are utilized to circulate water or other heat-transfer fluids through the collectors. Although passive systems are often less expensive, active systems are generally more effective. Active systems are more convenient to retrofit compared to passive systems since their storage tanks do not require mounting above or near the collectors.[4]

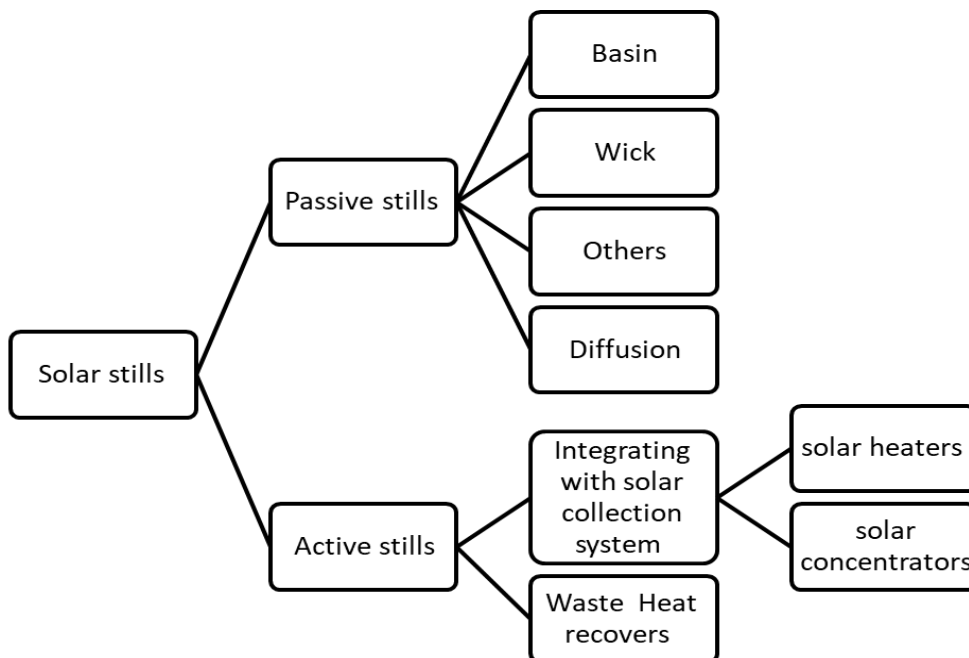


Figure (1.1): Classification of system for solar stills[4]

1.4 Kinds of passive solar stills

1.4.1. Single basin single slope solar still: The solar still consists of a basic horizontal basin and a glass cover plate inclined at a slope. Both components condense water vapor and collect the distilled water in separate compartments located on the side of the distillate. This type of solar still is commonly preferred over the double slope solar still due to its relatively lower initial cost. Figure (1.2) depicts the solar still with a single basin and a single slope.[5]

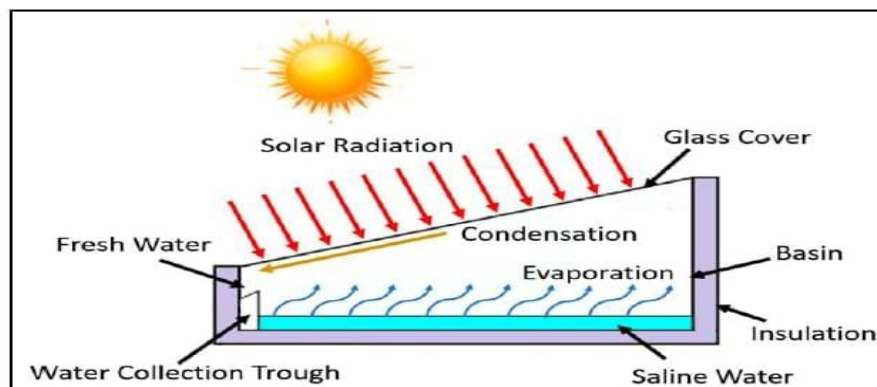


Figure (1.2): single basin single slope solar still [5].

1.4.2. Single basin double slope solar still: The solar still is comprised of a basic horizontal basin that is covered with two glass plates inclined at the same angle. Each plate condenses water vapor and collects the resulting distilled water in separate compartments located on either side of the distillate. This type of solar still is commonly employed due to its uncomplicated design and low initial cost. Figure (1.3) depicts a solar still with a single basin and double slope. [6]

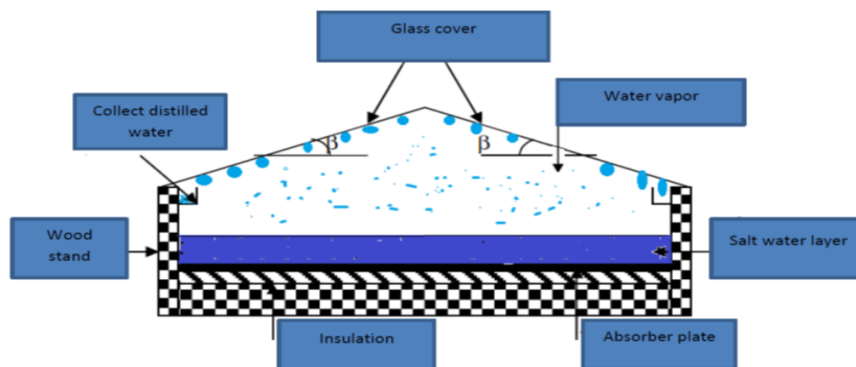


Figure (1.3): Single basin double slope solar still[6].

1.4.3. Tubular solar still: Horizontal solar tubular stills are the simplest to construct and can be used for both small and large-scale installations. The solar tubular still comprises a trough, a frame, and a tubular cover. The inside surface of the rectangular base is commonly darkened to efficiently absorb solar radiation. At the bottom of the glass cover, there is a mechanism for gathering the distilled output [7].

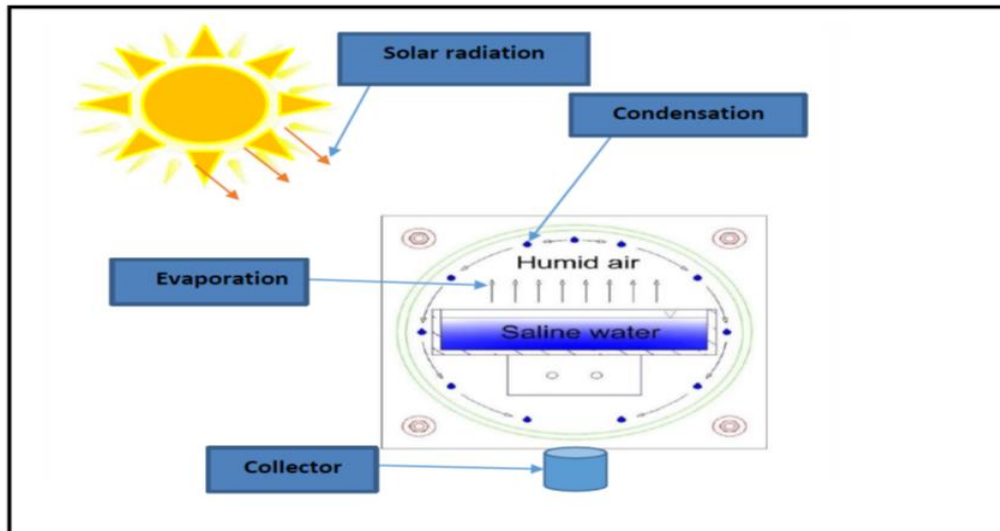


Figure (1.4): Tubular solar still [7].

1.4.4. Single basin triangular solar still: The triangular solar still is comprised of a pyramid-shaped design. The ideal angle for the pyramid glass cover to achieve maximum efficiency is 50° . Figure (1.5) Illustration depicting a solar still with a single basin in a triangular shape[8].

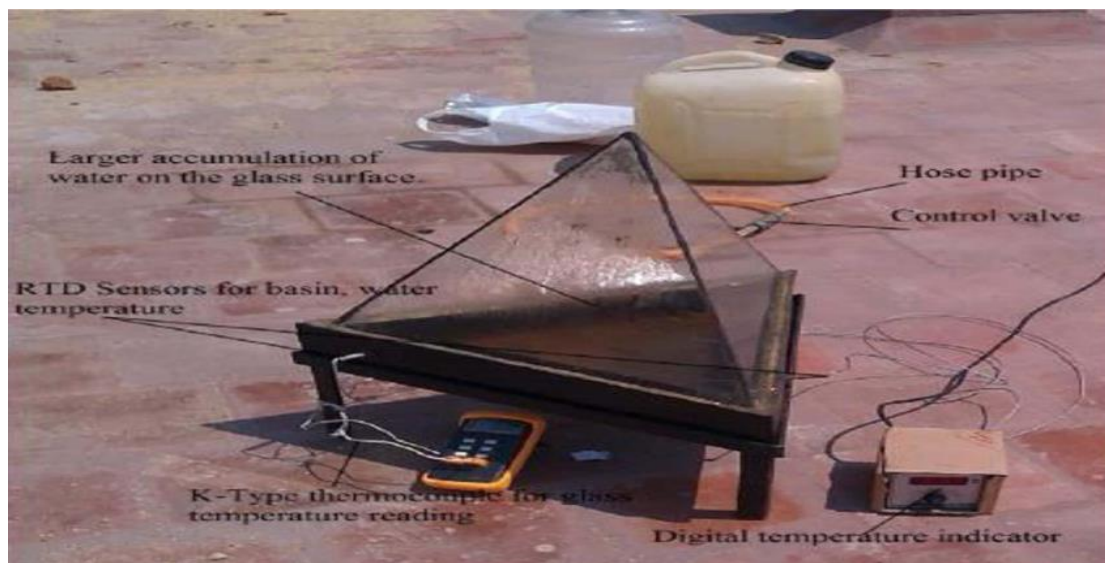
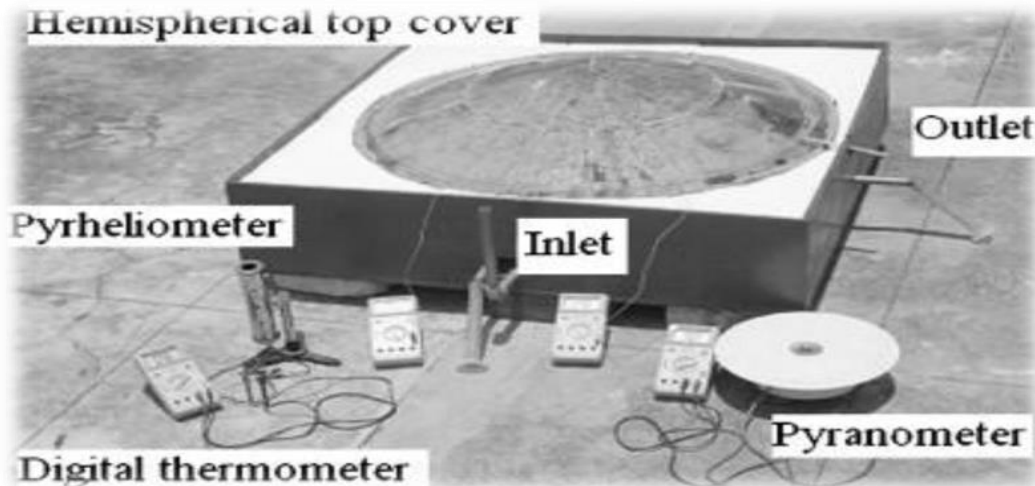


Figure (1.5): Photo for diagram of single basin triangular solar still [8].

1.4.5. Hemispherical solar still: Hemispherical coverings are employed to enhance the solar still's solar energy capture. The round solar distillers comprise a hemispherical condensation top and a circular basin for containing either salt water or ground storage water. Figure (1.6) depicts a schematic diagram of the hemisphere solar system[9].



Figure(1.6): Diagram of schematics the hemispheric solar system [9] .

1.4.6. Cylindrical solar still with a hemispherical dome (CSSHD):

Spherical coverings combined with cylinders are utilized to optimize solar energy absorption in the solar still. Circular solar stills consist of a curved, dome-shaped condensing surface and a round basin designed to hold brine or ground storage water. Figure (1.7) depicts a schematic of a cylindrical solar system featuring a hemispherical dome. Abbreviations Tw: Water surface temperature; Tb: Basin temperature; Tg-out: Outer glass temperature; Tg-in: Inner glass temperature.

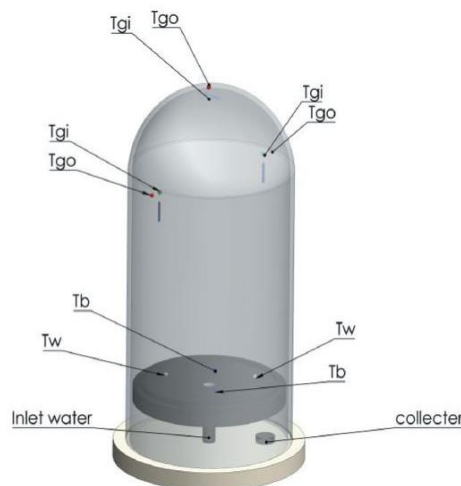


Figure (1.7): Schematic diagram of the CSSHD [16].

1.5. Research Background

Consumable water demand continues to rise as a result of increased population density. Solar desalination is a process of turning brackish water into drinkable water. Solar desalination is perhaps the earliest technique of water desalination. The sun's radiation evaporates water within a closed glass-covered chamber at a temperature is higher than the ambient temperature. A solar still is the device use the solar energy to evaporate the brackish water, and then condensate it, and convert to drinkable water.

1.6. Problem Statement

In recent years, numerous researchers have engaged in significant research and development of hemispherical solar stills to generate potable water for individuals in remote areas facing freshwater scarcity. Brackish water can be converted into drinkable water by sun desalination technology. Using the solar energy in declination of brackish water helped to reduce the of drinkable water. So, this problem can solve by improving the performance of solar still, by using cylindrical solar still with hemispherical dome equipped with fins in basin, to increasing the productivity per unit area.

1.7. Objective of present work:

The main objective of this work is conduct numerical simulations and experimental study to analyze the efficiency of a cylindrical solar still with a hemispherical dome. This can be achieved by incorporating fins in basin of solar still. Also, changing the length of cylinder. The aims of present work are listed below:

1. The performance of a modified solar still with fins was analyzed using COMSOL Multiphysics V.6.1.
2. Experimental study of the performance of the proposed solar still, based on the results of the numerical simulation that were reached.
3. Compare the simulation results with the experimental results.

Chapter Two

Literature Review

1.2. Introduction

Many researchers are seeking to develop alternative technologies to generate drinking water for daily use in remote areas due to the scarcity of fresh water; one of these options is the use of solar energy. Water desalination systems rely on traditional energy derived from the combustion of fossil fuels, which exposes them to many environmental and health risks, which represents an important potential solution to both the energy dilemma and the issue of toxic waste that endangers human health. This chapter discusses the studies conducted on the hemispherical solar still, including theoretical studies, experimental studies, and a combination of the two, and a summary of the results.

2.2. Experimental Studies

Attia et al (2021) [10] conducted enhance the efficacy of the solar still by employing reflective mirrors and aluminum foil sheets, affixed to the vertical internal surfaces of the distiller to augment the intensity of solar radiation incident on the distiller basin. Three hemispherical distillers were constructed and evaluated under identical conditions: Conventional Hemispherical Distiller with Black Painted Walls (CHSS-BPW), Modified Hemispherical Distiller with Reflective Mirror (MHSS-RM), and Modified Hemispherical Distiller with Reflective Aluminum Foil Sheets (MHSS-RAFS), as shown in the Figure (2.1). The experimental results indicated that the cumulative yield of reference distiller (CHSS-BPW) reached 4750 mL/m² day, while utilizations of reflective aluminum foil sheets (MHSS-RAFS) and reflective mirror (MHSS-RM) increases the

cumulative production to 6760, 7722 mL/m² day, with the enhancement of 42.3% and 62.6%, respectively.

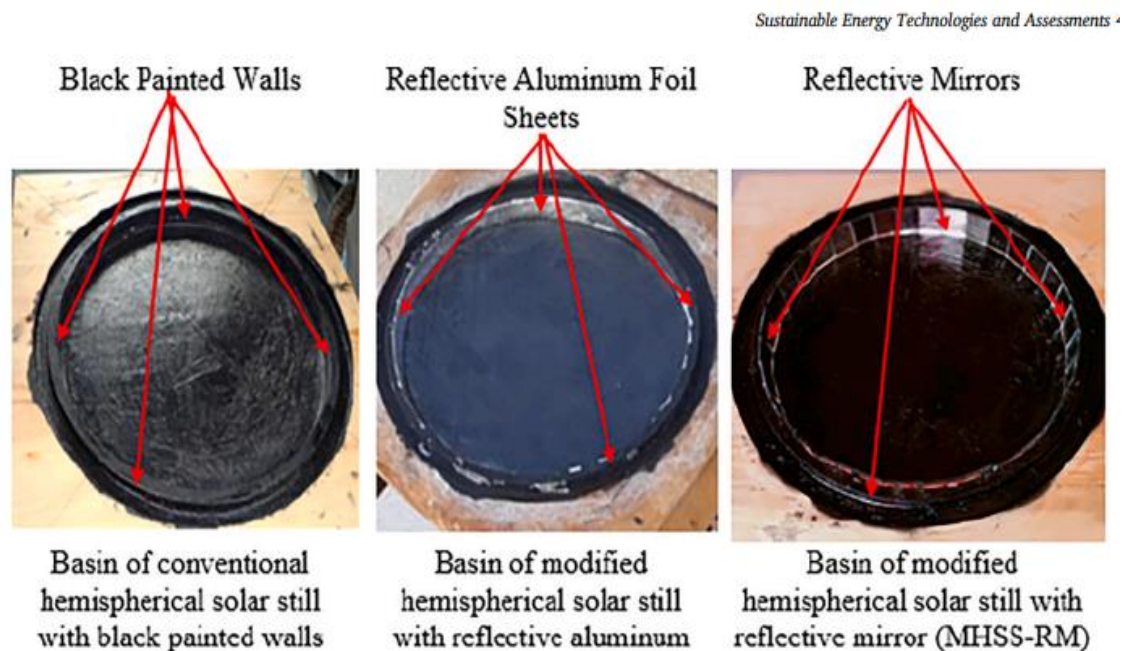


Figure (2.1): Photo of the present test rig [10].

Attia et al. (2021) [11] improved the performance of hemispherical distillers by using El Oued sand grains as sensible storage materials, which increase the absorption rate of solar radiation and improve heat transfer. The study tested eight different concentrations of El Oued sand grains and found that a concentration of 3% achieved the highest performance accumulative yield to 7270 mL/m²/day, resulting in a 52.1% improvement in accumulative yield and a 50.8% improvement in daily efficiency compared to the reference distiller.

Wisam A. Abd Al-wahid et al. (2021) [12] enhanced the efficiency of the cylindrical solar still by incorporating a vertical cylinder accompanied by a hemispherical dome as shown in the figure below.. Height increase initially raised productivity by 9.4%, but further increase led to a decrease. Different designs and materials can boost productivity without extra power. but height increase later decreased productivity. The

design can work well with passive or active heat transfer enhancements to saline water. Passive methods are crucial for productivity increase without additional power.

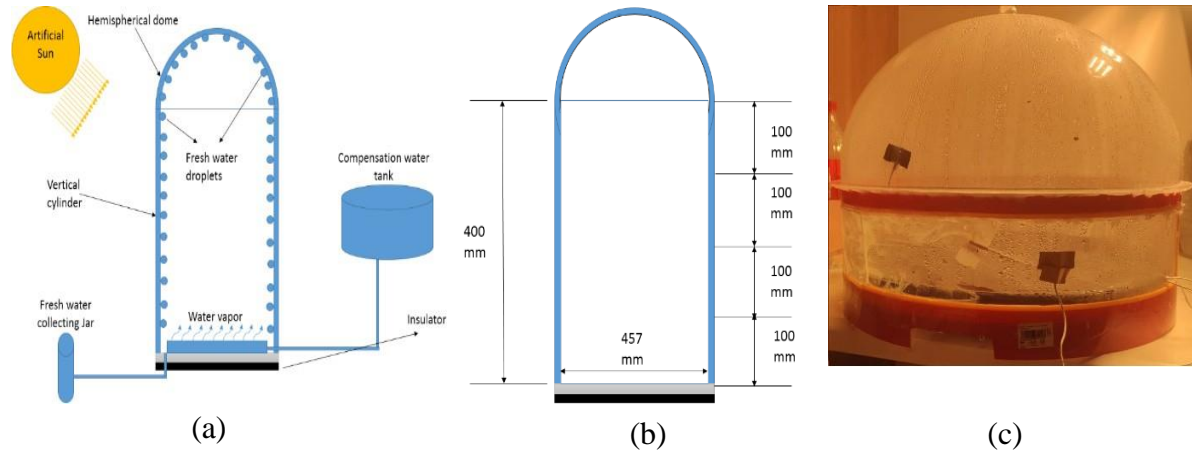


Figure (2.2): (a) Representative sketch of present work solar still, (b) measurements of still, and (c) photograph of used still for height of 10 cm [12].

Attia (2021) et al. [13] enhanced the productivity of hemispherical solar distillers by employing black gravel as an energy storage material, the . The productivity of black gravel was evaluated using sizes of 4, 8, 11, and 16 mm, as depicted in the images below (2.3), and it was found that the highest productivity was reached with the 16mm gravel reached 7.7kg/m^2 day. The utilization of black gravel resulted in significant enhancements in both cumulative yield and daily efficiency, exhibiting gains ranging from 16.3% to 57.1% in cumulative yield and from 16.2% to 56% in daily efficiency.



Figure (2.3): View of the basin of hemispherical distillers with black gravels [13].

Abd Elnaby Kabeel et al. (2021) [14] to enhance recommends the use of phosphate grains in hemispherical solar stills for their ability to increase efficiency and productivity, with a concentration of 30 g/L being optimal for achieving maximum performance gain resulting in a 57.9% improvement in cumulative yield and a 23% improvement in daily efficiency compared to traditional distillation methods .

Attia et al. (2021) [15] Enhanced the efficacy of the solar still by iron fins of varying lengths and spacing have been utilized on the absorber plate to enhance the absorption area and facilitate heat transfer from the heated basin plate to saline water. Three configurations have been evaluated under identical operating conditions. The traditional hemispherical distiller without fins serves as the reference case (CHSS). The modified hemispherical distiller with fins arranged at 5 cm intervals (MHSSIF5). The modified hemispherical distiller with fins positioned at 7 cm (MHSS-IF7), as shown in the Figure (2.4). The fin diameter remains constant at 1.2 cm, with tested lengths of 3 cm, 2 cm, and 1 cm. Findings demonstrate the respective collective yields for CHSS, MHSS-IF5, and MHSS-IF7 are 4.08, 5.65, and 6.22 L/m²/day at a fin length of 3 cm; 4.08,

5.86, and 6.38 L/m²/day at a fin length of 2 cm; and 4.08, 5.9, and 5.68 L/m²/day at a fin length of 1 cm. cm.

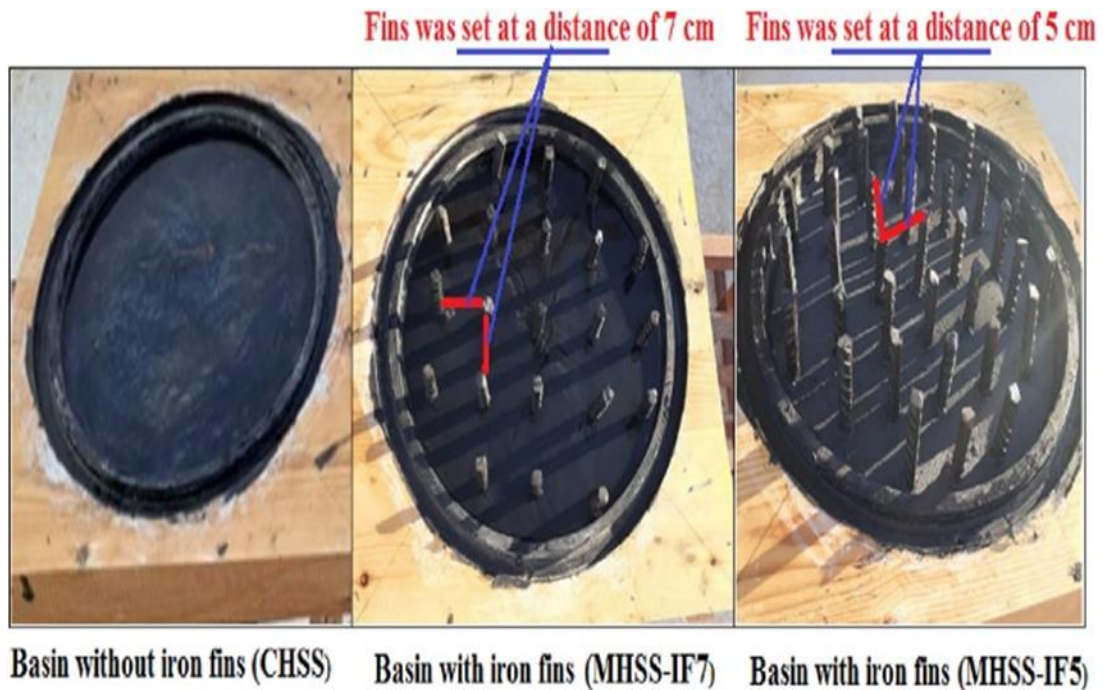


Figure (2.4): Photographic view of the basin with and without fins for three hemispherical distillers [15].

Mohammed Abd Al -Amir Khadim el at. (2021)[16] Developed the outer cover shape of the solar still to enhance production and thermal efficiency. This study introduces a novel glass cover design including a vertical cylindrical shape with a spherical dome atop. This design operates under the climatic conditions of Najaf, Iraq. A comparison conducted with a conventional single slope of identical basin area, as shown in the Figure (2.5). Three instances of cylinder height measured at 5 cm, 15 cm, and 20 cm. Two sets of trials were conducted, one in winter and the other in summer. On each experimental day, all climatic variables were recorded using a weather station, while additional recordings were made for still parts temperatures and hourly productivity. A yield of 5.8 l/m²·day at a height of 5 cm, 6.7 l/m²·day at 15 cm, 7.25 l/m²·day at 20 cm, and 4 l/m²·day for a single slope solar still. The measured thermal efficiencies were 18.8% for a height of 5 cm, 22% for 15 cm, 23.3% for 20 cm, and

15% for a single slope solar still. Summer measurements may indicate that the hemispherical solar still is more efficient than the cylindrical solar still with a hemispherical dome (CSSHD), whilst winter data reveal the contrary.

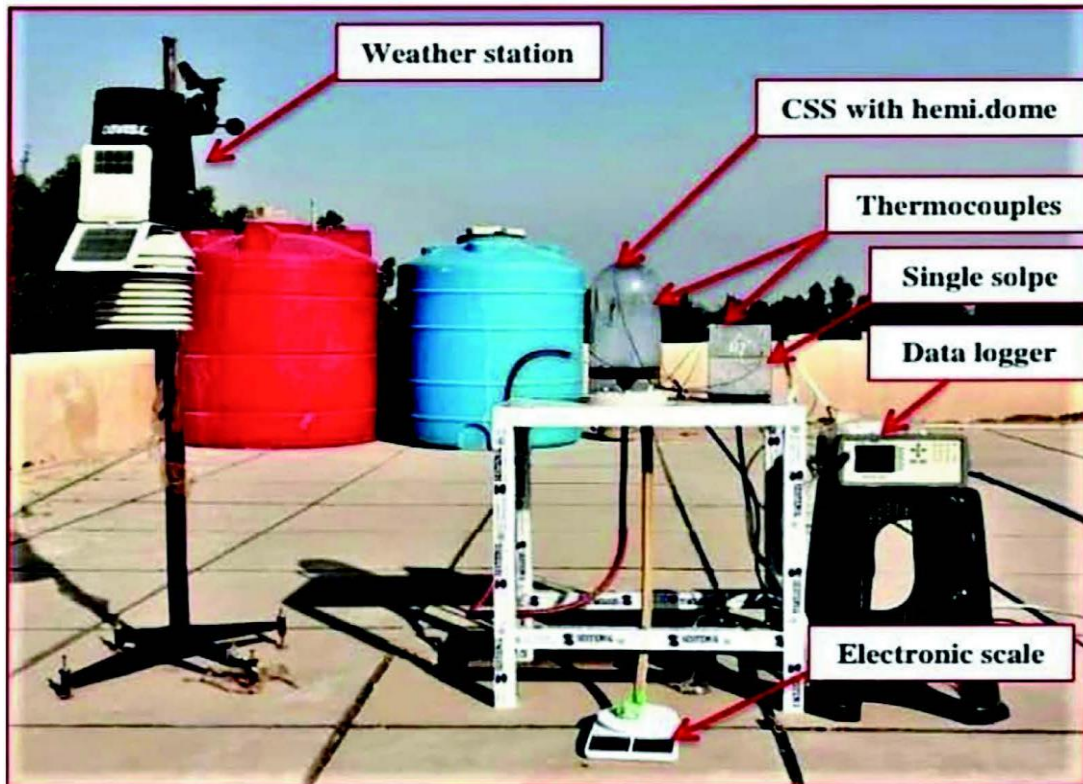


Figure (2.5): CSSHD and conventional single slope solar still used in present work [16].

Attia et al. (2021) [17] improved hemispherical solar still by use of phosphate pellets. Various pellet concentrations and configurations were compared. The results showed a significant productivity improvement when using a modified distiller with 2% phosphate pellets. The use of phosphate pellets enhanced productivity up to 47.9% compared to conventional distillers.

Attia et al. (2021) [18] enhanced the performance of the hemispherical solar still by incorporating zinc oxide into the device. Nanoparticles at concentrations of 0.1%, 0.2%, and 0.3% were utilized while cooling the glassy cover at varying flow rates of 1.5, 2.0, and 2.5 L/h. Three hemisphere solar stills were constructed for study purposes. The efficacy of a hemispheric solar still including nano-ZnO (HSS-Zn) and a hemispheric solar still with nano-ZnO featuring a cooled glass cover (HSS-ZnC) is examined and contrasted with a standard hemispheric solar still (CHSS) serving as a reference, as shown in the Figure (2.6). The findings indicated that the incorporation of ZnO nanoparticles and the cooling of the glassy cover with a hemispheric design further augment productivity. Tests indicate that the daily accumulated productivity of HSS with 0.3% ZnO nanoparticles and a cooling glassy cover with a flow rate of 2.5 L/h is 8.15 L/m²/day, representing an increase of 117.33% compared to CHSS. In this scenario, the daily efficiency of HSS with ZnO nanoparticles (0.3%) and cooling the glassy cover with a flow rate of 2.5 L/h is roughly 74.57%, whereas that of CHSS is around 79%.

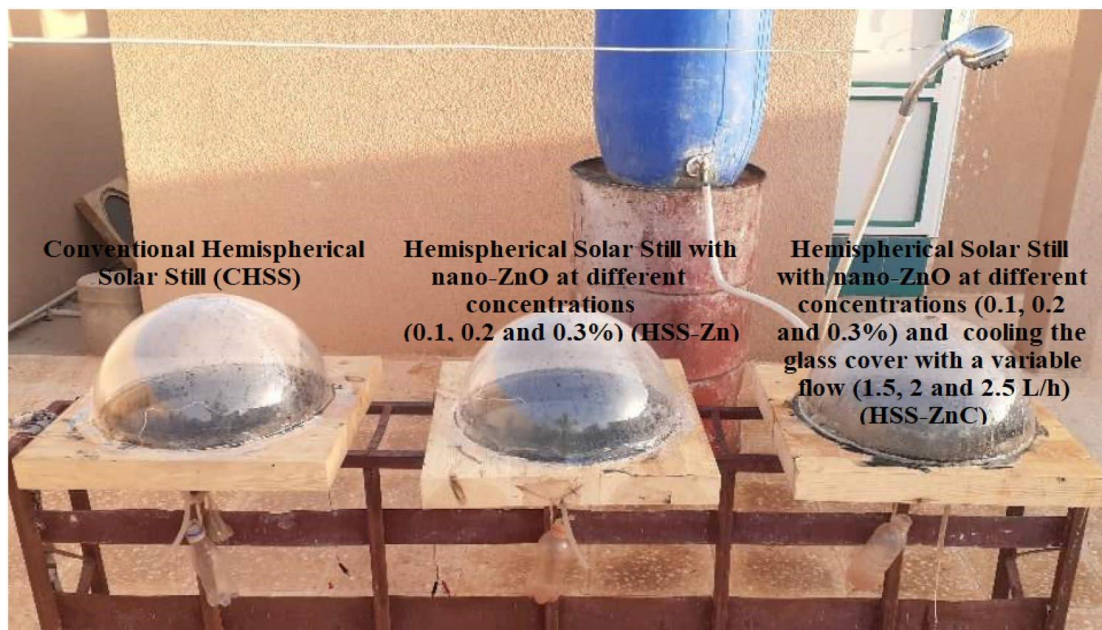


Figure (2.6): Photograph of experimental setup [18].

Attia et al. (2022) [19], the present investigation is centered on the augmentation of hemispherical solar distillers through the utilization of truncated circular cone-shaped reflector mirrors (TCC-RM) with varying inclination angles, as shown in Figure (2.7). The results of the experimental analysis have indicated that TCC-RM with a 25° inclination angle has yielded the highest cumulative output of 8.35 L/m^2 . This outcome represents a significant improvement of 42.74% when compared to traditional distillers. Conversely, altering the inclination angle to either 10° or 45° has had a detrimental effect on the overall yield of the distiller. Thus, it has been concluded that 25° is the optimal angle for achieving maximum performance and cost efficiency.

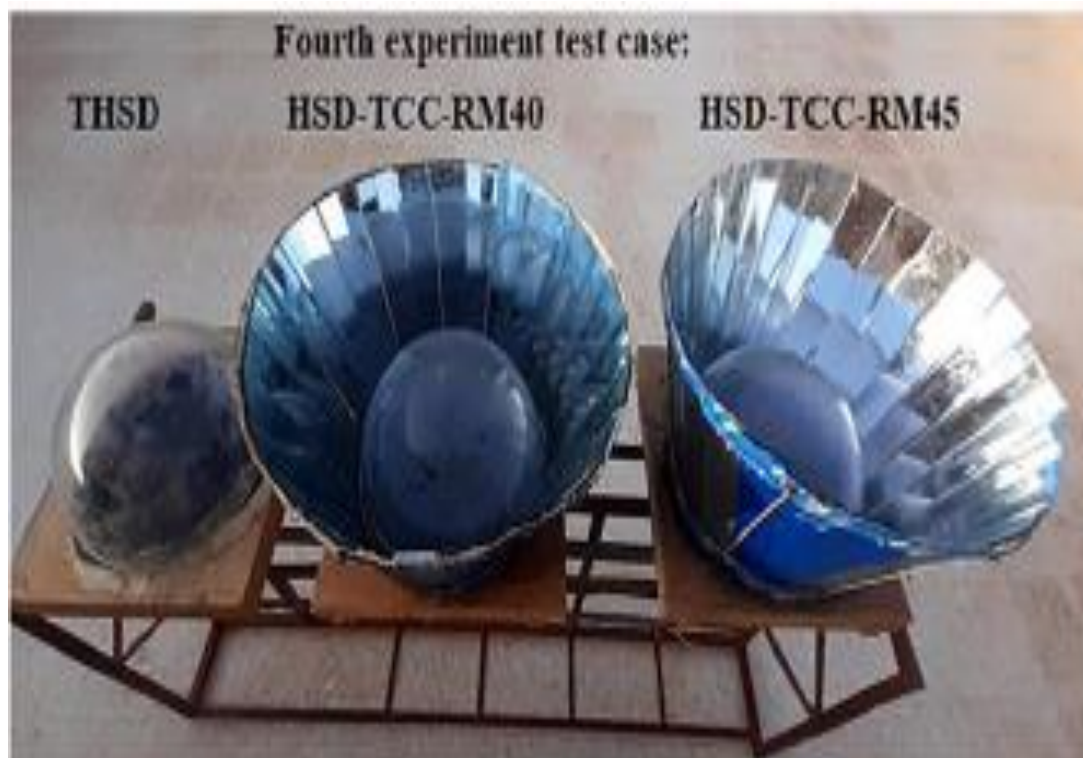


Figure (2.7): Photograph of experimental setup [19].

Abd Elnaby Kabeel et al. (2022) [20], the work aims to determine the optimal arrangement of cylindrical iron fins for solar distillers, as shown in Figure (2.8). Various experiments were conducted with different fin distances, revealing that filling the basin entirely with fins provides the highest yield. The adoption of extended cylindrical iron fins significantly

increases the cumulative yield compared to a traditional distiller. The result is that iron fins increased distiller yield and efficiency. The use of extended cylindrical iron fins with different distances (0, 1, 2, 3, 4, and 5 cm), improved the cumulative yield of a hemispherical solar distiller to 6.30, 6.10, 5.90, 5.65, 5.40, and 5.10 L/m²/day, respectively, compared to 4.80 L/m²/day achieved by traditional solar distiller without iron fins. Best results with extended cylindrical fins at 0 cm distance.

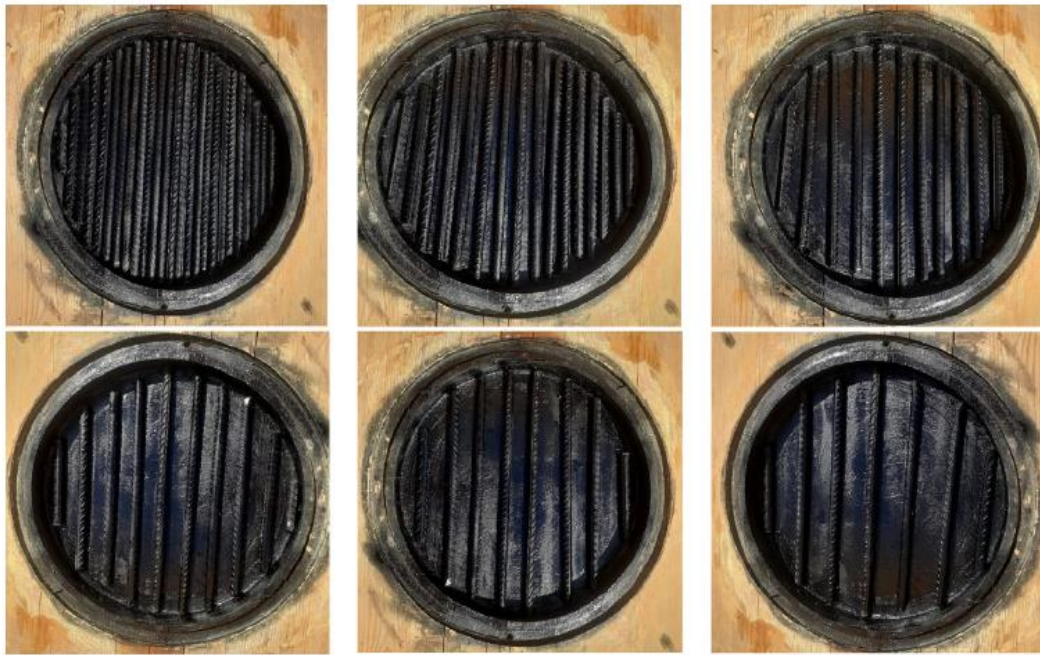


Figure (2.8): A photograph of the position of the iron fins inside the distilled basin as the distance between them changes (0, 1, 2, 3, 4, and 5 cm)[20].

Abdelkader Bellila et al. (2020) [21] improve the solar still by adding Al_2O_3 nanoparticles were initially added to the basin water to enhance the evaporation rate, followed by the implementation of glass cover cooling technology to augment the condensation rate. This study examines the effects of Al_2O_3 -water nanofluid and glass cover cooling technology utilizing a water sprinkler on the performance of hemispherical solar distillers. Three hemispherical solar distillers were developed and evaluated under identical climatic circumstances. The first case is the reference model (traditional hemispherical solar distiller), the second is the

modified hemispherical solar distiller utilizing Al_2O_3 -water nanofluid, and the third is the modified hemispherical solar distiller employing Al_2O_3 -water nanofluid in conjunction with a water sprinkler. Three distinct concentrations of Al_2O_3 nanoparticles, namely 0.1%, 0.2%, and 0.3%, were examined. The results indicated that the cumulative yield of the conventional hemispherical solar distiller attained 3280 ml/m²/day, whereas the application of Al_2O_3 -water nanofluid and the water sprinkler enhanced the cumulative yield to 6750, 6900, and 7250 ml/m²/day, Reflecting improvements of 105.8%, 110.4%, and 121% for volume fractions of 0.1%, 0.2%, and 0.3%, respectively. The enhancement in daily efficiency from the application of Al_2O_3 nanoparticles and water sprinklers achieved 105.7%, 109.7%, and 120.1% for nanoparticle concentrations of 0.1%, 0.2%, and 0.3%, respectively, in comparison to the reference instance.

Ravishankar Sathyamurthy et al. (2022) [22], this study examines the use of low-cost nanoparticles in a solar distillation device to improve yield. The addition of nanoparticles resulted in a significant increase in yield compared to conventional methods. By utilizing renewable energy and nanotechnology, fresh water production can be enhanced in a cost-effective manner. The study demonstrated improvements in fresh water production using composite PCM without negative environmental impact. The daily yields for each method were 4.85, 6.2, and 8.3 L/m²/day, respectively, as shown in Figure (2.9).

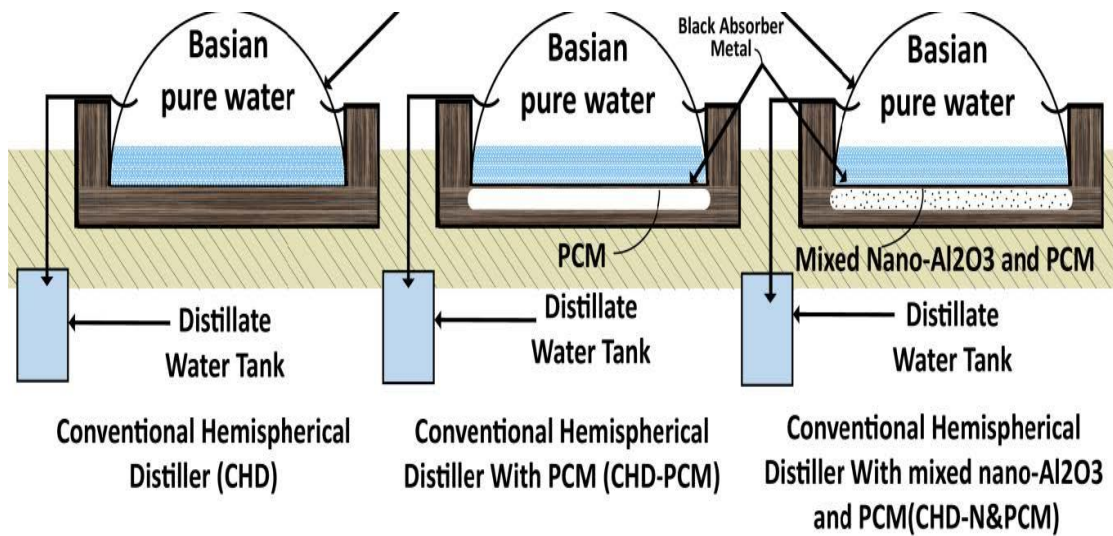


Figure (2.9): (a) Graphical representation of the different configurations[22].



Figure (2.9): (b) Experimental setup [22].

Attia et al. (2022) [23] improve the performance of the hemispherical solar still using rock salt balls in solar still systems to improve fresh water production, as shown in Figure (2.10). The results show that spacing the balls at 4.0 cm the accumulative freshwater reached 7.0 kg/day.m² is optimal for energetic-economic performance. This arrangement increases freshwater production by 38.3%, 49.0%, 27.65%, and 13.84%. Daily energy efficiency is enhanced by 55.92%, 60.10%, 51.46%, and 45.98% for the same arrangements, respectively. The

proposed hemispheric distillers using rock salt balls decrease the cost per 1.0 L of freshwater by 25.23%, 31.0%, 19.84%, and 10.77%, respectively, compared to conventional hemispheric solar stills. Overall, implementing rock salt balls significantly improves freshwater production, daily energy efficiency, and cost-effectiveness.



Figure (2.10): (a) detailed experimental setup of the hemispheric solar distilleries [23].



Figure (2.10): (b) Photograph depicting a basin with rock salt balls arranged at varying intervals of 3.0, 4.0, 5.0, and 6.0 cm [23].

Abd Elnaby Kabeel et al. (2022) [24] enhanced the efficiency of the hemispherical solar still by Flax fiber was included into a hemispherical still as a natural porous substance. Three basic hemispherical stills were designed and fabricated, and their efficacy was evaluated under identical climatic conditions. The initial simple hemispherical still (SHD)

functioned as the standard, while the subsequent stills were improved with natural yellow flax fiber (SHD-YF) and black dyed flax fiber (SHD-BF), respectively. The findings indicated that black dyed flax fiber (SHD-BF) yielded the highest daily output of 7.05 L/m²/d, while SHD-YF produced 6.55 L/m²/d, in contrast to 5.05 L/m²/d from the reference still. Additionally, the cumulative yield increased by 29.7% and 39.6%, respectively, with the use of natural yellow flax fiber (SHD-YF) and black dyed flax fiber (SHD-BF) compared to the reference still.

Attia et al. (2022) [25] improved the performance of the solar still by utilized a double-face absorbing solar thermal receiver integrated with a solar concentrator ,as shown in the Figure (2.11) ,to improve the productivity, energy efficiency, and exergy efficiency of a hemispherical solar distiller, resulting in significant improvements over the traditional distiller. The modified distiller achieved an 8.65 l/m²day productivity compared to 5.75 l/m².day for THSD with an improvement of 50.4%. Consequently, due to this great increase in yield of MHSD-DFASTR&SC, the energy efficiency of MHSD-DFASTR&SC was increased by 50.56% compared to THSD. Furthermore, the daily exergy efficiency of MHSD-DFASTR&SC is 68% compared with 2.47% for THSD.



Figure (2.11): Photographic view of MHSD-DFASTR&SC and THSD [25].

Attia et al. (2022) [26] Improved performance of hemispherical solar stills by incorporating extended hollow cylindrical fins filled with phase change material (EHCF-PCM), as shown in Figure (2.12). The research investigated four distinct distances between the EHCF-PCM, and three designs of hemispherical distillers were evaluated in Algerian climatic circumstances. The findings indicated that the EHCF-PCM with no gap spacing was the most effective configuration for optimal performance. This arrangement attained an aggregate productivity of 8.75 L/m²/day, representing an enhancement of 80.4% relative to the conventional hemispherical solar distiller (CHSD). Furthermore, the daily efficiency increased from 39.6% for CHSD to 71% for HSD-EHCF-PCM.



Figure (2.12): Photo of EHCF position inside distilled basin with the change of the distance between them (0, 2, 3, and 4 cm) in order [26].

Milad Mohsenzadeh et al. (2022) [27], the researchers developed a new floating solar still with low vacuum conditions, using solar heat localization and capillary water circulation to prevent salt accumulation. The system generated 4.3 L m⁻² d⁻¹ of distilled water with a distillation efficiency of 35.6% in Melbourne, Australia. The cost per liter of drinking

water generated was 4.7 US ϕ L⁻¹, making it a cost-effective solution for remote or disaster-stricken areas. The system outperformed existing designs by 64% in terms of water yield and had a multi-layer basin for improved water evaporation and salt rejection. The capillary water circulation reduced the need for maintenance, Figure (2.13) displays images depicting the researcher's experimental study.

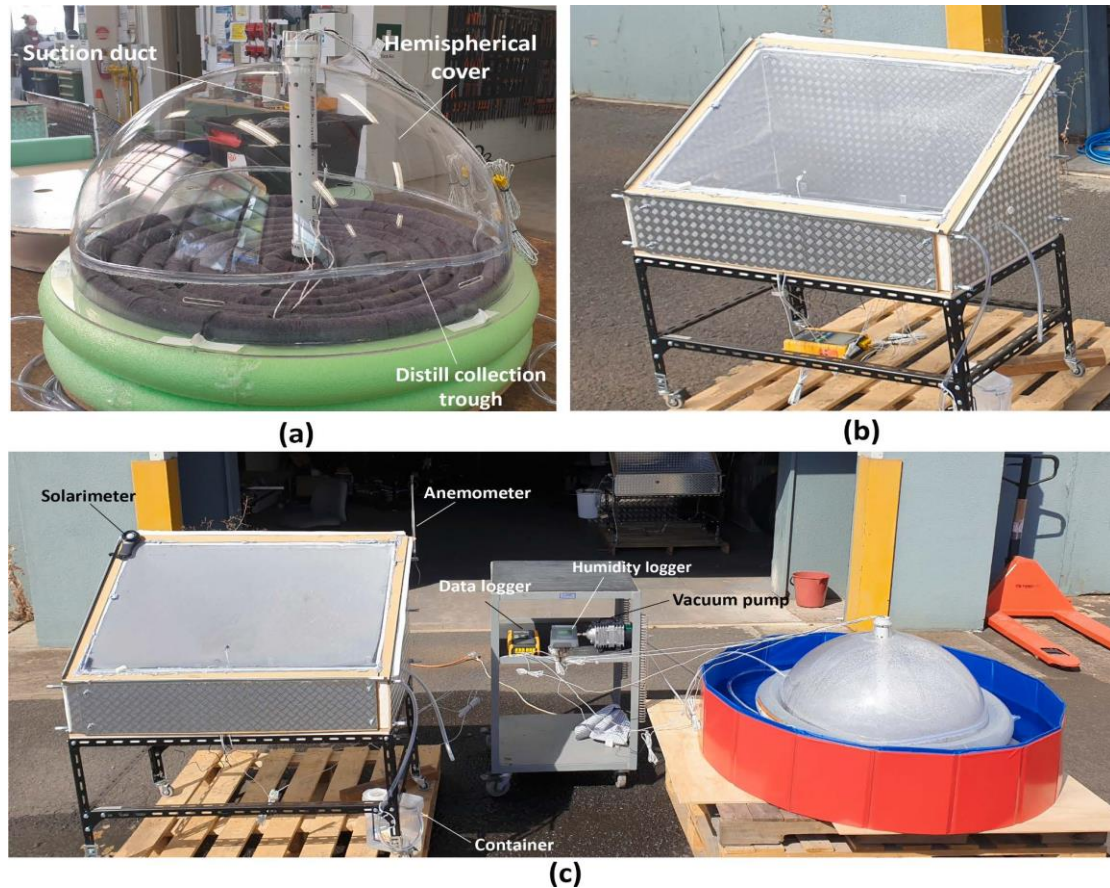


Figure (2.13): Photographs of the experimental setups: (a) Floating Hemispherical Solar Still (FHSS); (b) Reference Passive Solar Still (RPSS); (c) Outdoor experiments of FHSS next to RPSS [27].

B. Thamarai Kannan et al. (2022) [28] enhanced the efficiency of the hemispherical solar still. Utilizing paraffin wax as a phase change material (PCM) contained in discarded aluminum cans, arranged in two distinct configurations: a square pattern (four PCM cans) and a triangular pattern (three PCM cans), as shown in the Figure (2.14). A comparative investigation of traditional HSS versus modified HSS with PCM in two distinct configurations was conducted to determine the optimal mass of PCM. The results indicated that

PCM encapsulated in aluminum cans arranged in square and triangular patterns within an HSS basin enhanced clean water production by 92.80% (full-day water generation of 5.63 kg/m²) and 67.12% (full-day water generation of 4.88 kg/m²), respectively, compared to the bare HSS without any PCM (full-day water generation of 2.92 kg/m²). The efficient use of heat from aluminum cans containing paraffin wax enhanced potable water production by increasing water evaporation.



Figure (2.14): Photograph of the experimental set-up with the PCM-loaded [28].

V. Savithir el at. (2022) [29] Conducted a study explores the efficacy of modified hemispherical solar still (MHSS) with rubber and wick materials at the basin in enhancing yield compared to conventional hemispherical solar still (CHSS) , as shown in Figure (2.15). The yield increases with black rubber and wick material thickness. To experimentally studied the effect of rubber materials at different thicknesses (2.5, 5, 7.5, and 10 mm) and wick materials at a different thickness (1.5, 3, 4.5, and 6 mm), under the same operating conditions, three equal HSS units are designed and constructed. The experiments were conducted in four days, under the climatic conditions of the city of El Oued-Algeria. The experimental results showed that a rubber material at a different thickness (2.5, 5, 7.5, and 10 mm) improves the yield by 14.29, 26.53, 35.71, and

46.94%, respectively as compared to the CHSS. Also, using wick materials at different thicknesses (1.5, 3, 4.5, and 6 mm) improves the yield by 12.24, 22.45, 30.61, and 40.81%, respectively, as compared to the CHSS. This modification is very efficient and inexpensive because rubber and wick materials are available at a cheap price. After comparing the yield of HSS according to the thickness of the rubber and wick materials used, we found that the more thickness of the materials (rubber and wick), the better the yield. Therefore, we recommend using thicker materials.



Figure (2.15): Photograph of three units of the experimental HSS [29].

Attia et al. (2022) [30] modified the design of a hemispherical solar distiller by using metal trays with high thermal conductivity and reflective mirrors. He tested three different metal trays (steel, zinc, and copper) with reflective mirrors under the same climate conditions to determine the optimal selection for the highest performance. Four distillers were fabricated as shown in Figure (2.16). And tested Hemispherical Solar Distiller with Black Silicone Walls (HSD-BSW) which represent the reference case, Hemispherical Solar Distiller with Steel Trays and Reflective Mirrors (HSD-ST&RM), Hemispherical Solar Distiller with Zinc Trays and Reflective Mirrors (HSD-ZT&RM), and Hemispherical Solar Distiller with Copper Trays and Reflective Mirrors (HSD-CT&RM). The experimental results presented that the utilization of copper trays

incorporated with reflective mirrors increases the cumulative production to 9.5 l/m²day, being the most effective option. The cumulative production of the HSD-BSW distiller increased by 104.3%, and the daily thermal and exergy efficiencies improved by 102.4% and 194.9% compared to the HSD-BSW. Additionally, the use of copper trays with reflective mirrors reduced the cost of distilled water by 44.1%.

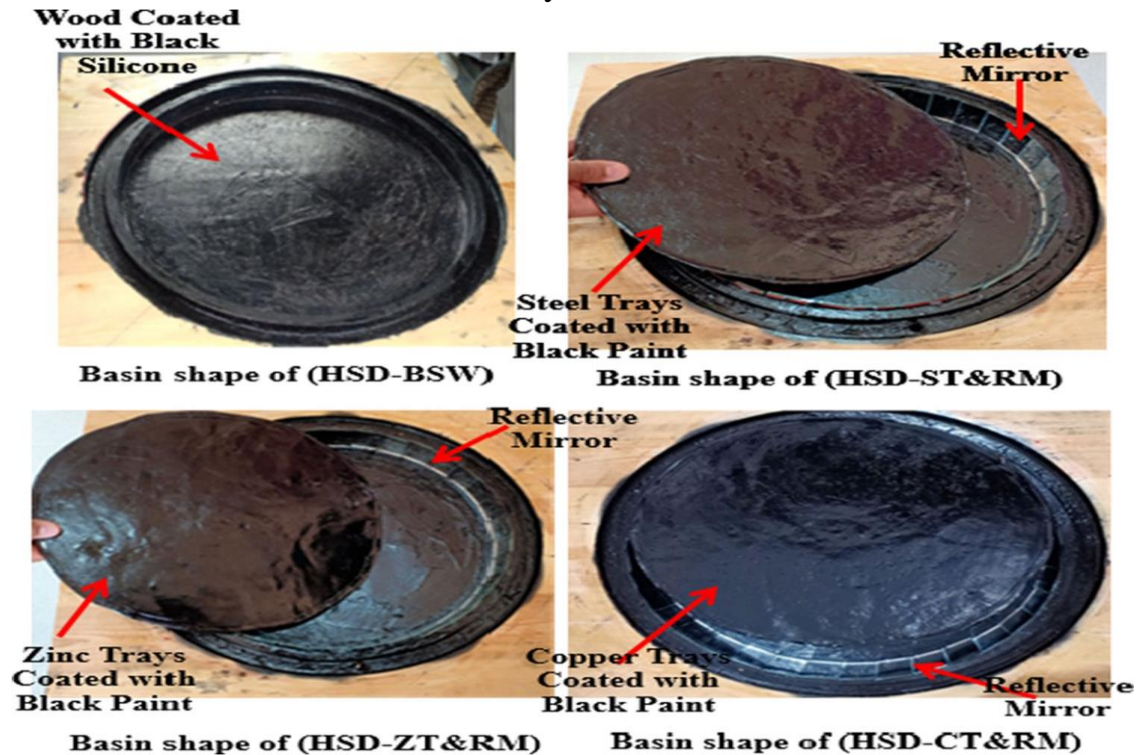


Figure (2.16): Photo of the basin configuration of the four hemispherical distillers

[30].

Bassem F. Felemban et al. (2022) [31], the researchers aimed to enhance freshwater productivity of a solar distiller by increasing absorber surface area and evaporation rate. They studied the effect of three absorber liner shapes and using a cotton wick to enlarge wetted surface area. The corrugated absorber, wick, and energy storing material showed the highest productivity improvement of 183%. The stepped absorber had a maximum improvement of 125% at a water depth of 2 cm, while the corrugated absorber with wick had an improved productivity of 160%, as shown in Figure (2.17).



Figure (2.17): Photo of tested dish solar still (DSD) [31].

Wisam A. Abd Al-wahid et al. (2022) [32] explored the use of hemispherical solar stills with rock as heat transfer enhancers to convert saltwater to freshwater with solar energy, as shown in Figure (2.18). Adding rocks increased water productivity by 52% and 58% for volumes of 300 mL and 600 mL, respectively, due to greater solar energy absorption. Rocks functioned as heat storage materials and extended the still's operating hours. The study's steady state tests showed that the rocks improved solar energy absorption and overall efficiency. The study's results suggest that hemispherical solar stills with rocks are a practical solution for converting saltwater into freshwater with solar energy.



Figure (2.18): (a) River rocks used in experiments [32].



Figure (2.18): (b) Experimental setup used in the work [32].

Abd Elnaby Kabeel et al (2023) [33], studied the impact of diverse shapes of corrugated absorbers on the performance of a solar still in arid regions. Four shapes were experimentally tested and compared to a conventional design, as in Figure (2.19). The findings reveal that the use of corrugated absorbers enhances the yield of freshwater, with the triangular shape exhibiting the highest efficiency. Corrugated absorbers possess the potential to improve the efficiency of solar stills in remote areas. The augmented contact surface area enhances the transfer of heat and absorption of solar radiation, resulting in increased water temperatures and productivity. The average productivity of hemispherical solar distillers with different corrugated absorber shapes range from 5.60 kg/m²/day to 7.15 kgm²/day, compared to 4.80 kg/m²/day for the conventional design. The overall freshwater yield of the diverse corrugated absorber shapes (HSD-FA, HSDSA, HSDSCA, HSDTA) exhibited an improvement of 16.67%, 27.08%, 39.58%, and 48.96% respectively, compared to the conventional design (CHSD).

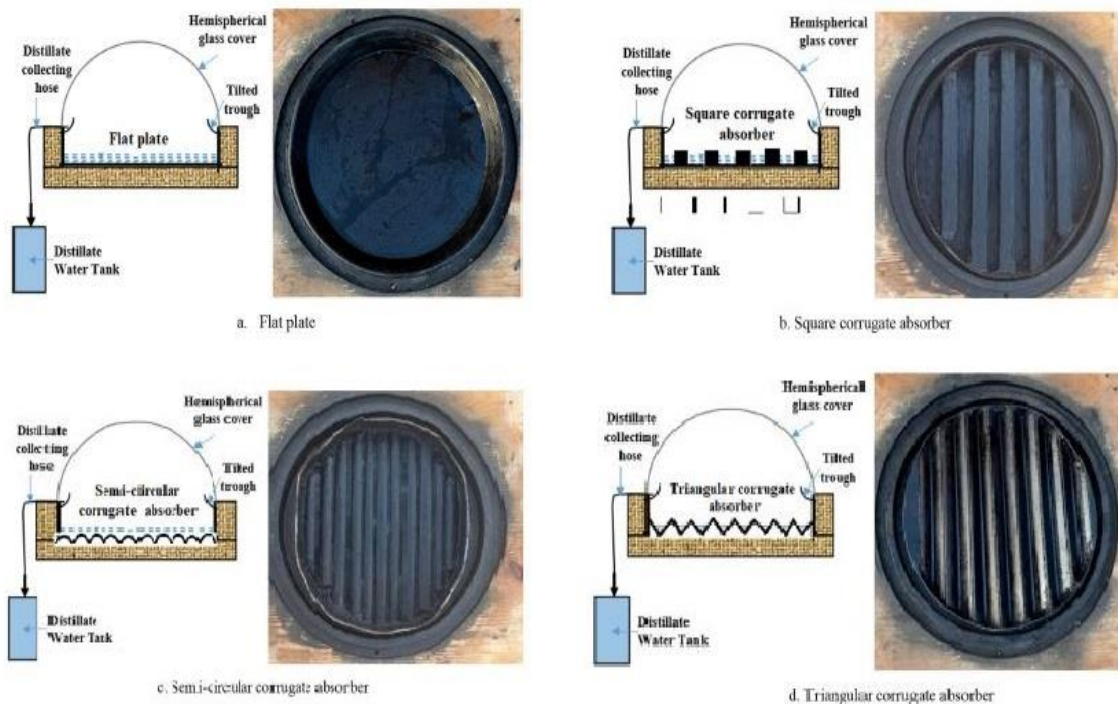


Figure (2.19): Photographic view of different corrugated absorbers, a.Flat plate, b. Square corrugate absorber, c. Semi-circular corrugate absorber, d. Triangular corrugate absorber [33].

Ibrahim M. Elsayy el at. (2023) [34] aimed to enhance freshwater production and reduce costs using a hemispherical solar still with activated agricultural waste materials. Modified distillers using charcoal and carbonized corncobs show improvements in the daily productivity of 4455 mL/m², and efficiency compared to a conventional unit. The study enhances photo thermal properties through chemical and physical activation, resulting in improved efficiency. The experiment is conducted in Karle sheikh, Egypt with seawater and lake water. The modified distillers using activated agricultural waste materials show significant improvements in productivity, efficiency, and cost reduction. Future research includes exploring different methods of chemical activation and investigating the impact of different salinity degrees, as shown in Figure (2.20).

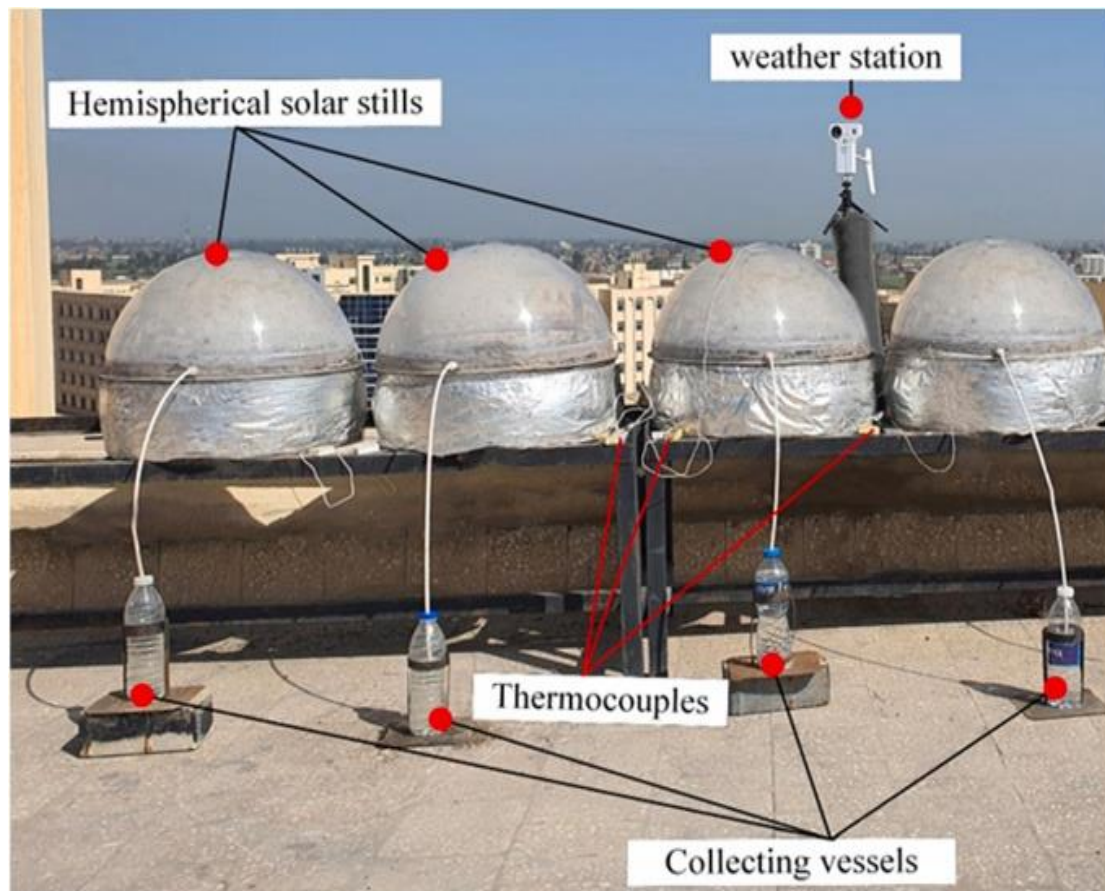


Figure (2.20): Experimental setup photograph [34].

Attia et al. (2023) [35] conducted a study in El Oued, Algeria, examined the impact of reflective aluminum foils, metal sheets, and phosphate granules on the productivity and efficiency of hemispherical solar stills. A traditional solar still was modified by adding reflective aluminum foils, zinc metal sheets, and copper sheets to its side walls. The modified stills showed increased productivity of 8.67%, 29.08%, and 42.35%, respectively, compared to the standard still. This could be due to the foils and metals reflecting more radiation and storing energy, which raises the temperature of the saltwater in the basin. In the second experiment, three modified solar stills containing aluminum foil and phosphate granules (30 g/L), as shown in Figure (2.21). The productivity of the modified solar still with aluminum foil and phosphate granules (improvement rate 30.61%) was on the far side of the productivity of the still with zinc metal sheets and phosphate granules (improvement rate 49.961%) and copper metal sheets and phosphate granules (improvement rate 62.24%).

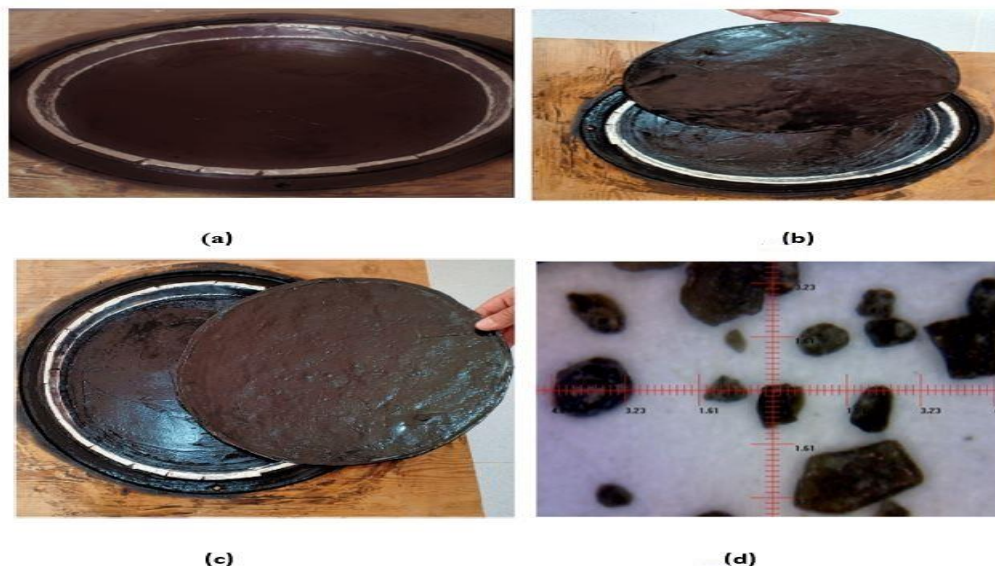


Figure (2.21): (a) Basin with phosphate granulate. (b) Basin with zinc metal sheet and phosphate granulate. (c) Basin with copper metal sheet and phosphate granulate. (d) Micrograph of Phosphate pellets [35].

Azzeddine Beggas et al.(2023) [36] Improved hemispherical solar stills using waste aluminum as heat absorber and storage material as shown in Figure (2.27). Which increases productivity and improves heat transfer, the productivity reached 6150 ml/m^2 . The incorporation of waste aluminum increases productivity by 48.19% and improves thermal efficiency. This also reduces the cost of distilled water production by 32%. In general, waste aluminum is an effective and low-cost material for improving hemispherical solar stills.



Figure (2.22): (a) A photograph of the hemispherical solar still basin without and with aluminum waste [36].

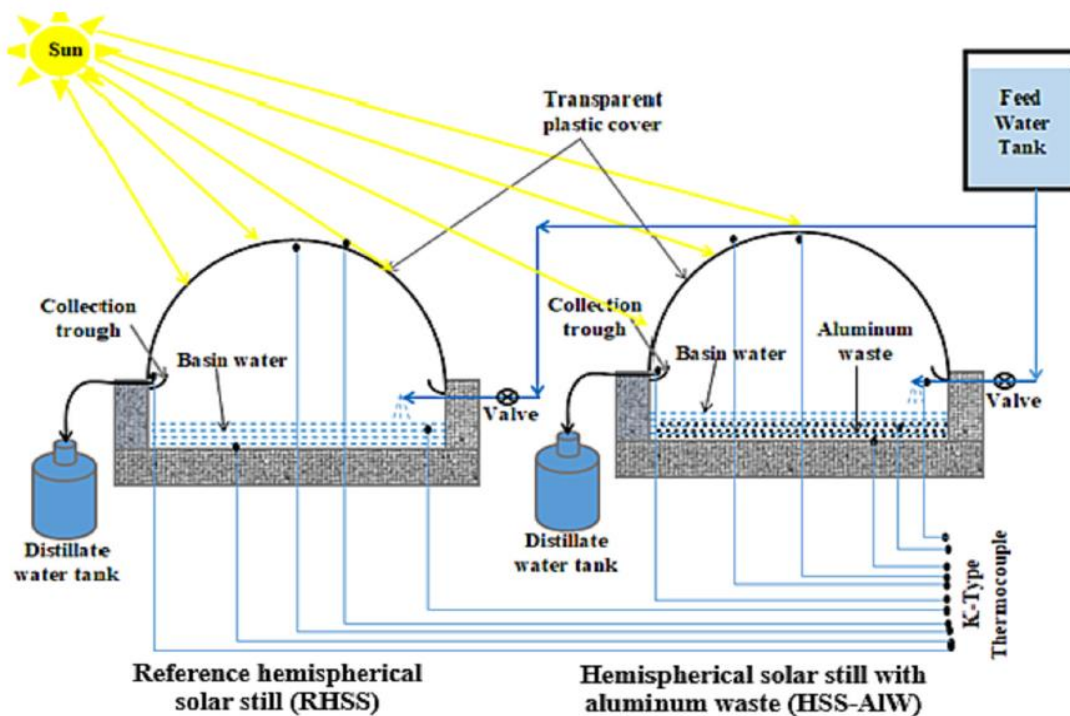


Figure (2.22): (b) A schematic of two hemispherical distillers (RHSS and HSS-Awls) [36]

Attia et al. (2023) [37] enhanced the performance of hemispherical solar distillers by optimizing the construction of marble pieces as thermal energy storage materials. Experimental results show that among four types of marble pieces tested as in Figure (2.23). Red marble provides the highest improvement for cumulative productivity, thermal efficiency, and cost reduction. Specifically, red marble pieces increase the cumulative productivity of distillers by 61.46%, achieving 7.75 l/m² days. The thermal efficiency of distillers improves from 39.25% to 62.98% with the use of red marble pieces. Moreover, the use of red marble pieces results in a 35.6% reduction in distillate cost.

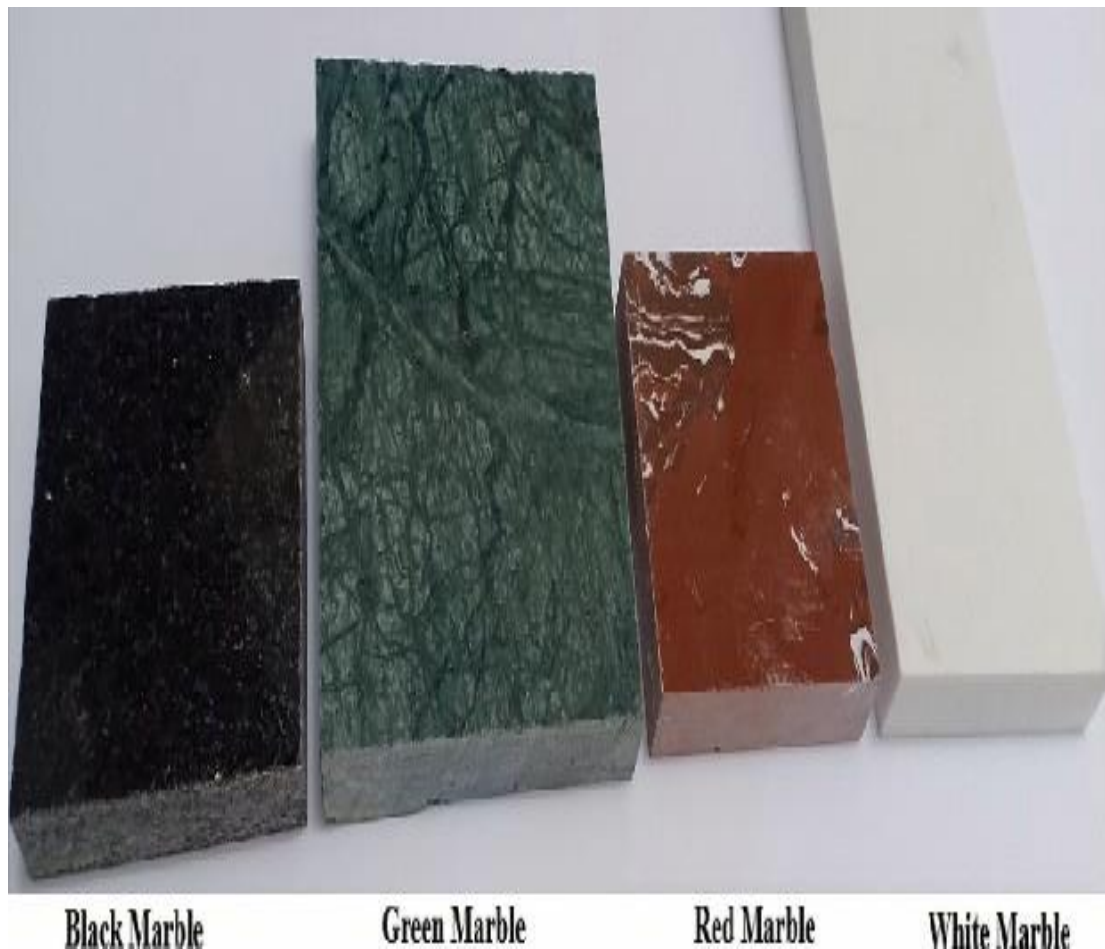


Figure (2.23): Marble pieces at different colors used in the experiment [37].

Attia et al. (2023) [38] developed a method to improve the efficiency of hemispherical solar stills, which have an extensive condensation surface area. He used pocket and semi-circular liners to increase the heat transfer area between the basin water and the absorption surface. These liners were integrated with an inverted solar collector to expedite the evaporation process. Three hemispherical stills were constructed: the traditional hemispherical solar still (THSS), the hemispherical solar still with a pocket liner combined with an inverted solar collector (SHSS-ISC), and the hemispherical solar still featuring a semi-circular liner integrated with an inverted solar collector (HCHSS-ISC), as in Figure (2.24). The results showed that the modified HCHSS-ISC and SHSS-ISC increased daily yields by 63.40% and 54.00%, respectively. The economic feasibility analysis showed that the implementation of semicircular liners combined with an inverted solar collector reduced the cost of distilled water by 30% compared to THSS.



a) Traditional hemispherical solar still (THSS) and hemispherical solar still with a sinusoidal liner incorporated with an inverted solar collector (SHSS-ISC)



b) Traditional hemispherical solar still (THSS) and hemispherical solar still with a half-circle liner incorporated with an inverted solar collector (HCHSS-ISC)

Figure (2.24) : A photograph of experimental stages[38].

Attia et al. (2023) [39] use unique convex basin design was utilized in place of a flat absorption basin to enhance the exposure and evaporation surface area. Additionally, a layer of jute fabric was employed over the convex basin as an absorbent medium to augment the evaporation rates within the modified still, as in Figure (2.26). The impact of employing phase change material (PCM) thermal storage on the thermoeconomic performance of the still was also examined. Three hemispherical stills were built and evaluated: a modified hemispherical still with a convex wick absorption basin (MHD-WCAB), a modified hemispherical still with a convex wick absorption basin and phase change material (MHD-WCAB+PCM), and a reference hemispherical still (RHD), as shown in Figure (2.25). The daily production of distilled product was 7.95 kg/m²/day for MHD-WCAB+PCM, 6.90 kg/m²/day for MHD-WCAB, and 4.25 kg/m²/day for RHD, representing improvements of 87.06% and 62.35% relative to RHD. Furthermore, the daily energy efficiency of MHD-WCAB+PCM and MHD-WCAB was assessed at 46.90% and 34.04%, respectively, indicating an enhancement rate of 85.67% and 61.74% in comparison to RHD. The daily energy efficiencies of MHD-WCAB+PCM and MHD-WCAB were 3.88% and 3.39%, respectively, reflecting increases of 128.24% and 99.41% compared to RHD.

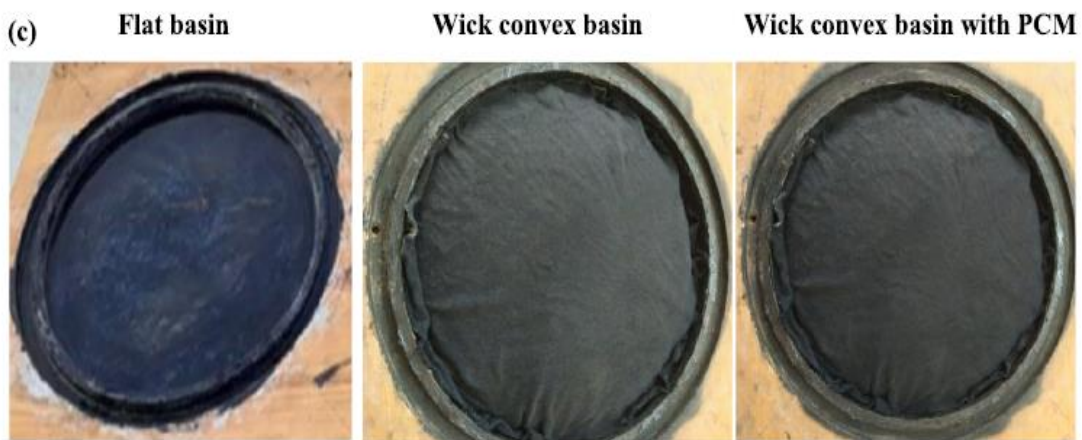


Figure (2.25) :(a) Pictorial view of the designed absorber basins in each distiller [39].

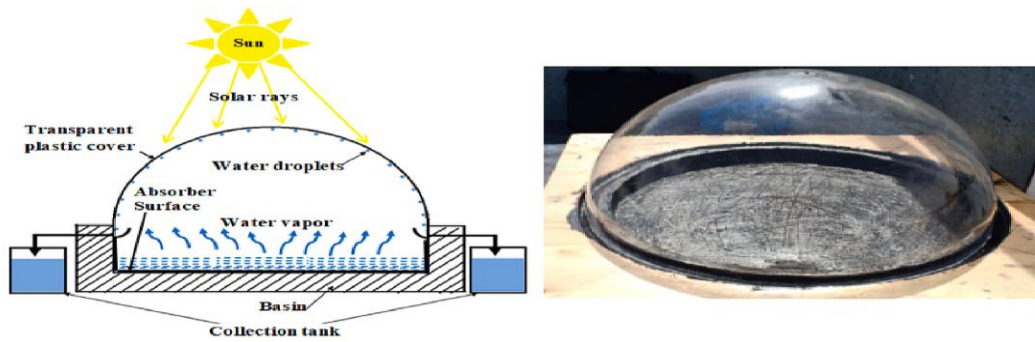


Figure (2.25) : (a) Schematized diagram; (b) Pictorial view [39].

Abd Elnaby Kabeel et al. (2023) [40] improved hemispherical solar distillers by using scrubber steel wire coils as porous materials and energy store materials. Two configurations of coils, spiral and cake form, were tested in the distiller basin as in Figure (2.26). The cake-shaped coils provided the highest distiller performance, with 1.472 times more distillate than traditional distillers. Thermal and exergy efficiencies also increased significantly. The use of scrubber steel wire coils in the shape of a cake is a good choice for enhancing the performance of hemispherical distillers. The accumulation totals of HSD-SSCSSW and HSD-CSCSSW reached 6315 mL/m^2 and 7110 mL/m^2 , respectively, while THSD accumulation totaled 4830 mL/m^2 . This can effectively address freshwater shortage issues in remote areas, where population increase and climate changes pose challenges.



Basin of traditional hemispherical solar distiller (THSD)

Basin of hemispherical solar distiller with cake-shaped coils of scrubber steel wire (HSD-CSCSSW)

Basin of hemispherical solar distiller with spiral-shaped coils of scrubber steel wire (HSD-SSCSSW)

Figure (2.26): Basin photo of the three hemispherical distillers [40].

Mohamed A. Dahab et al. (2023) [41] experimental investigations were conducted on integrating evacuated tubes (EVT) in a hemispherical solar still (HSS) to enhance its performance, as in Figure (2.27). EVT integration significantly improved distillate performance and achieved higher energy and exergy efficiency values compared to the traditional design. The highest daily distillate production rate was achieved with EVT integration, ranging from 91% to 551%. The proposed HSS-EVT system showed improved energy and exergy efficiency compared to the traditional HSS, with a maximum daily production of 6.69 L/m² at 8 tubes of EVT. The estimated cost of the system varied between 0.00237 and 0.0101 USD/L.

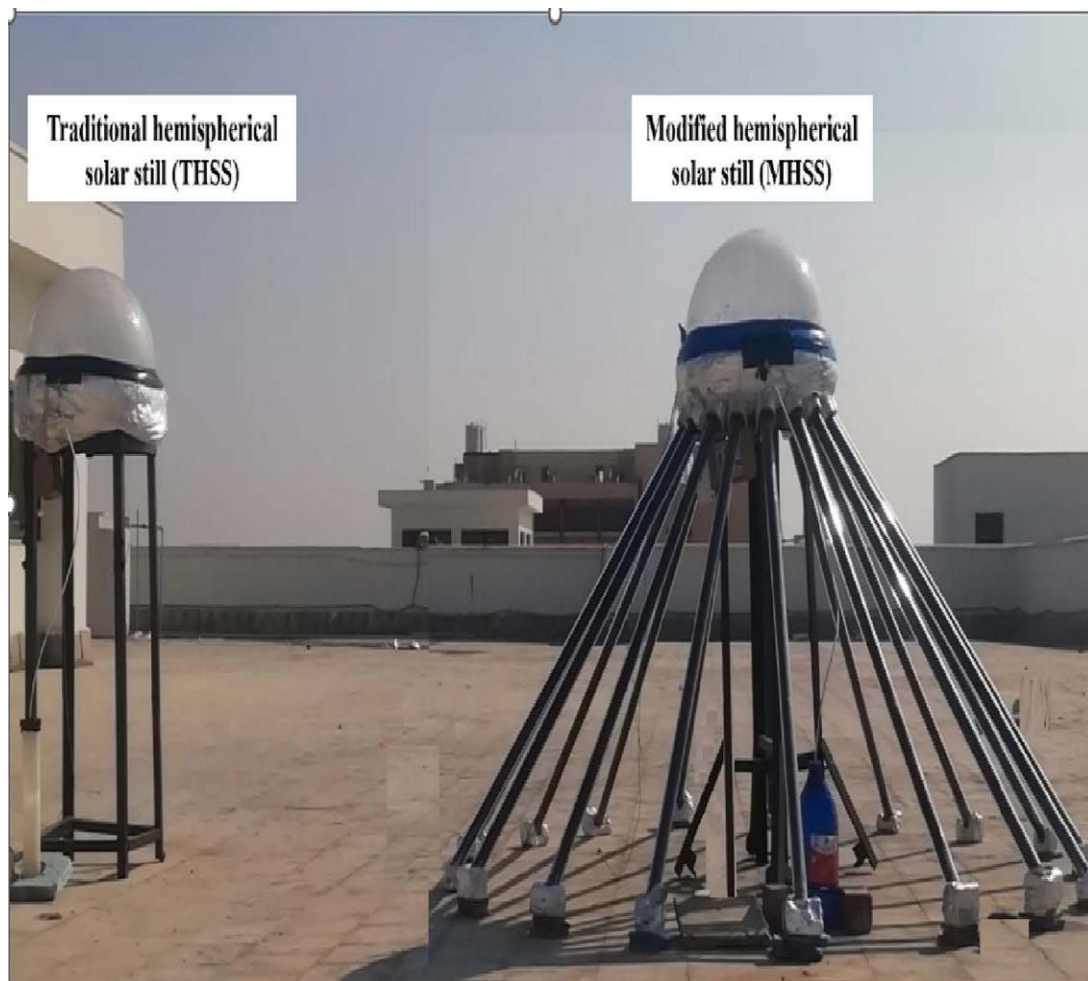


Figure (2.27): Photograph of the experimental test rig [41].

Swellam W. Sharshir et al. (2023) [42] sought to improve to enhance the performance of a hemispherical solar still (HSS) by applying various modifications. The modifications included copper absorbers covered with black cotton fabric and paraffin wax or sheep fat as phase change materials (PCM), as well as graphite Nano fluid in the basin as in Figure (2.28). The final case involved using a Nano-based sheep fat with dispersed graphite nanoparticles. The modified HSS yielded daily improvements ranging from 43% to 95.2%, with the best thermoeconomic performance achieved in the final case. The modifications also led to a decrease in freshwater price by 33.90% and a reduction of 6.27-ton CO₂/year in CO₂ emissions. These results highlight the potential of utilizing different energy storage materials and Nano fluids to enhance efficiency and reduce environmental impact in solar desalination systems.

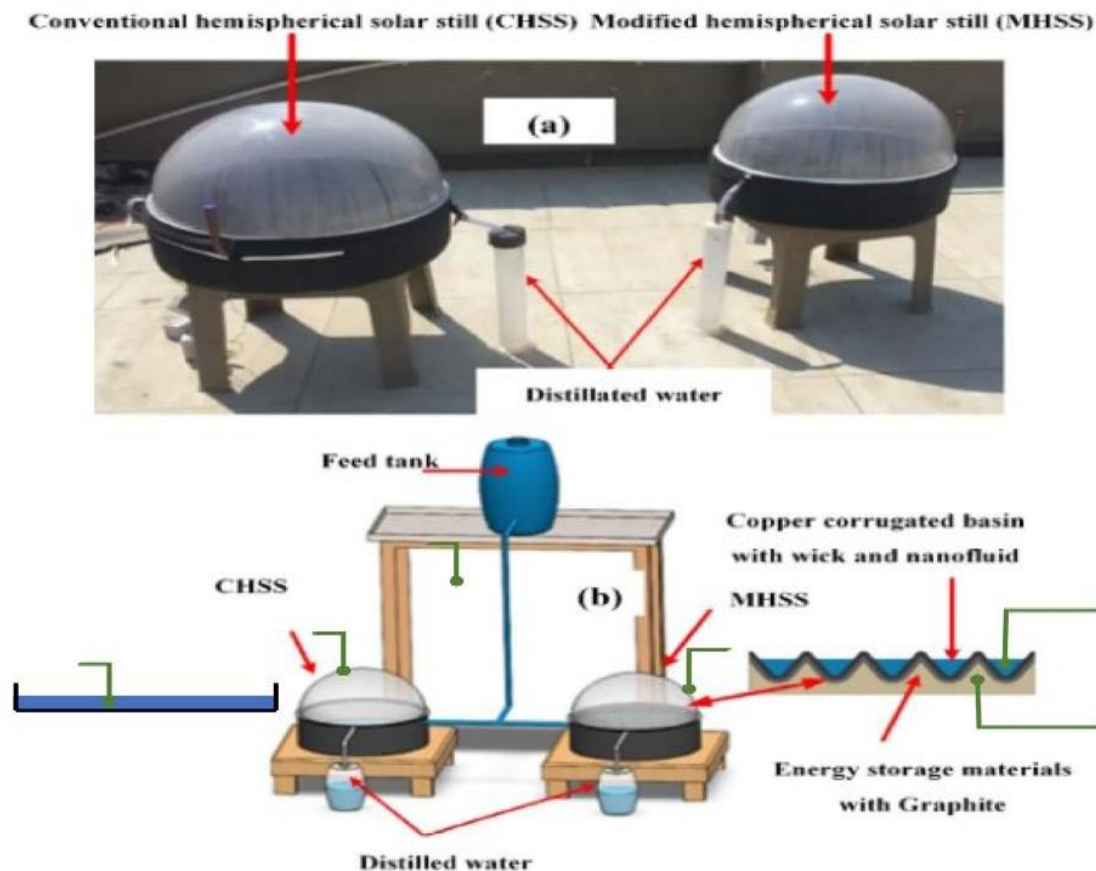


Figure (2.28): The experiment set up (a) photograph, (b) the schematic [42].

2.3 Theoretical Studies:

Dhafer M Hachim et al. (2021) [43] presented a simulation model that was developed to investigate the performance of a novel cylindrical solar still design, as shown in Figure (2.29). The aim of the study was to enhance the efficiency of solar distillation technology by achieving a maximum level of productivity of 6.1 kg/m^2 per day in terms of freshwater output. The findings of the study revealed that the new design displayed a higher level of daily freshwater productivity compared to conventional single slope solar stills. Moreover, the simulation results were consistent with the available experimental data, thereby attesting to the accuracy of the simulation model.

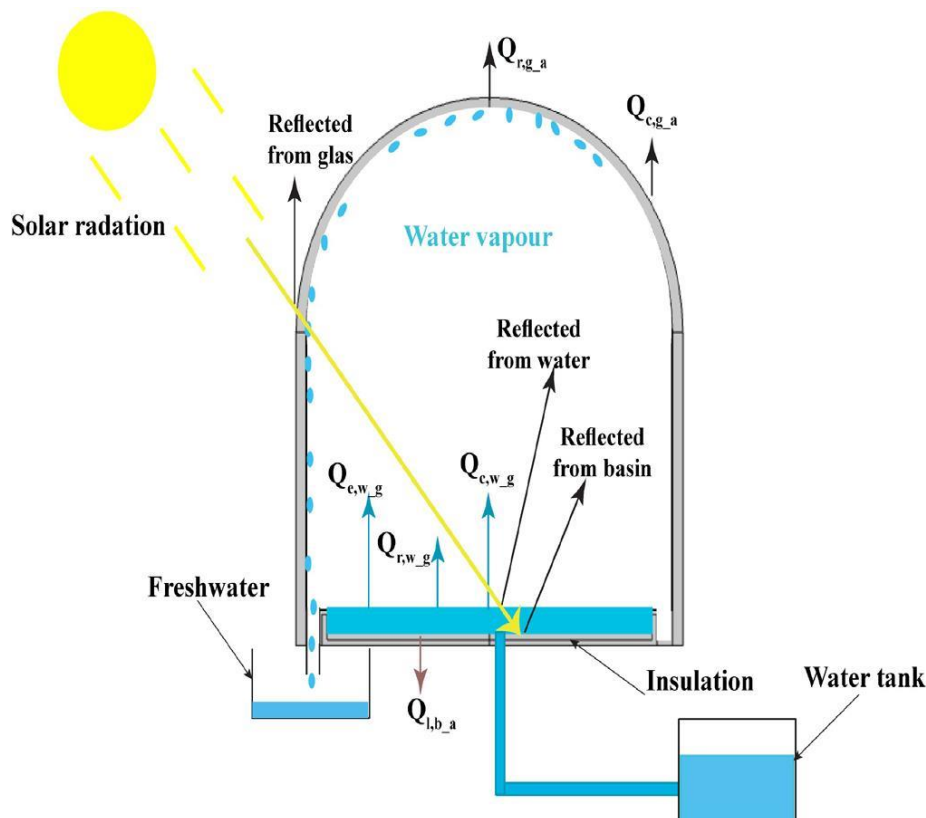


Figure (2.29): The cylindrical solar still is depicted in a cross-sectional view, showing various heat losses and gains [43].

Mohd Zaheen Khan et al. (2021) [44] performed an investigation on a solar still equipped with a hemispherical glass enclosure and water cooling. The study was done at Jamia Millia Islamia's Department of Mechanical Engineering and monitored key parameters. The results showed that water cooling increased efficiency from 34% to 42%, and using a hemispherical glass cover with water cooling increased efficiency by 1.25 times. The study suggests that top cover cooling enhances performance and daily yield.

Theoretical and Experimental Studies:

R. Fallah Zadeh et al. (2020) [47] modified simple hemispherical solar still was evaluated both theoretically and experimentally in the outdoor conditions of Mashhad, Iran (latitude $36^{\circ}18'0''$; longitude $59^{\circ}34'0''$). Following multiple experimental tests, the daily production of distilled water from the still was recorded to vary between 2.72 and 3.17 liters per day. Upon comparing experimental results with those derived from modeling the solar still, it was shown that Clark's model exhibited greater consistency with the experimental data than other prevalent thermal models. Moreover, the modeling findings demonstrated that the efficiency of the still improved by over 1% with a reduction in the thickness of the glass cover. Furthermore, the thermal conductivity and thickness of insulation significantly influenced the still's efficiency, allowing for an enhancement of 60% by reducing thermal conductivity and increasing insulation thickness, respectively.

Mohamed Abdelgaied et al. (2022) [48], this study compared a modified hemispherical solar still with traditional ones, using PCM and CuO nanoparticles additives, as shown in Figure (2.30). Three MHSS cases were examined, showing significant improvements in productivity and energy efficiency compared to THSS. The dual usage of PCM and CuO/water Nano fluid further enhanced productivity. The daily energy efficiency of the MHSS with PCM and CuO/water Nano fluid was found to be 63.61%. The economic feasibility analysis indicated a cost reduction of 75% compared to THSS. Overall, the usage of PCM and CuO/water Nano fluid in the MHSS proved to be an effective and cost-efficient tool.



(1) THSS (2) MHSS with
PCM container (3) MHSS with 0.3
wt.% CuO/water NF (4) MHSS with PCM container
and 0.3 wt. %CuO/water NF

Figure (2.30): Photographic view of the proposed hemispherical solar stills [48].

Panchal et al (2013) [49], the hemisphere solar still model was utilized. The two-dimensional three-phase mechanism of evaporation and condensation in ANSYS CFD is compared to experimental results of hemispheric solar stills under Mehsana climate conditions (latitude $23^{\circ} 59'$ and longitude $72^{\circ} 38'$). The simulation yields data for variables such as water temperature, vapor temperature, and distillation output. The water temperature and distillate output were consistent with the experiment's real

results. The study demonstrates that ANSYS CFD is highly effective and valuable for designing and comparing hemispheric solar stills.

2.4 Summary of Literature Survey

Through the literature review, there has been a significant amount of interest in the field of design pertaining to hemispherical solar stills. The Numerical research encompasses experimental research, numerical research, as well as combined experimental and numerical research. Vestigations have been carried out to examine the impact of various adjustments on the output of solar distillates. These modifications encompass the utilization of rock salt balls, sand, fin sets, as well as the incorporation of Al_2O_3 nanoparticles, phase change materials PCM and CuO additives nanoparticles, reflective mirrors, aluminum panels, and paraffin wax, among others. Despite thoroughly examining all previous studies, were unable to identify any instances of utilizing a cylindrical solar still hemispherical dome with fins. These behaviors are investigated to maximize the maximum productivity of different types of solar stills.

The study is summarized in Table (2.1), which includes the studied parameter, cumulative productivity, productivity per square meter per hour, and cost. In the present work, a new model used by improving the cylindrical solar still with hemispherical dome with and without fins in basin. As far as know, this is the first time such work has been done in Iraq. The use of cylindrical solar stills, which are fitted with a hemispherical dome and fins, is employed to desalinate water and improve production in order to enhance the effectiveness of solar stills.

Table (2.1): Summarizes literature studies

NO.S	Author and work place/year	Research type	Used	Results	cost	complexity
1	Attia (2021) [10]	Experimental	Reflective mirror and reflective aluminum foil sheets	increases the cumulative production to 6760, 7722 mL/m ² day, improves cumulative yield and thermal efficiency by 42.3% and 37.5%	0.0066 \$/Liter	Simple
2	Attia (2021) [11]	Experimental	using El Oued sand grains as sensible storage materials	improves the accumulative yield to 7270 mL/m ² /day, representing a 52.1% improvement in accumulative yield	N.A	Simple
3	Wisam A. Abd Al-wahid [12]	Experimental	adding a vertical cylinder with ahemispherical dome.	increase productivity by 9.4%	N.A	simple
4	Mohammed El Hadi Attia (2021) [13]	Experimental	black gravel, especially with 16 mm size	increase ranging from 16.3% to 57.1% and 16.2% to 56%, respectively, with a corresponding rate of 7.7 kg/m ² /day.	0.0034 7\$/Liter	simple
5	Abd Elnaby Kabeel (2021) [14]	Experimental	using phosphate grains as energy storage materials	The utilization of 30 g/L phosphate grains (HSS-PG30) resulted in a cumulative yield of 6 L/m ² /day, which was a 57.9% improvement compared to THSS.	N.A	simple
6	Attia (2021) [15]	Experimental	iron fins	the productivity can be reduced by up to 56.73% with a maximum of 6.38 L/m ² /day	0.0103 \$/liter	simple
7	Mohammed. Abd Al -Amir Khadim (2021) [16]	Experimental	a new solar still glass cover design was implemented. It comprises a vertical cylinder with a spherical dome on top.	the yield amount ranging from 5.8-7.25 l/m ² .day and the thermal efficiency ranging from 18.8-23.3%	N.A	simple
8	Attia (2021) [17]	Experimental	phosphate pellets	4.6, 6.32, 6.15, and 6.85 L/m ² .day for different configurations of the distillers tested	N.A	simple

NO.S	Author and work place/year	Research type	Used	Results	cost	complexity
9	Attia (2022) [18]	Experimental	new reflector mirrors called truncated circular cone-shaped reflector mirrors (TCC-RM)	achieved the maximum cumulative yield of 8.35 L/m ² , which is a 42.74%	0.0057 \$/Liter	Simple
10	Abd Elnaby Kabeel (2022) [20]	Experimental	extended cylindrical iron fins	6.30 L/m ² increase of total output ranging from 6.25% to 31.25%, depending on the distance of the fins from 0-5 cm.	0.0368 \$/Liter	complex
11	Abdelkader Bellila (2021) [21]	Experimental	Al ₂ O ₃ nanoparticles to increase evaporation and used glass cover cooling technology	The yield and efficiency increased by over 100% for various concentrations of Al ₂ O ₃ nanoparticles	0.0725 \$/Liter	simple
12	Ravishankar Sathyamurthy (2022) [22]	Experimental	Paraffin wax with aluminum oxide nanoparticles used as a PCM in a solar distiller.	further improved the yield to 8.3 L/m ² /day, achieving a 71.13% increase over the conventional distiller	0.4518 \$/Liter	complex
13	Attia (2022) [23]	Experimental	use of rock salt balls in solar distillation systems to improve freshwater production.	The accumulative freshwater production is increased by 49.0% for rock salt balls with gap spacing of 4.0cm f 7.05 L/m ² /day The utilization of black-dyed flax fibers in a hemispherical	0.0075 \$/Liter	simple
14	Abd Elnaby Kabeel (2022) [24]	Experimental	black dyed flax fibers	distiller resulted in a 7.63% increase in distillate water production and a maximum daily thermal efficiency of 57.31%, which was 39.34% higher than the reference distiller.	0.42 \$/Liter	simple
15	Attia (2022) [25]	Experimental	a double-face absorbing solar thermal receiver integrated with a solar	achieved an 8.65 L/m ² .day productivity, a 50.56% increase in energy efficiency	N.A	complex

NO.S	Author and work place/year	Research type	Used	Results	cost	complexity
16	Attia(2022) [26]	Experimental	expanded copper fins filled with PCM	productivity of 8.75 L/m ² /day and an improvement of 80.4%	N.A	Simple
17	Milad Mohsenzadeh (2022) [27]	Experimental	solar energy is used to localize heat and capillary action is employed to prevent salt buildup.	daily rate of 4.3 L m ⁻² d ⁻¹ with a distillation efficiency of 35.6%	N.A	simple
18	B. Thamarai Kannan(2022) [28]	Experimental	paraffin wax as a phase change material (PCM)	increased clean water production by 92.80% and 67.12%	0.0111 \$/liter	N.A
19	V.Savithir (2022) [29]	Experimental	rubber and wick materials at the basin	5.63	0.0057 \$/liter	complex
20	Attia (2022) [30]	Experimental	thermal conductivity metal trays and reflective mirrors	daily exergy efficiency, reaching 9.5 L/m ² day	0.0066 \$/liter	Complex
21	Bassem F. Felemban (2022) [31]	Experimental	Various absorber liners such as convex dish, stepped, and corrugated surface	improvement in productivity, amounting to 183%, and thermal efficiency, which was 69.5%.	N.A	simple
22	Wisam A. Abd Al-wahid (2022)[32]	Experimental	amounts of river rocks	show an increase in water productivity by 52% and 58%	N.A	Simple
23	Abd Elnaby Kabeel (2023) [33]	Experimental	triangular corrugated absorber shape enhancing the performance of the hemispherical solar still	the conventional design has 4.80 kgm ² /day.	N.A	simple
24	Ibrahim M. Elsayy (2023) [34]	Experimental	two floating agricultural waste materials, namely charcoal derived from guava tree wood (CHL) and carbonized comcobs (CCC).	The daily productivity, thermal, and exergy efficiencies for H.CCC.LW were 4455 mL/m ² , 41.19%, and 3.85%	N.A	Complex

NO.S	Author and work place/year	Research type	Used	Results	cost	complexity
25	Attia (2023) [35]	Experimental	solar still with copper sheets, phosphate granules, and reflective aluminum foils	6.36 kg/m ² improvement rates for aluminum foils, aluminum foil with phosphate granules, and zinc metal sheets with phosphate granules were 62.24%, 30.61%, and 49.961%, respectively.	0.438 \$/liter	simple
26	Azzeddine Beggas (2023) [36]	Experimental	waste aluminum as a heat absorber and storage material	6.15 kg/m ² /day The inclusion of waste aluminum leads to a 48.19% rise. The cost of manufacturing distilled water falls by 32%.	0.0087 \$/Liter	N.A
27	Attia (2023) [37]	Experimental	four types of marble pieces tested	Red marble fragments enhance distillers' total productivity by 61.46%, resulting in 7.75 l/m ² days	0.0074 \$/Liter	simple
28	Attia (2023) [38]	Experimental	incorporating sinusoidal and half-circle basin liners with inverted solar collectors	the highest daily yield of 8.25 L/m ² /day and an efficiency of 66.9%.	0.006 \$/Liter	complex
29	Attia (2023) [39]	Experimental	convex absorber basins and phase change material (PCM)	7.95 kg/m ² /day, an 87.06% increase	0.0085 \$/Liter	Complex
30	Abd Elnaby Kabeel (2023) [40]	Experimental	scrubber steel wire coils The cake-shaped	reaching 7110 mL/m ²	N.A	Simple
31	Mohamed A. Dahab (2023) [41]	Experimental	integrating evacuated tubes(EVT) in ahemispherical solar still (HSS)	daily production of 6.69 L/m ² at 8 tubes of EVT.	0.0023 7, and 0.0101 \$/Liter	Complex
32	Dhafer M Hachim (2021) [43]	Theoretical	COMSOL multiphysics and the simulations	greater daily freshwater productivity than the SSS, with a difference of 2.92 kg/m ² .	N.A	simple
33	Mohd Zaheen Khan (2021) [44]	Theoretical	A glass cover that is hemispherical and cooling with water	increased efficiency by 1.25 times The cumulative yield and daily efficiency experienced an	N.A	simple

NO.S	Author and work place/year	Research type	Used	Results	cost	complexity
34	R.Fallahzadeh (2020) [47]	Experimental and Theoretical	through theoretical modeling and experimental tests	water output ranging between 2.72 and 3.17 Liter/day	0.031 \$/Liter	N.A
35	Mohamed Abdelgaied (2022) [48]	Experimental and Theoretical	PCM and CuO nanoparticles additives	Productivity increased by 80.20%. MHSS with PCM and CuO/water nanofluid has 63.61% energy efficiency, leading to a 79.08% daily efficiency improvement compared to THSS.	0.00645 \$/Liter	Complex
36	Panchal et al (2013) in India [49]	Experimental and Theoretical	A model is developed in ANSYS-CFD to compare parameters. Compared with actual experimental results,	ANSYS CFD simulation are very important tool for analyzing a solar still function	N.A	simple

Chapter Three

Numerical Analysis

3.1. Introduction

This chapter analyzes the models demonstrated in the numerical simulation with COMSOL Multiphase 6.1 software, then establish the governing equations employed in the numerical solution, along with the initial and boundary conditions and the assumptions made in the numerical solution. Furthermore, it assesses the accuracy of the network and compare it with previous studies.

3.2. Proposed Model Geometry

In order to test the performance of the cylindrical solar still with a hemispherical dome, the COMSOL V.6.1 program was used to perform numerical simulation of the proposed model. The proposed distiller consists of the following parts:

The glass cover, the structure of glass cover was made of a cylindrical glass, with a length of 0.35 m, a diameter of 0.166 m, and a thickness of 0.003 m, with hemispherical dome has diameter of 0.166. The basin of still circular shape made of brass its diameter 0.13 m, with thickness 0.002 m, and height of the circumference is 0.01 m. The fins have circular shape positioned in basin of still at specific heights of 0.004m, 0.006m, and 0.008m, with thickness 0.002 m, used different number (4 fins, 5 fins, 6 fins). The thermal insulator is circular in shape, with a diameter of 0.166 m and a thickness of 0.028 m, made of foam as shown in Figure (3.1).

The outcomes of computational simulations, encompassing the temperatures of basin, salt water, inner glass, outer glass, and productivity are exhibited for four months, namely January, March, July, and October. Each month is assessed for a single day. A total of twenty-eight cases were

meticulously examined in order to ascertain the impact of impact of augmenting the height of the cylinder and height of the fins as well as the number of fins on the performance of still, as shown in Table (3.1)

In which the mechanism of fins operates (a) The solar light incident on the fins is absorbed. An increase in the number of fins correlates with a greater surface area exposed to solar radiation. (b) The fins conduct heat to the water between them by convection. This facilitates the elevation of water temperature, hence enhancing the evaporation process. (c) The dimensions of the fins affixed within the tank diminish the water volume, therefore augmenting the rate of evaporation relative to a tank devoid of fins, since the reduced water quantity necessitates less thermal energy and time for evaporation.

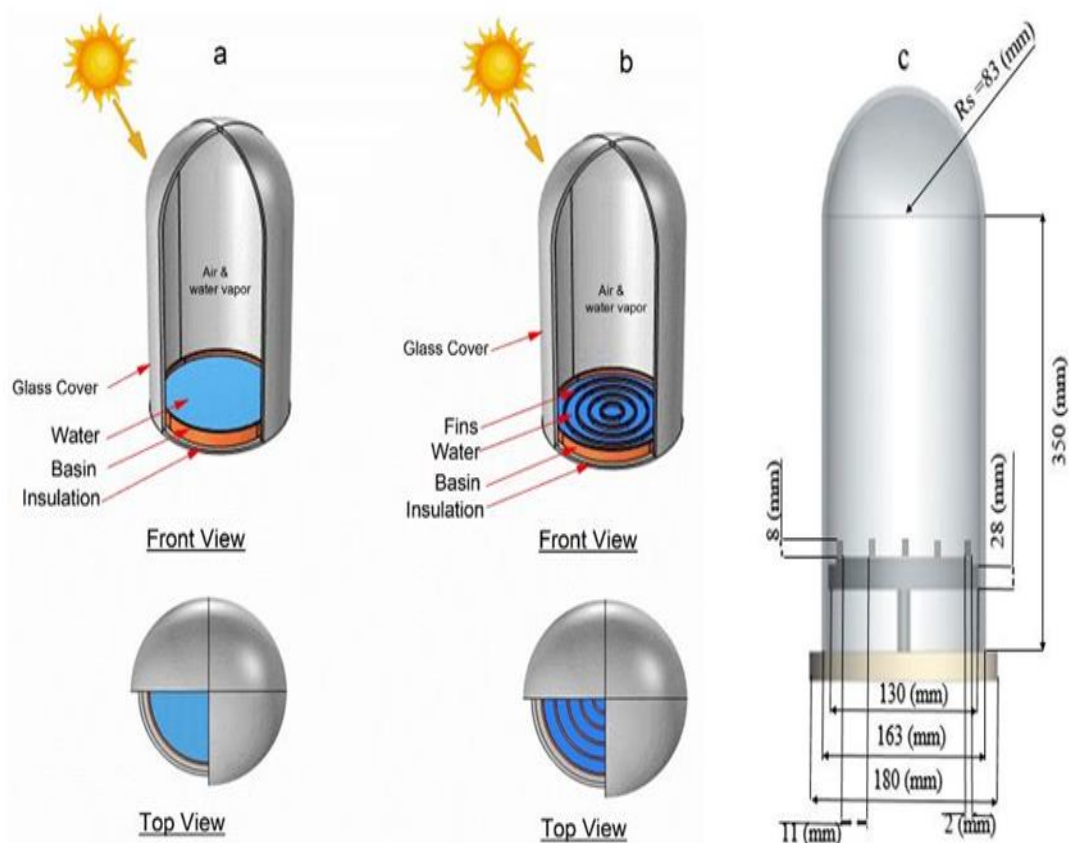


Figure (3.1): The diagram presented depicts cylindrical solar still with a hemispherical dome, (a) without fins in basin, and, (b) with fins in basin, (c) Dimensions of the solar still

Table (3.1): The parameters that effect of area of condensation and area of basin

No.	Height of the cylinder L _w (mm)	height of fins h _f (mm)	Number of fins N _f	Area of basin A _b (m ²)	Area of glass A _g (m ²)
Case 01	0	0	0	0.023475	0.031674
Case 02	50	0	0	0.023475	0.053972
Case 03	200	0	0	0.023475	0.12088
Case 04	350	0	0	0.023475	0.18777
Case 05	0	4	4	0.026877	0.031674
Case 06	0	6	4	0.029252	0.031674
Case 07	0	8	4	0.031627	0.031674
Case 08	50	4	4	0.026877	0.053972
Case 09	50	6	4	0.029252	0.053972
Case 10	50	8	4	0.031627	0.053972
Case 11	200	4	4	0.026877	0.12088
Case 12	200	6	4	0.029252	0.12088
Case 13	200	8	4	0.031627	0.12088
Case 14	350	4	4	0.026877	0.18777
Case 15	350	6	4	0.029252	0.18777
Case 16	350	8	4	0.031627	0.18777
Case 17	0	4	5	0.028456	0.031674
Case 18	0	6	5	0.031621	0.031674
Case 19	0	8	5	0.034787	0.031674
Case 20	50	4	5	0.028456	0.053972
Case 21	50	6	5	0.031621	0.053972
Case 22	50	8	5	0.034787	0.053972
Case 23	200	4	5	0.028456	0.12088
Case 24	200	6	5	0.031621	0.12088
Case 25	200	8	5	0.034787	0.12088
Case 26	350	4	5	0.028456	0.18777
Case 27	350	6	5	0.031621	0.18777
Case 28	350	8	5	0.034787	0.18777

3.3. Proposed Modeling and numerical simulation

3.3.1. Assumptions for Modeling

In order to streamline the resolution of the suggested modules, the following assumptions are utilized:

- The fluid dynamics and thermal exchange in the mentioned components exhibit two-dimensional symmetry.
- Characteristics are unsteady and follow a laminar behavior.
- There is no water vapor leakage between the glass cover and original frame in all models.
- The outlet thermal conduction coefficient is wind speed dependent.
- The water vapor present on the surface of the water is in a state of saturation.
- The evaporation flux is equivalent to the condensation flow.
- Properties of variables that vary in response to changes in temperature.

3.3.2. Governing Equations

The concepts of conservation of continuity, momentum, energy, and concentration are employed to mathematically represent the equations that regulate the behavior of flow, energy, and concentration. The initiation of the heat transfer process takes place when solar energy interacts with the modules. To carry out an initial study, the system examines a small rate of liquid flow and assumes that the movement of the liquid layer follows a smooth and orderly pattern known as laminar behavior. The flow in the suggested hybrid modules is characterized as incompressible, unstable, two-dimensional, symmetric, and laminar. This characterization leads to the application of the following equations.

3.3.2.1. Conservation of Mass Equation

The mass within an isolated system remains constant, as it cannot be generated or eliminated; however, it has the ability to change from one state to another. The equation of continuity represents a mass conservation for the air mixture and it can be expressed as:

$$\rho \nabla \cdot (u) = 0 \quad (3 - 1)$$

3.3.2.2. Conservation of Momentum Equations

The conservation of momentum is a fundamental principle in physics, asserting that the total momentum of a system remains constant in the absence of external forces. This concept is encapsulated in Newton's First Law, also known as The Law of Inertia. Experimental evidence strongly supports the law of conservation of momentum, and it can be logically derived through mathematical reasoning under the assumption of uniform space. The momentum equation for the air mixture can be given as:

$$\rho \left(\frac{\partial u}{\partial t} + u \cdot \nabla u \right) = -\nabla p I + \nabla \cdot (\mu (\nabla u + (\nabla u)^T)) + (\rho - \rho_{ref})g \quad (3 - 2)$$

The equation represents the different forces acting on a fluid at a certain position. The first term represents the inertial forces, the second term represents the pressure forces, the third term represents the viscous forces, and the fourth term represents the gravitational forces. The identity matrix is represented as I.

3.3.2.3. Conservation of Energy Equation

The principle of conservation of energy dictates that energy cannot be generated or annihilated; rather, it can only change from one state to another. When considering all types of energy, the overall energy within a closed system remains consistent. All forms of energy adhere to the principle of conservation of energy. In essence, the principle of conservation of energy asserts that

$$\rho C \frac{\partial T}{\partial t} + \rho C u \nabla T + \nabla q = q_o \quad (3 - 3)$$

Where:

$$q = -K \nabla T \quad (3 - 4)$$

3.3.2.4. The equations of concentration

The movement of diluted substances through the pore space is controlled by the combined influence of diffusion and convection. This can be mathematically represented by the equation mentioned in the reference[48]:

$$\frac{\partial c}{\partial t} + u \nabla c = \nabla (D_{AB} \nabla c) + R \quad (3 - 5)$$

The hourly productivity (P_h) of pure water can be calculated as:

$$P_h = \frac{(-3600 * D_{ab})}{L} \int_0^x \frac{dc}{dy} dx \quad (3 - 6)$$

And the cumulative productivity (P_{cum}) can be obtained from the following:

$$P_{cum} = \sum_{working\ time} hr P_h \quad (3 - 7)$$

The daily efficiency of the solar still can be derived using the subsequent equation.

$$\eta_h = \frac{ph(t) lw,av}{G(t).Ap} \times 100\% \quad (3-8)$$

3.3.3 Models Boundary and Initial Conditions

The equations (1-7) shown above are resolved by employing the subsequent boundary and initial conditions.

A. Boundary Conditions

The numerical simulation employed the initial and boundary conditions, which are specified in Table (3.2), along with an accompanying explanation of boundary conditions.

B. Initial Conditions

The initial conditions for the governing equations, previously mentioned, act as the initial state for the simulation at time $t=0$. The initial circumstances can be presented in a tabular fashion as illustrated in Table (3.3).

Table (3.2): Boundary Conditions

Model layers	Settings
Outer glass layer of still	Convection to ambient, $Q_{cgout-amb} = h_{out} (T_{gout} - T_{amb}(t))$ Radiation to ambient, $Q_{rgout-sky} = \alpha_g \sigma (T_{gout}^4 - T_{sky}^4)$ Heat source, $R_g = G(t) \cdot \alpha_g \cdot A_{g_out}$ $h_{out} = 5.7 + 3.8 V_{wind}(t)$ $T_{sky} = 0.0552 T_{amb}(t)$
Inner glass layer of still	Heat Condensation, $Q_{cond} = M_{evap} H_{evap}$ Radiation from inner glass to water surface, $Q_{rgin-w} = \alpha_g \sigma (T_{g_in}^4 - T_w^4)$ Concentration on inner glass surface, $c_g = \frac{P_{sa-g}}{R T_g}$
Water surface	Heat source, $R_w = G(t) \cdot \alpha_w$ Heat Evaporation, $-Q_{evap} = M_{evap} H_{evap}$

	Radiation from water surface to inner glass, $Q_{rw-gin} = \alpha_w \sigma (T_w^4 - T_{gin}^4)$ Concentration on water surface, $c_w = \frac{P_{sa-w}}{R T_w}$
Basin of still	Heat source, $R_b = G(t) \cdot \alpha_b \cdot A_b$ Heat Losses, $Q_{cb-amb} = h_{ins} (T_b - T_{amb}(t))$ $h_{ins} = K_{ins}/t_{ins}$

Table (3.3): Initial conditions

Equations	Settings
Continuity and momentum equation	The initial value of the velocity field is zero; $u(r, z, 0) = v(r, z, 0) = w(r, z, 0) = 0$
Energy equation	$T(r, z, 0) = T_{amb}(0)$
Concentration equation	$c(r, z, 0) = 0$

3.4. CFD Time-Dependent Solver

Utilize the Time-Dependent Solver for addressing time-dependent issues (referred to as dynamic or unsteady problems) by employing implicit time-stepping techniques such as Backward Differentiation Formula (BDF) or generalized- α , or an explicit approach from the array of Runge–Kutta methods, alongside an Adams–Bashforth method for resolving ordinary differential equations (ODEs). This computational tool is activated automatically when a Time Dependent study is incorporated into the model. To explain how the simulation process of present work. The flow chart to show numerical progression into the depicted in Figure (3.2).

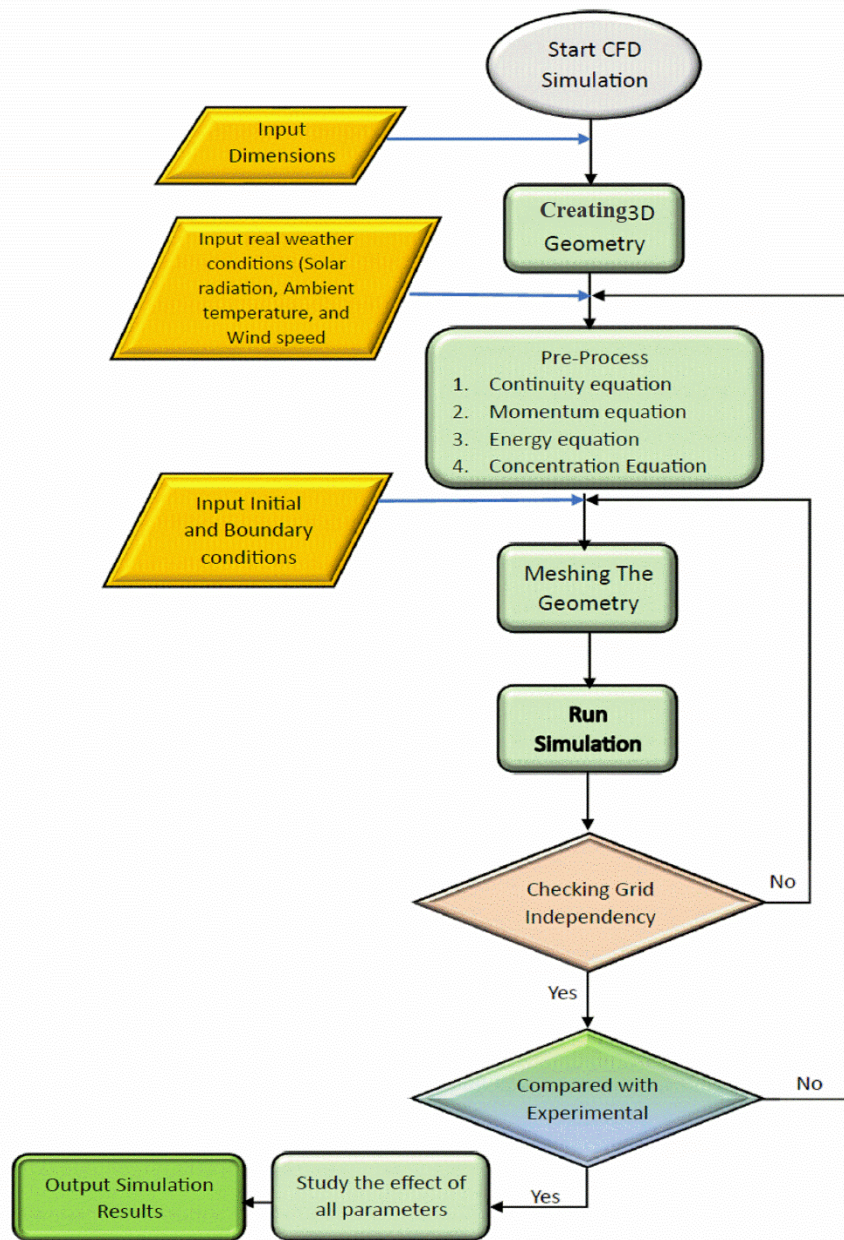


Figure (3.2): The flow chart to show the simulation process of present work.

3.5. Meshing and Grid Dependence Test

In COMSOL Multiphysics software V6.1 used a triangular network comprising 5506 elements was utilized, featuring a minimum element quality of 0.02388 and an average element quality of 0.8002, as illustrated in Figure (3.3) (b). To assess network independence, simulations were performed across various element counts to identify the optimal configuration yielding maximal results with minimal elements and expedited simulation time. Figure (3.3) (a) depicts the relationship between element count and cumulative productivity, indicating that exceeding 10061 elements yields no additional benefits. Consequently, a reduced element count was selected that maintained consistent results with higher counts. The finalized element count of 5506 was determined to optimize both result accuracy and program execution speed.

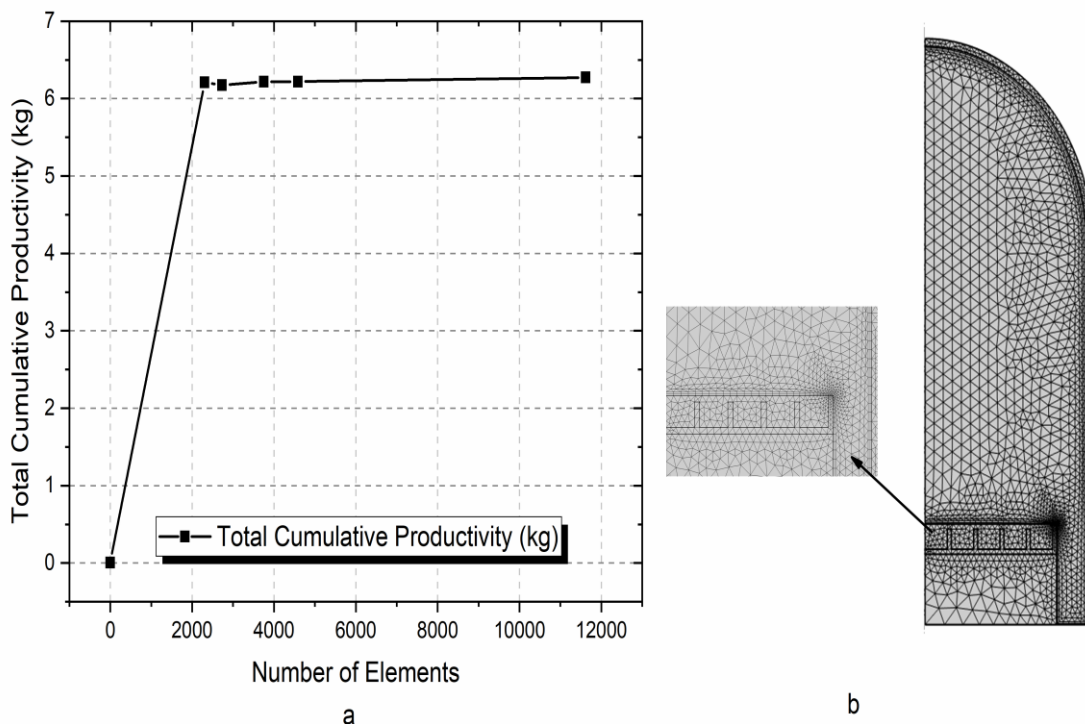


Figure (3.3) :(a) Grid created at the CSSHD with different numbers of elements
(b) mesh generation.

3.6 Validation of the current model

In order to verify the accuracy of the "numerical simulation" results, a comparison was made between the practical inquiry carried out by Elsayw et al [34] and the numerical findings of the current study regarding productivity and water temperature. The climatic circumstances outlined in the experimental investigation conducted by [34], and the design parameters presented in Table (3.4) were utilized to evaluate and contrast the performance of the CHSSD with fins in this validation configuration. The concept of study is depicted or exemplified in Figures (3.4), (3.5). The root mean squared percent deviation was employed to establish comparability between the results generated from the numerical model utilized in this investigation and the results obtained by [34]. This was achieved by utilizing equation (3-9).

$$\text{RMSD}(\%) = 100 \times \sqrt{\frac{\sum_1^n \left(\frac{X_{sim,i} - X_{exp,i}}{X_{sim,i}} \right)^2}{n}} \quad (3-9)$$

Where: $X_{sim,i}$, $X_{exp,i}$, i and n are the simulated value, the experimental value and the data number, respectively. A percentage error of 10.83% and 11% shows that the results are close and in good agreement.

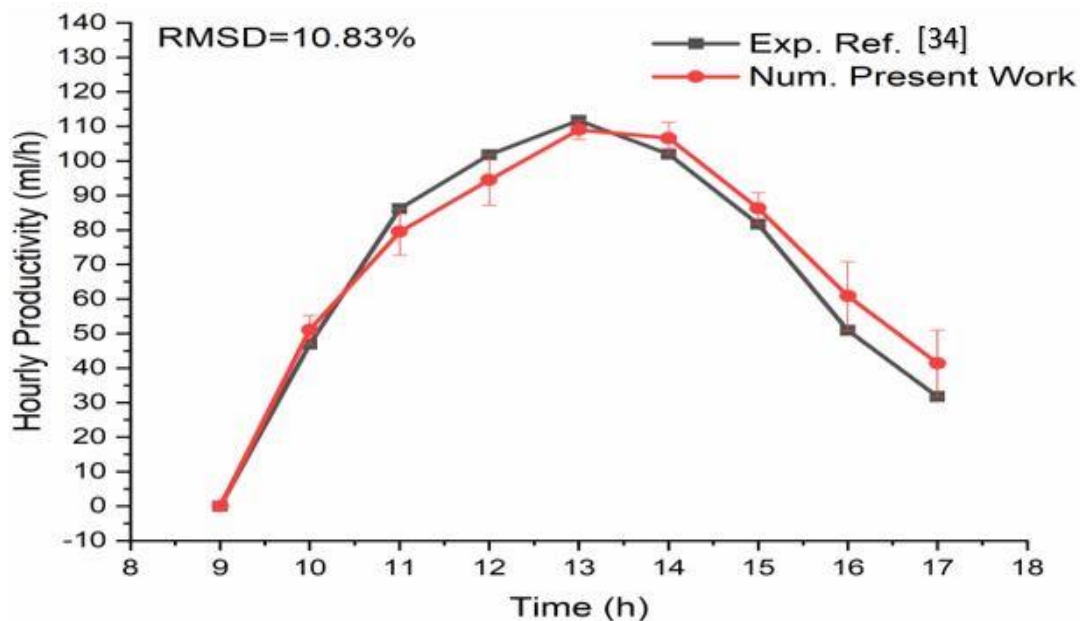


Figure (3.4): Comparison of hourly productivity with experimental work of [34]

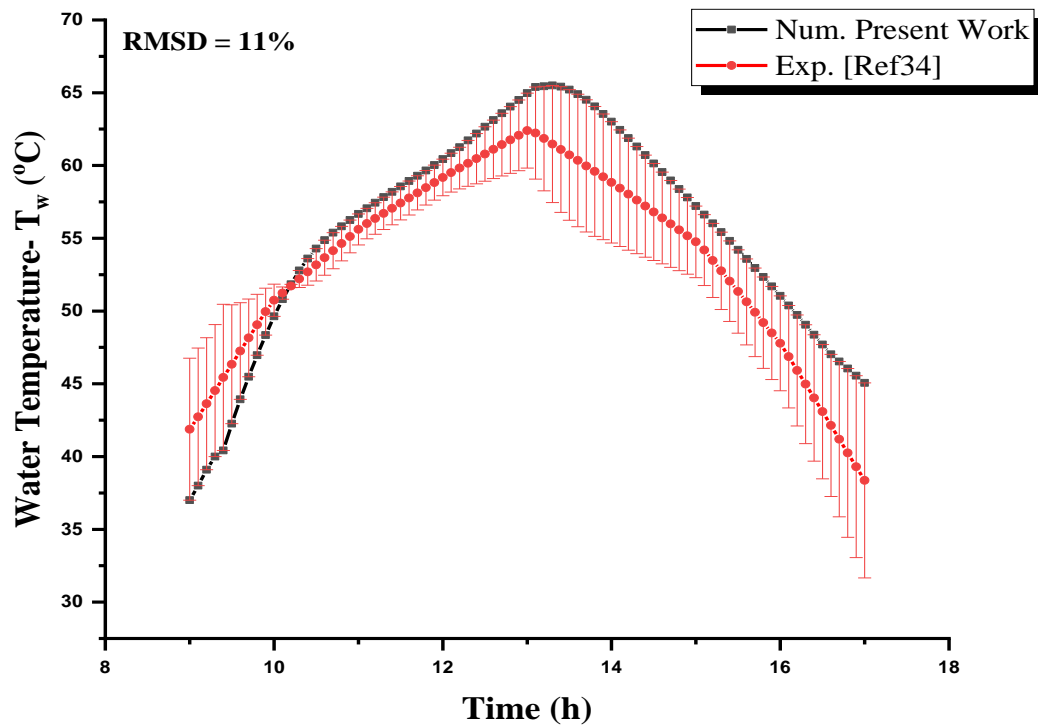


Figure (3.5): Comparison of hourly water temperature with experimental work of [34]

Table (3.4): The parameters of design used for validation setup of hemispherical solar still [34]

Validation Design Parameters	Value (m)
Circular basin made of stainless-steel thickness	0.0015
Diameter	0.5
Dome-shaped cover of molten acrylic poured into Diameter steel mold	0.5

Comparison was also conducted with the study conducted by researcher Al-Amir Khadim [16], as their study employed the same type of distiller. The climatic circumstances outlined in the experimental investigation conducted by [16], the design parameters are presented in Table (3.5) The comparison between the two studies can be observed in Figure (3.6) which showcases the “cumulative productivity” of the practical results achieved by the aforementioned researcher [16] in comparison to the simulation results of the current study. It is important to note that this particular comparison is particularly significant, as it allows for a comprehensive evaluation of the findings obtained from both studies. The obtained results indicate that the root mean square percent deviation (RMSD) amounted to 4.62%, which suggests a relatively minor deviation between the practical and simulated results.

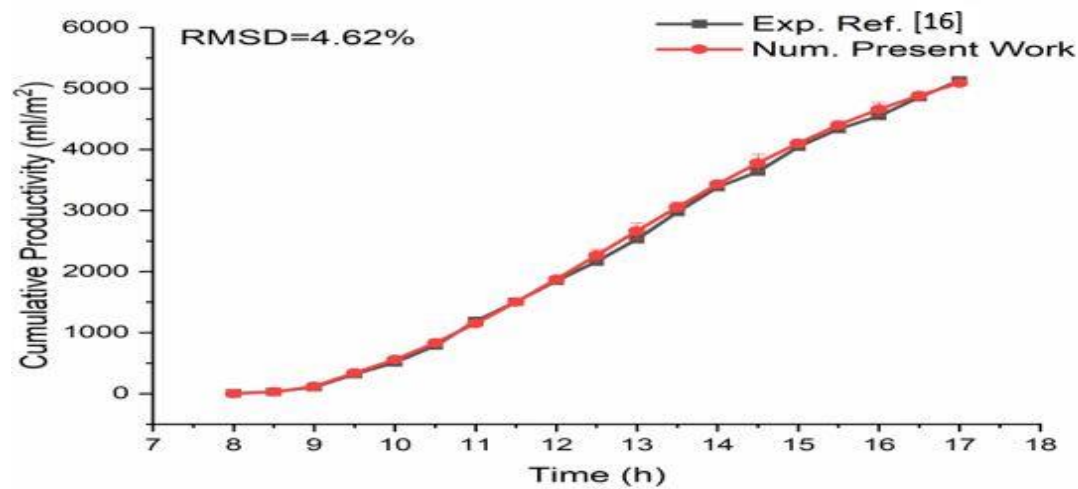


Figure (3.6): Comparison of cumulative productivity with experimental work of [16]

Table (3.5): The parameters of design used for validation setup of CHSSD [16]

Validation Design Parameters	Value (m)
Glass cylinder length	0.3
External diameter	0.15
Internal diameter	0.142
Thickness of glass	0.004
The basin is made of brass with a diameter	0.13
Height	0.02
Depth	0.08

Chapter Four

Experimental Work

4.1 Introduction

This chapter includes the experimental study of the present work, explains construction two cylindrical solar distiller with hemispherical dome with and without fins. Also, measurement devices used to test the performance of solar stills Finally, proceeding of testing the solar stills.

4.2 Construction of (CSSHD)

Cylindrical solar distiller with hemispherical dome using fins (CSSHD) is constructed using various materials to serve specific purposes. The selection of materials for a solar still is typically determined by an understanding of the existing circumstances in various areas of the still, as well as an evaluation of the material's cost. The subsequent passage provides an account of the primary components of solar stills. The experimental rig for testing the two models of still (with and without fins) is shown in Figure (4.1). as well as Figure (4.2) show schematic of experimental rig with devices used in measurement of weather conditions and productivity.

4.2.1. Basin

Both solar still types, with and without fins, have a brass material basin of identical size. The solar basin has a diameter of 0.13 m. The solar still basin has a thickness of 0.02 m and a water-filled depth of 0.008 m. fin solar still type is fitted with five fins, each measuring 0.008 m in height. The thickness is 0.002m. The basin-shaped circular black color to absorb sunlight, as depicted in Figure (4.3), The thermal properties of the material of basin are listed in Table (4.1).

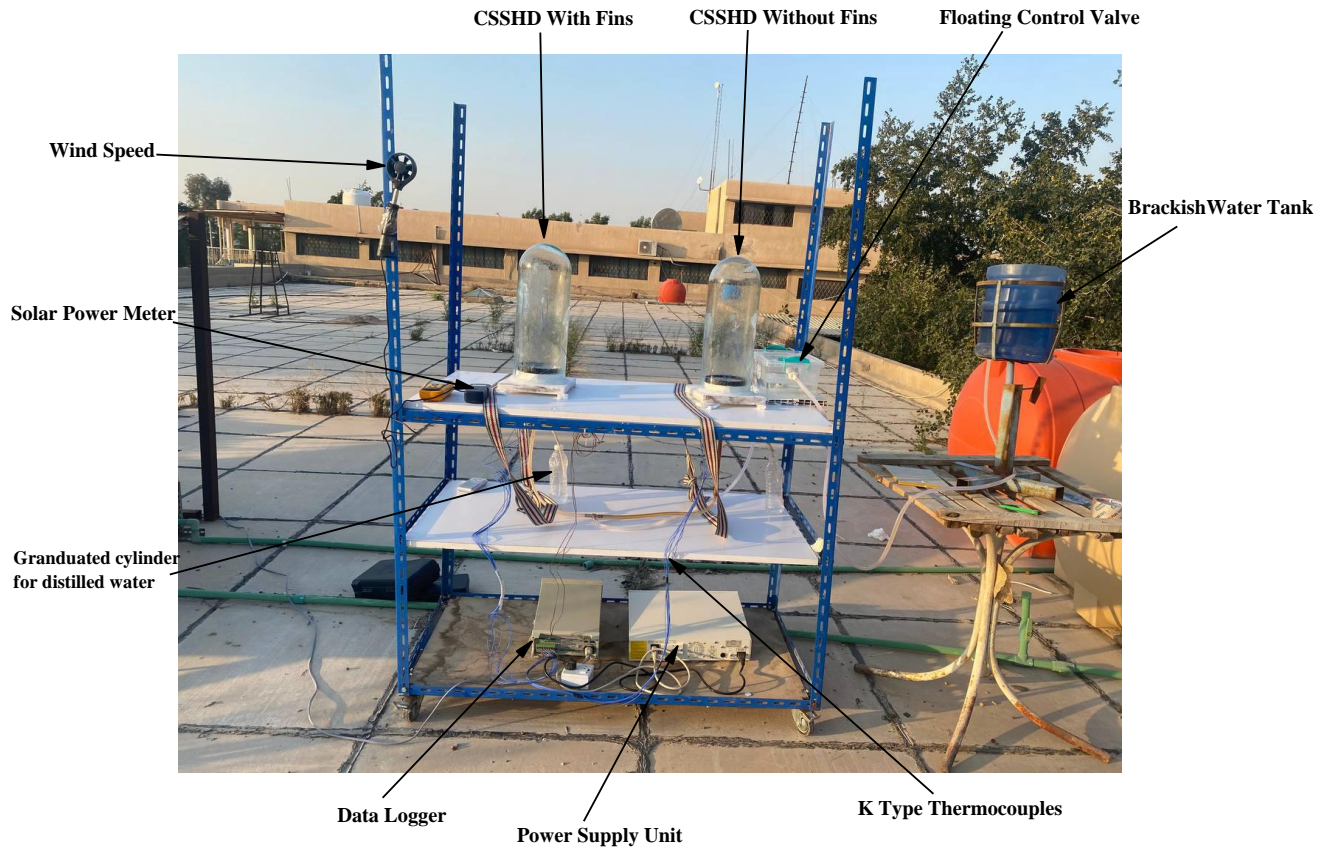


Figure (4.1): Experimental rig

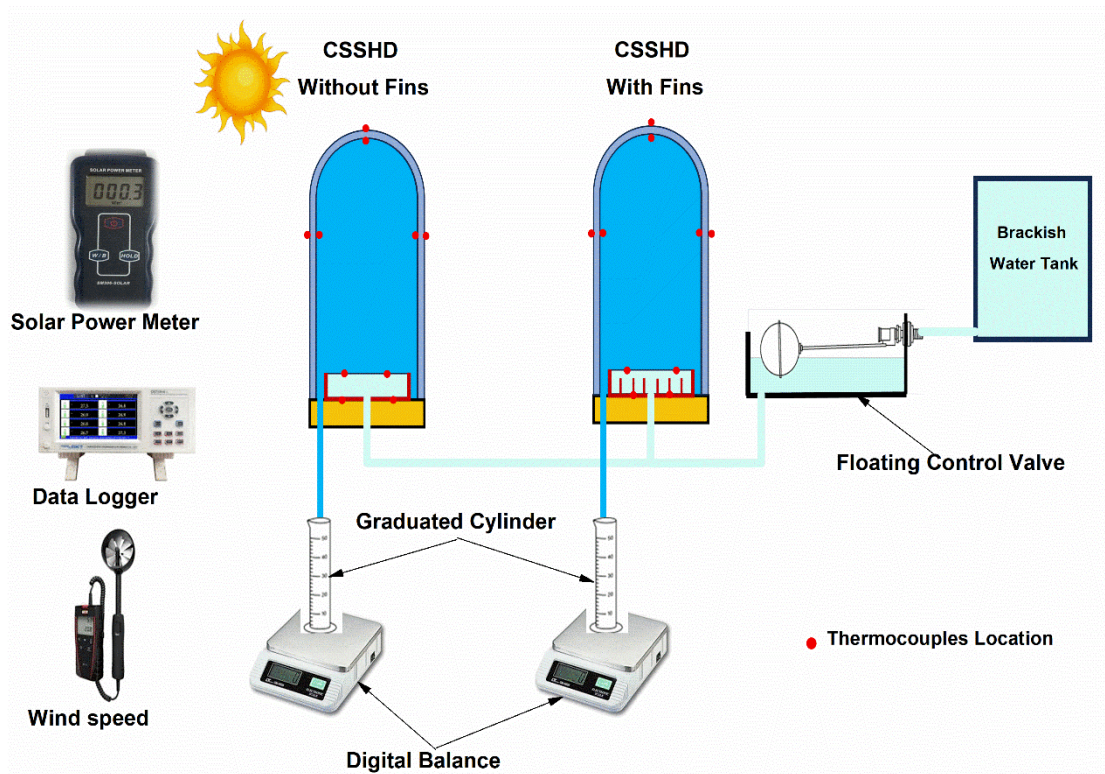


Figure (4.2): Schematic of Experimental rig

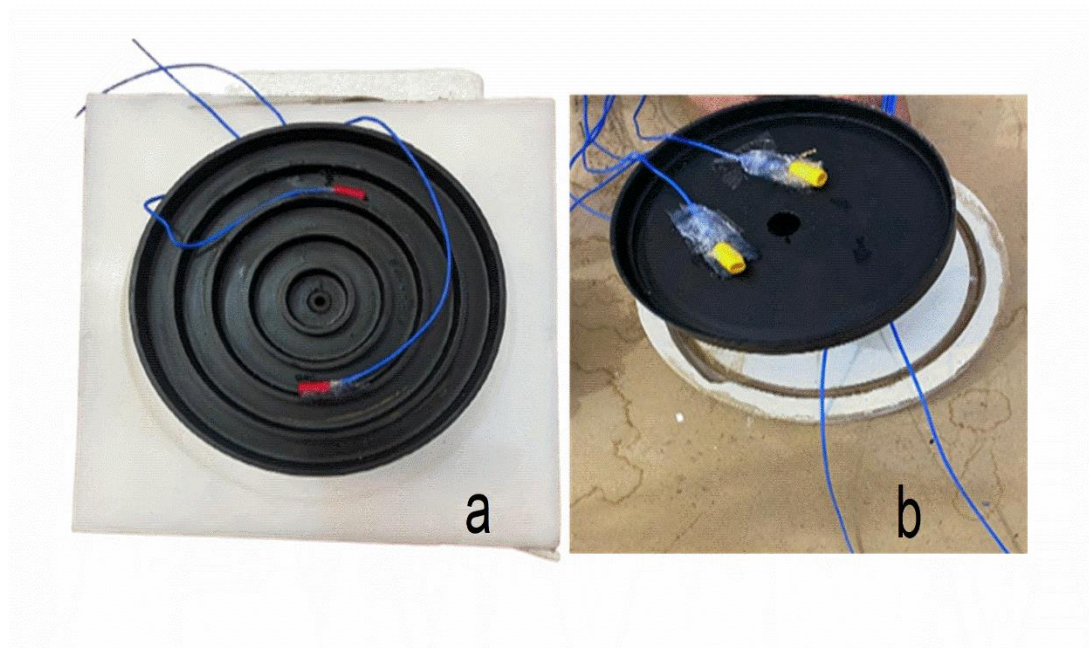


Figure (4.3): Photographic view of the basin hemispherical distillers (a) with fins (b) without fins.

Table (4.1): Thermal properties of basin

Properties	Value	Units
Density (ρ)	8960	kg/m ³
Specific heat capacity (C_p)	385	J/kg. k
Thermal conductivity(k)	400	W/m. k
Emissivity (ϵ)	0.85	-

4.2.2. Glass Cover

The solar still cover should exhibit low absorption and reflection of solar radiation across the whole solar spectrum. Furthermore, it serves as an obstacle to impede the transfer of heat from the salt through water to the atmosphere by means of thermal radiation. The protective material must exhibit excellent heat resistance and be capable of enduring the impact of solar radiation, wind erosion, and severe weather conditions. Ordinary glass is commonly used to enclose solar stills since it has the necessary qualities to fulfill the given criteria. The cylindrical glass has a length of 0.35 m. The out diameter of the object measures 0.15m, while the inside

diameter is 0.142m. The glass thickness is 0.003m. Figure (4.4) shows the glass cover used in experimental work. The thermal properties of glass cover are shown in Table (4.2).



Figure (4.4): Photographic view of solar still glass cover

Table (4.2): Thermal properties of glass cover

Properties	Value	Units
Density (ρ)	2210	kg/m ³
Specific heat capacity (C_p)	730	J/kg. k
Thermal conductivity(k)	1.4	W/m. k
Emissivity (ϵ)	0.85	-
Thickness (t)	4	mm

4.2.3. Solid Teflon Base

This base makes from Teflon material ,as shown in Figure (4.5). the function of this base is to installing the basin and glass cover, as well as cumulative the water production from still.

4.2.4. Sealant and Piping ports

Sealant: To prevent the escape of steam and the leakage of water from the connection between the cover and the solid Teflon, it is crucial to use an appropriate sealant for the solar cover. Typically, glass covers are used to protect rubber molds, metal cover plates, asphalt caulking compounds, and silicone rubber. Among these materials, silicone rubber is the most effective sealer. It has the ability to adhere to glass and various other materials rapidly. It possesses adaptability and may be swiftly executed. The experimental model utilized silicone rubber as the sealant to effectively seal the necessary joints, as shown in Figure (4.5).



Figure (4.5): Photograph displaying the sealant used in a solar still.

Piping ports: The solar stills' base is equipped with two types of pipe, one for cumulative distilled water production and the to supply brackish water, as shown in Figure (4.6).

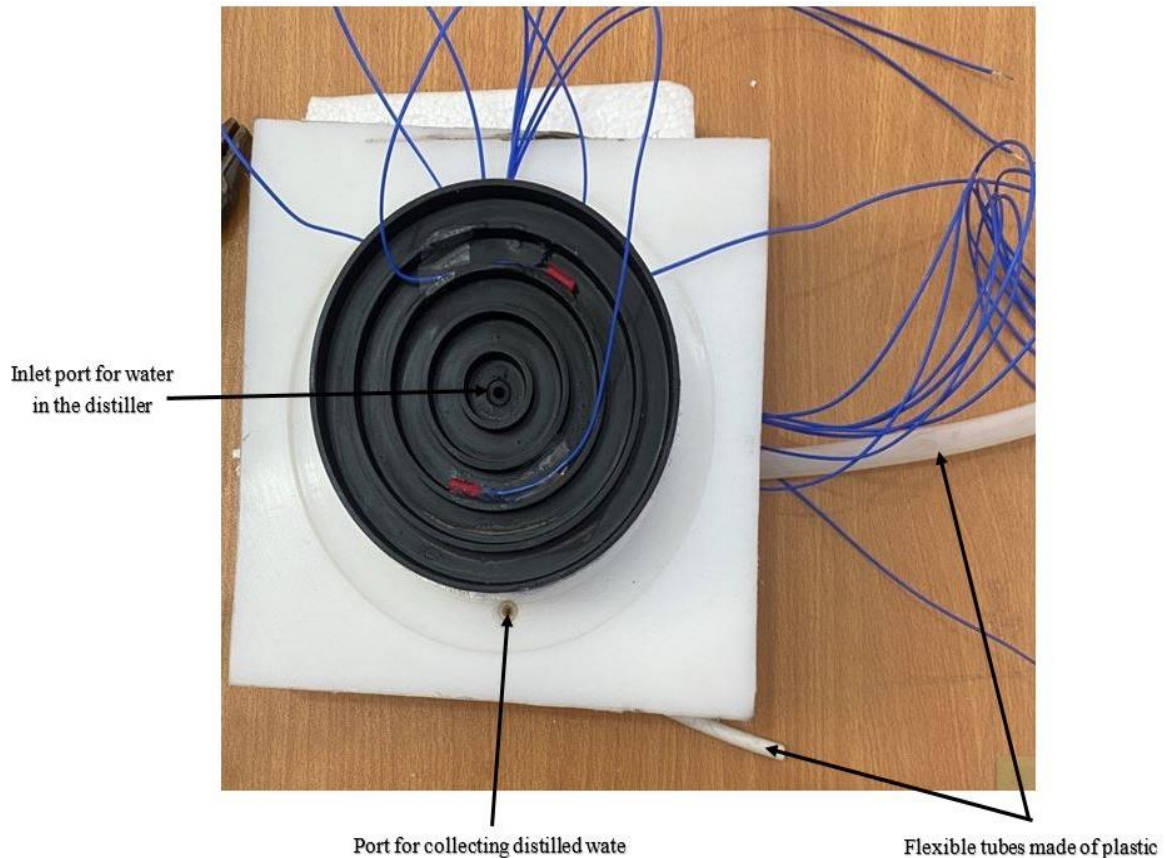


Figure (4.6): Photograph depicting CSSHD pipe ports

4.3. Measurements Devices

The study was carried out in Iraq, specifically in Najaf (latitude 31.59 N, longitude 44.19 E), for the duration of March 2024. The experiments were conducted utilizing substantial equipment. Each of these devices will be described in the following way. Once the solar distillation basin releases clean water, it flows down from the distillation channel and is collected in a plastic container. The weight of the empty bottle is measured prior to and subsequent to filling it with distilled water at 10-minute intervals.

4.3.1. Data Logging Equipment

The temperature is measured in order to study the impact of the design change on the operating temperature. We strategically positioned the thermocouples in various areas, such as the interior and outside cover, saltwater, trough temperatures, and ambient temperatures. Figure (4.7) illustrates a data logger, which is a device capable of detecting temperatures and including many channels. The CKT4000 is a specific model of data logger that was selected, boasting a total of 32 channels. This instrument is compatible with both Type K and Type T thermocouples. The read accuracy of the instrument is 0.2% per 1C°. All of the thermocouples have been calibrated in the laboratory is illustrated in Appendix A.

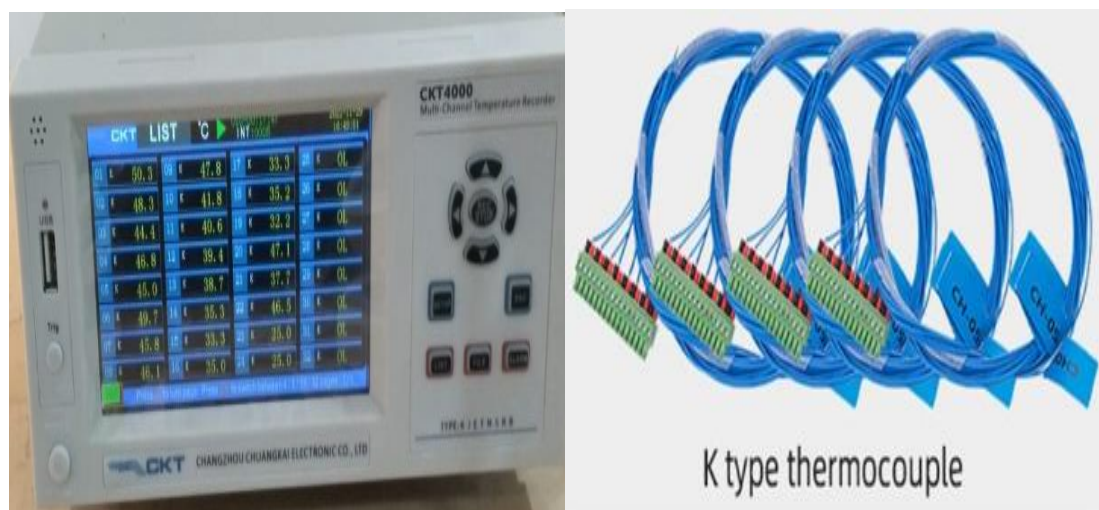


Figure (4.7): Data logger and k-type thermocouple

4.3.2 Solar Power Meter

Solar radiation is essential in determining the formation of distilled water. This energy meter is utilized to quantify the intensity of solar radiation that is received by the solar still. The TENMARS SM-206 solar power meter is fitted with a calibration button that enables the operator to set the instrument's reading to 0 W/m² when measuring the device in the absence of light. The range spans from 0 to 1370 W/m² Measurements of solar radiation are taken every 10 minutes from sunrise to sunset. The

device used to obtain these readings is shown in Figure (4.8). The Solar Power Meter have been calibrated is illustrated in Appendix B.



Figure (4.8) Solar Power Meter

4.3.3 Wind speed measurement

Wind speed is a significant aspect that affects the output of the solar distillery. Where the wind speed is empirically assessed to demonstrate its impact on production. The airflow, particularly when it comes into contact with the glass surface of the solar still, significantly enhances the condensation process. Consequently, the anemometer model GM8902 is used to measure the speed of the wind. The velocity of the device ranges from 0.0 to 45.0 m/s, and it is powered by a 9V power supply. The precision

of the device is within $\pm 3\% +0.1$ m/s, as depicted in Figure (4.9). The Wind speed measurement have been calibrated i is illustrated in Appendix C.



Figure (4.9): Wind speed measurement

4.3.4 Digital Scale

The digital scale is polygonal in shape and has dimensions of 120*62*20 mm. The device is equipped with a digital screen that displays the weight includes a protective covering. The device is operated by a pair of batteries. The weight range extends from 0.5 g to 2 kg as depicted in Figure (4.10). The measurement of purified water output occurs at ten-minute intervals throughout the day, from sunrise to sunset. The typical duration of measurement is around 9-10 hours per day. The Digital Scale have been calibrated is illustrated in Appendix D.



Figure (4.10): Digital Scale.

4.4. Experimental Procedure

Process for the experimental work: see the flow chart Figure (4.11).

1. After the all components of the experimental rig connected to the two model (with and without fins), then start testing the solar still as following:
 - a) The temperature is measured at eighteen different points on two solar stills using a thermocouple probe. The cylindrical solar still with a hemispherical dome is outfitted with fins and connected to eight thermocouples. The temperature is measured at two internal places within the still, one external point adjacent to the still, and two locations on the surface of the still. The water's surface as shown in Figure (4.2). There are two areas where the temperature of the water inside the basin can be tested. These locations are in different positions within the basin. The temperature of the inner surface of the cylindrical cover determines two distinct places. The outside temperatures of the cylinder cover were recorded at two distinct locations. Thermocouples are frequently employed for the determination of ambient temperature.
 - b) Quantify by attaching eight thermocouples to the cylindrical solar still with a hemispherical dome without fins. Measure the temperature at

two points within the still, two points outside the still, two points on the water's surface within the still, and two points within the small basin to gauge the temperature of the water within the basin, as shown in Figure (4.2).

- c) Solar radiation intensity sensor: utilizing a solar radiation measurement equipment. To obtain an hourly estimate of the direct sun radiation, measurements of the direct solar radiation should be taken every 10 minutes.
 - d) Wind speed measuring gadget: Utilizing the wind speed measuring apparatus employed at the Renewable Energy Research Laboratory in the Engineering Technical College in Najaf Al-Ashraf. In order to estimate the direct sun radiation reading on an hourly basis, measurements are performed every 10 minutes.
 - e) The fresh water jug range refers to a plastic bottle that is utilized to gather water from the hose's output. The collection process occurs every 10 minutes.
2. Periodic measurements would be conducted on all measuring equipment from 8:00 A.M to 17:00 P.M. to collect data.
 3. The thermometer logger autonomously records data. Productivity, sun radiation, and wind speed are manually measured at ten-minute intervals.
 4. The trials are carried out on the rooftop of the Engineering Technical College building in Najaf. For all of these tests. The studies were done in March 2024 to study and compare the productivity of two distillers in terms of tractor degree, solar radiation, wind speed, and daily productivity.

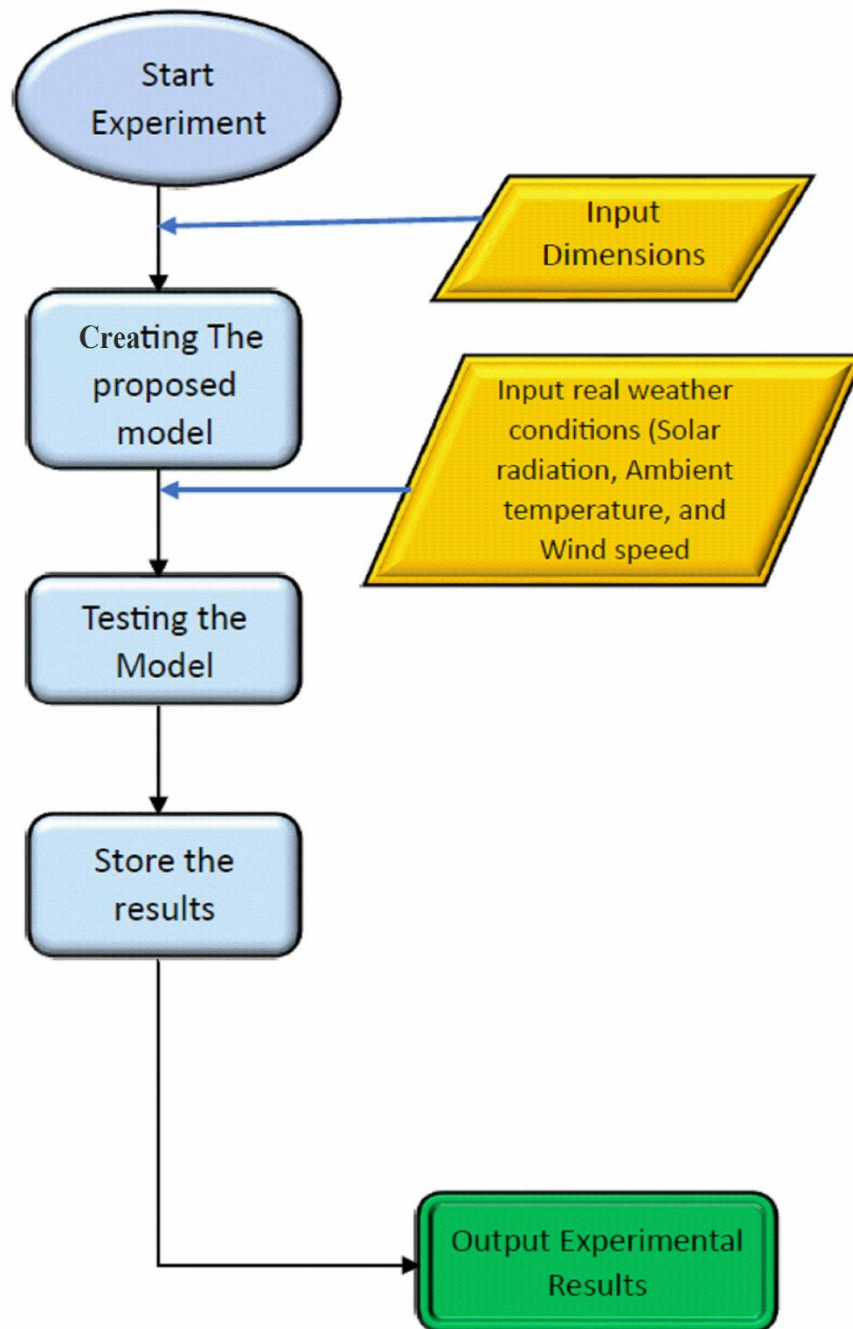


Figure (4.11): The flow chart Process for the experimental work

Chapter Five

Results and Discussion

5.1. Introduction

This chapter provides an analysis of the findings and debates derived from both experimental work and numerical simulations, along with a comparison of the two models. The primary input parameters for the numerical simulation utilizing COMSOL V.6.1 comprise atmospheric conditions, including ambient temperature, wind speed, incident radiation, and key characteristics specific to the climate of Najaf city in central Iraq (latitude 31.59 N, longitude 44.19 E).

5.3. Numerical Results

The COMSOL V.6.1 application was utilized to authenticate its validity. The program compares the input parameter with the experimental and simulation findings. Additionally, it calculates the percentage divergence between the simulation and experimental results. In order to compare and analyze the difference between the simulated and experimental findings, a time period of more than one month was selected due to the significant amount of readings. These data are adequate for analyzing and elucidating the disparities between them. This section also examines the impact of the many seasons of the year, including summer, winter, spring, and autumn, on the efficiency and output of the solar still.

5.3.1. Study the effect of weather conditions

In this section, the effect of seasonal variations on the adopted model in the experimental study will be examined and evaluated through numerical simulation using COMSOL V.6.1 software. Data on solar radiation, ambient temperature, and wind speed were obtained from the meteorological station at Najaf Technical College of Engineering for four

specific months. Specifically, Figure (5.1 to 5.4) display the weather data for 15 January 2024, 15 March 2024, 15 July 2024, and 15 October 2024, respectively. These data were utilized in the numerical simulations to analyze the influence of weather conditions on the performance of the proposed model.

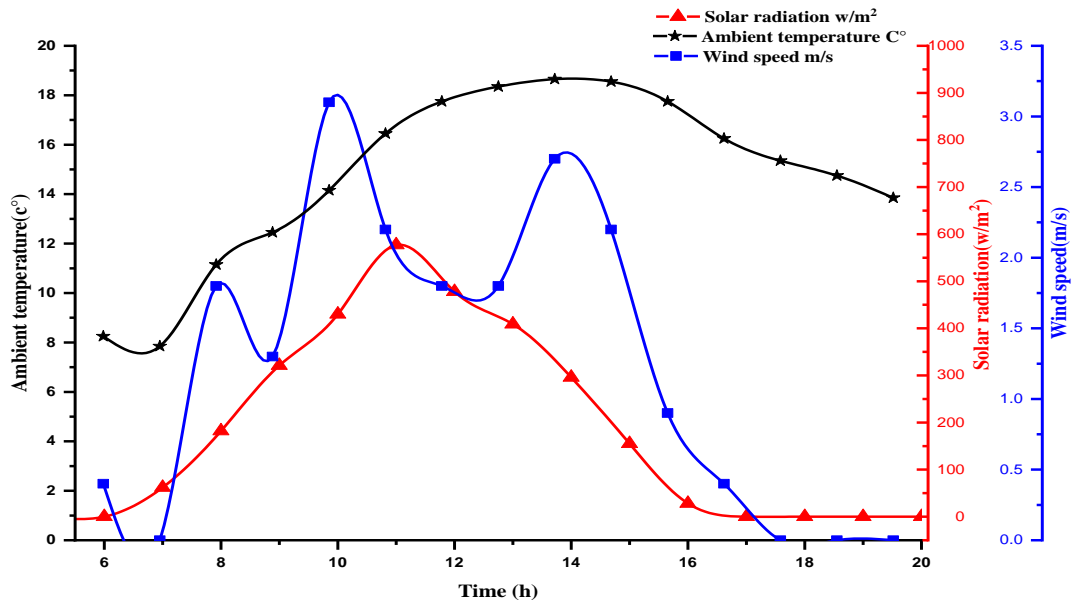


Figure (5.1): Weather Conditions of 15-January 2024

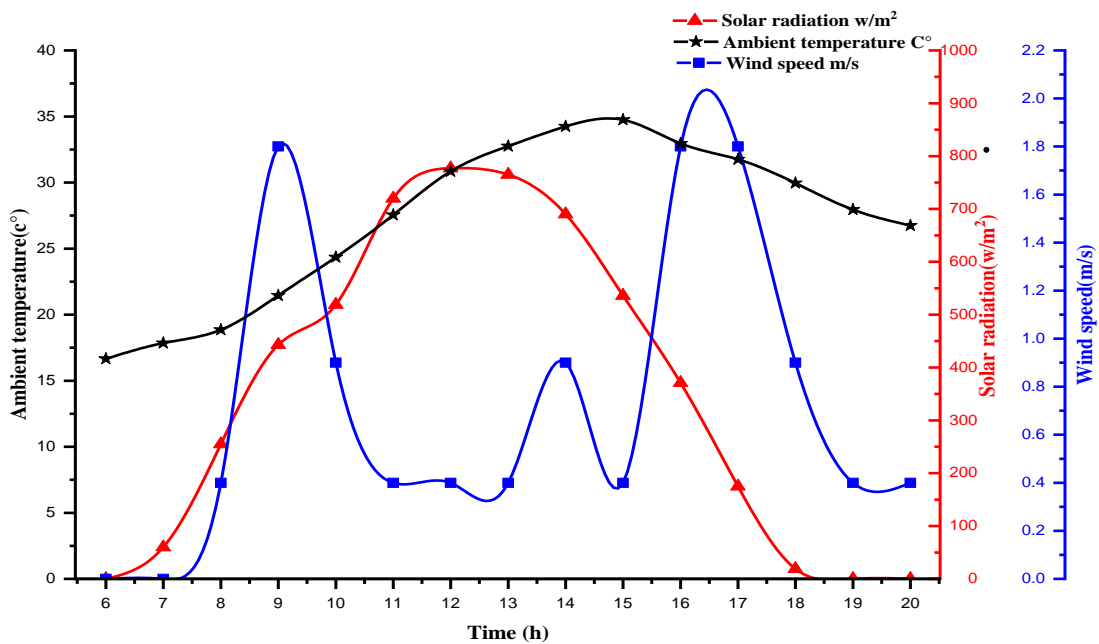


Figure (5.2): Weather Conditions of 15-March 2024

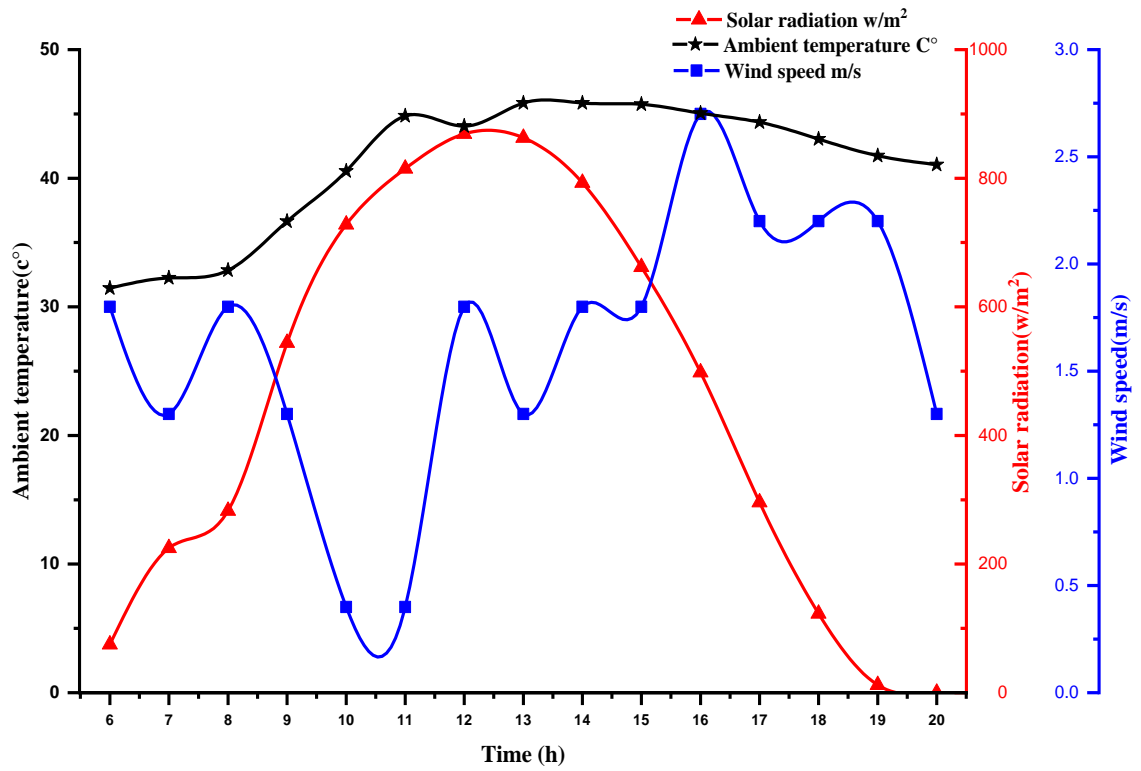


Figure (5.3): Weather Conditions of 15-July 2024

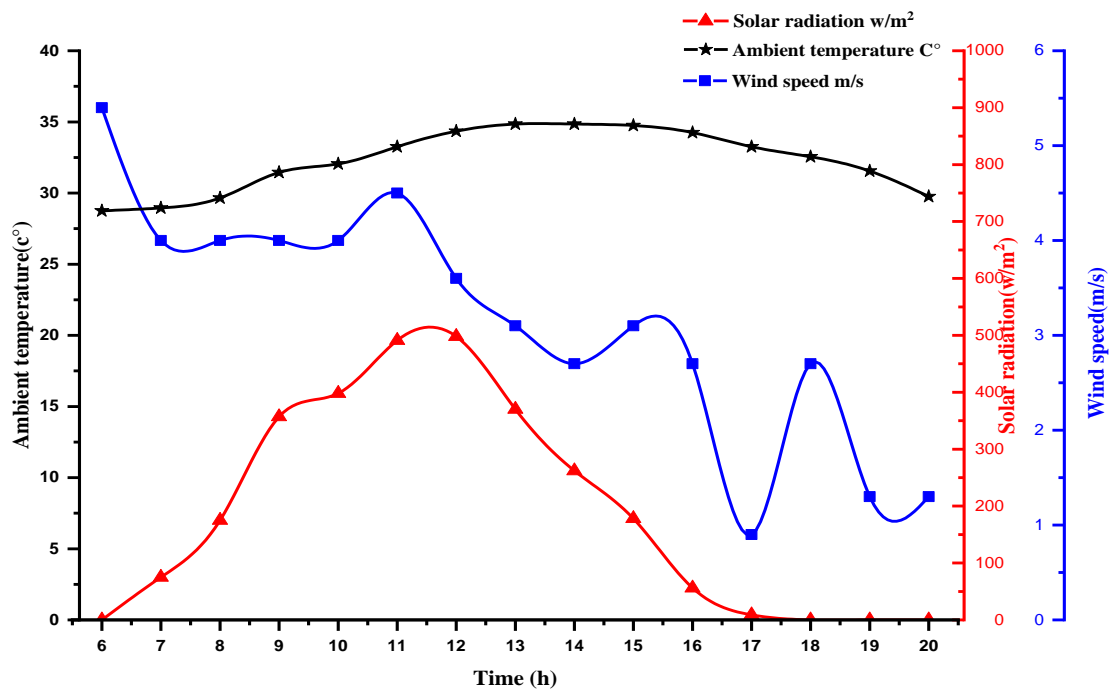


Figure (5.4): Weather Conditions of 15-October 2024

5.3.2. Study the Effect of Fins Number

To study the effect of changing the number of fins in the solar still basin, Figure (5.5 to 5.9) are shown. Comparison water surface temperature T_w , basin temperature T_b , and cover temperature of inner glass T_{g-in} and outer glass T_{g-out} at a cylinder height of 350 mm and a fin length of 8 mm for two cases. Case (a) represents four fins, while case (b) represents five fins. The simulation was done at different seasons. The results revealed a significant correlation between the number of fins and the temperature of both the aquarium T_b and the water surface T_w . The water temperature reached a maximum of $61.04\text{ }^\circ\text{C}$ and It attained a value of $59.484\text{ }^\circ\text{C}$ with four fins. during the month of July, coinciding with the presence of 5 fins. Figure (5.7) shows the basin temperature for July, comparing configurations without fins and with four and five fins, yielding maximum temperatures of 57.375 , 60.192 , and $61.04\text{ }^\circ\text{C}$ respectively. In addition, the temperature of the internal and external glass covers is taken into account.

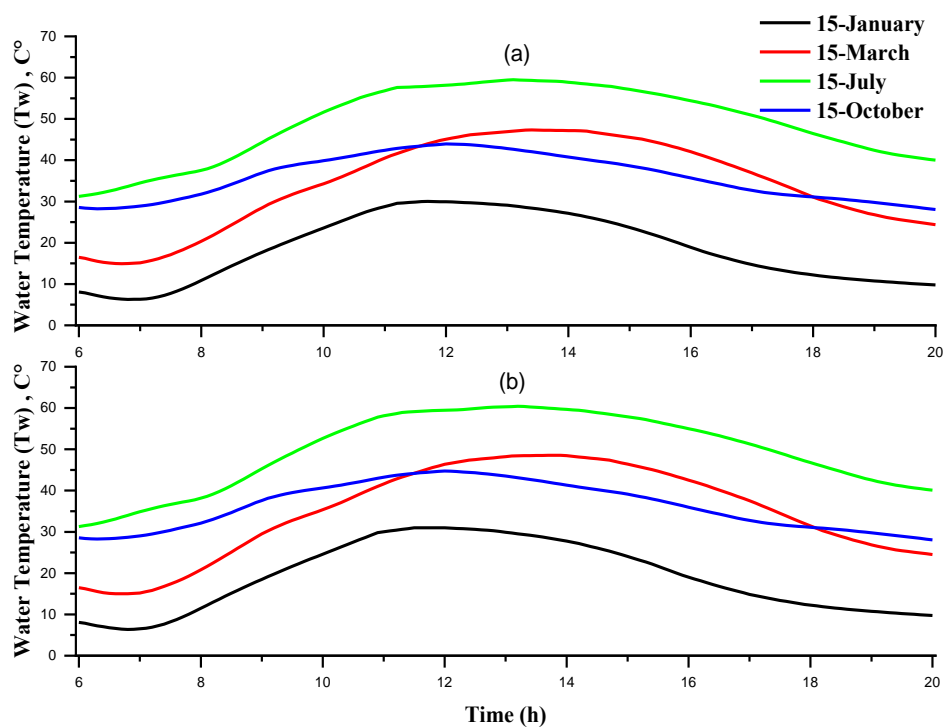


Figure (5.5): Variations of Water Temperature for CSSHD at $H_f = 8\text{ mm}$, $L_w = 350\text{ mm}$ (a) $N_f = 4$ (b) $N_f = 5$

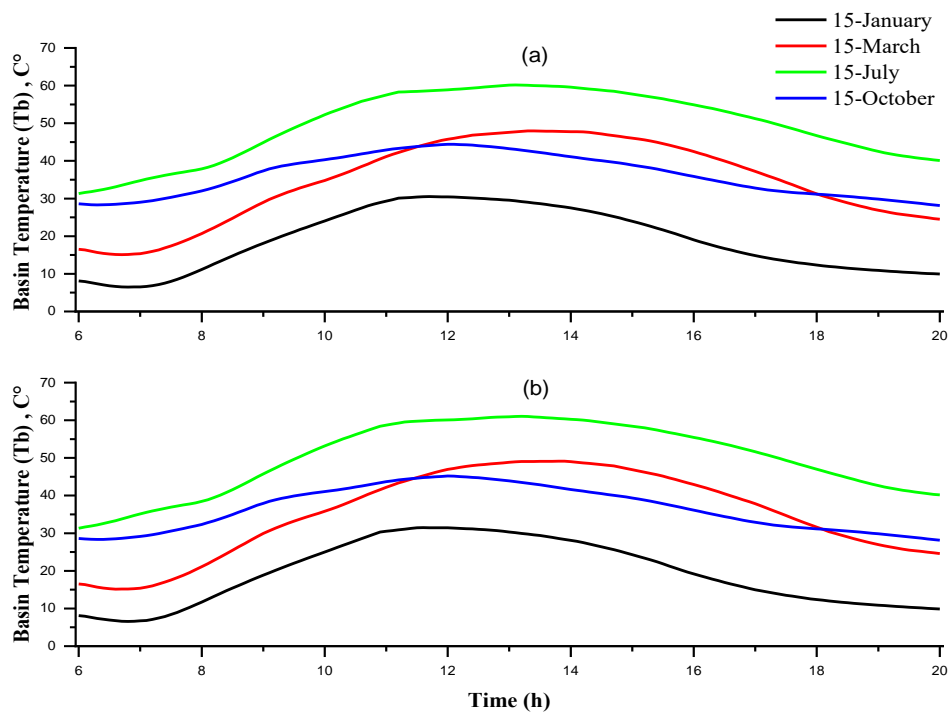


Figure (5.6): Variations of Basin Temperature for CSSHD at $H_f = 8$ mm, $L_w = 350$ mm (a) $N_f = 4$ (b) $N_f = 5$

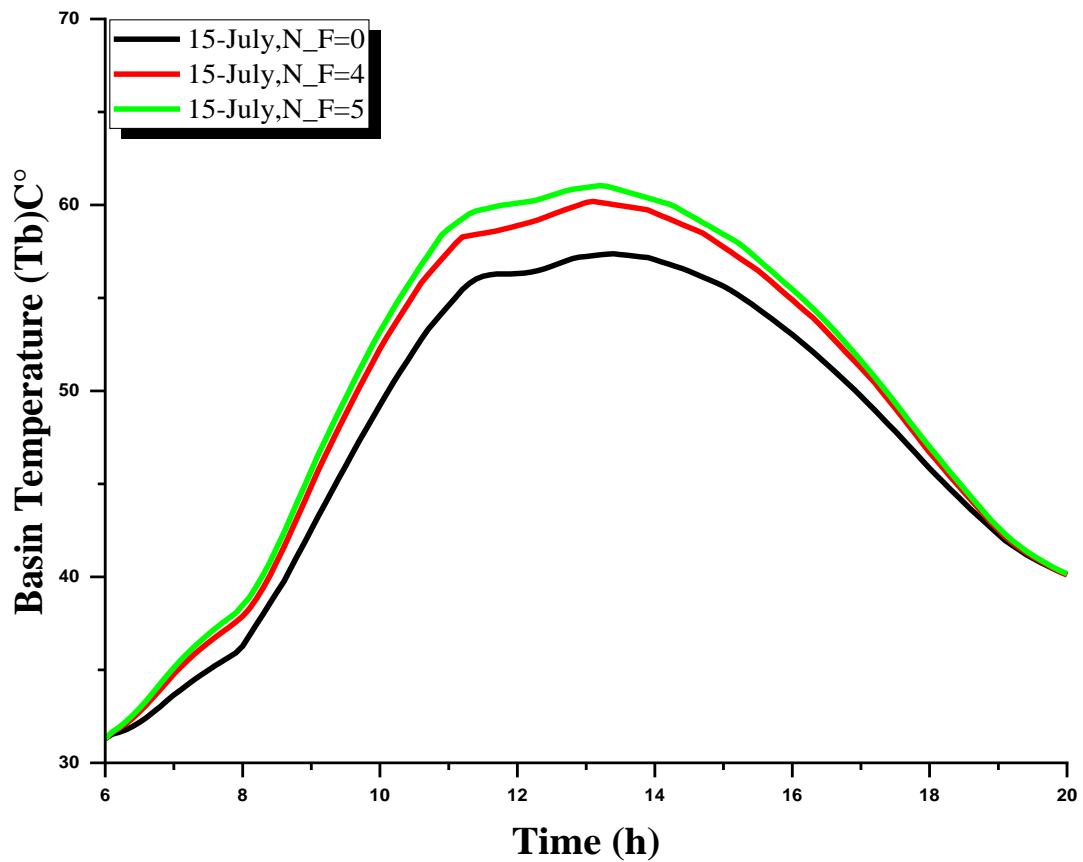


Figure (5.7): Variations of Basin Temperature for CSSHD $L_w = 350$ mm at $N_f = 0$, $N_f = 4$ and $N_f = 5$ for July

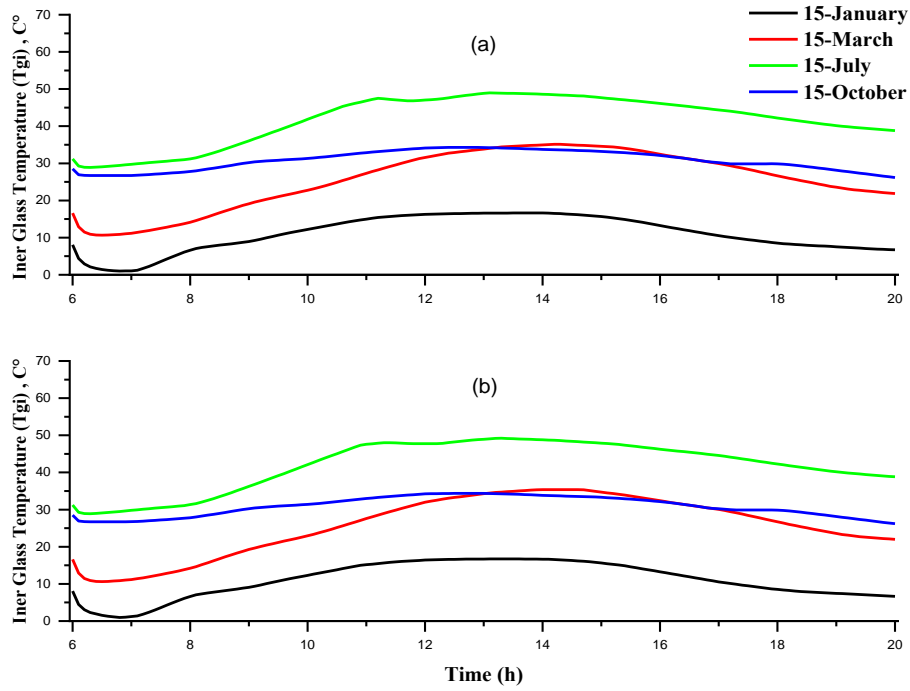


Figure (5.8): Variations of Inner Glass Temperature for CSSHD at H_f = 8 mm, L_w = 350 mm (a) N_f = 4 (b) N_f = 5

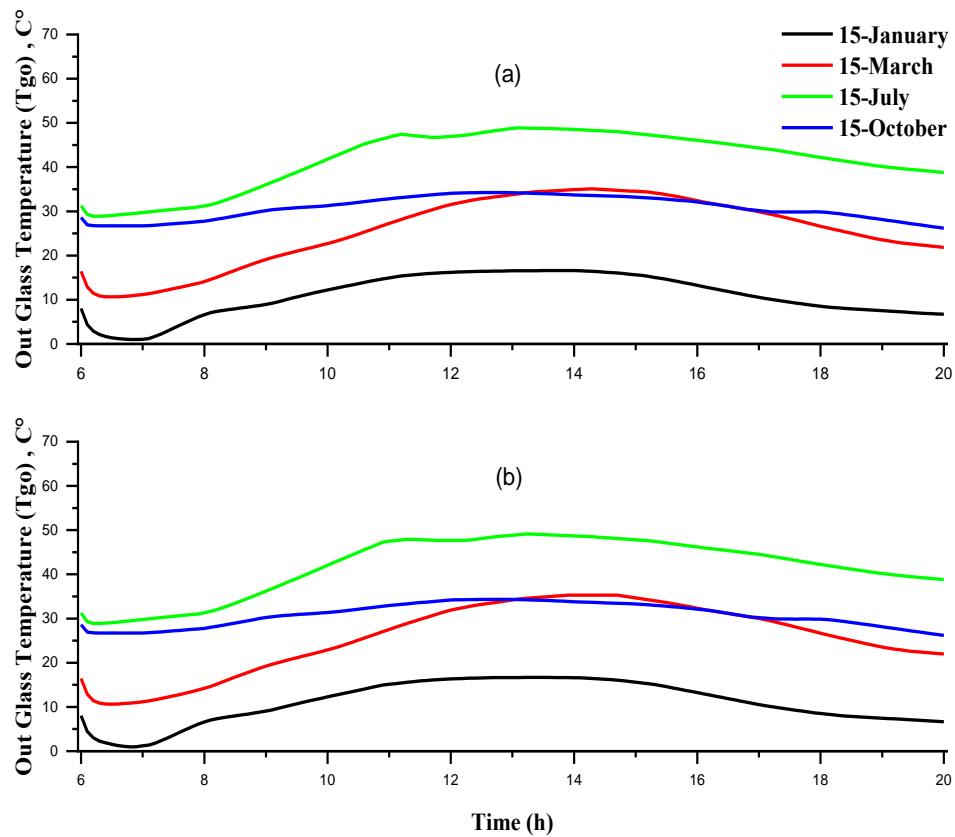


Figure (5.9): Variations of Out Glass Temperature for CSSHD at H_f = 8 mm, L_w = 350 mm (a) N_f = 4 (b) N_f = 5

An increase in the number of fins leads to a proportional increase in the total cumulative growth, as seen in Figure (5.10). The greatest yield in July reached 11.8534 kg/m², while the minimum output in January was 4.279 kg/m² with the use of 5 fins. With the addition of four fins, the production reached its peak level. In July, the output yield reached 9.565 kg/m², while in January, a lower yield of 3.420 kg/m² was achieved, suggesting a growth increase of 10.6% compared to the utilization of 4 fins.

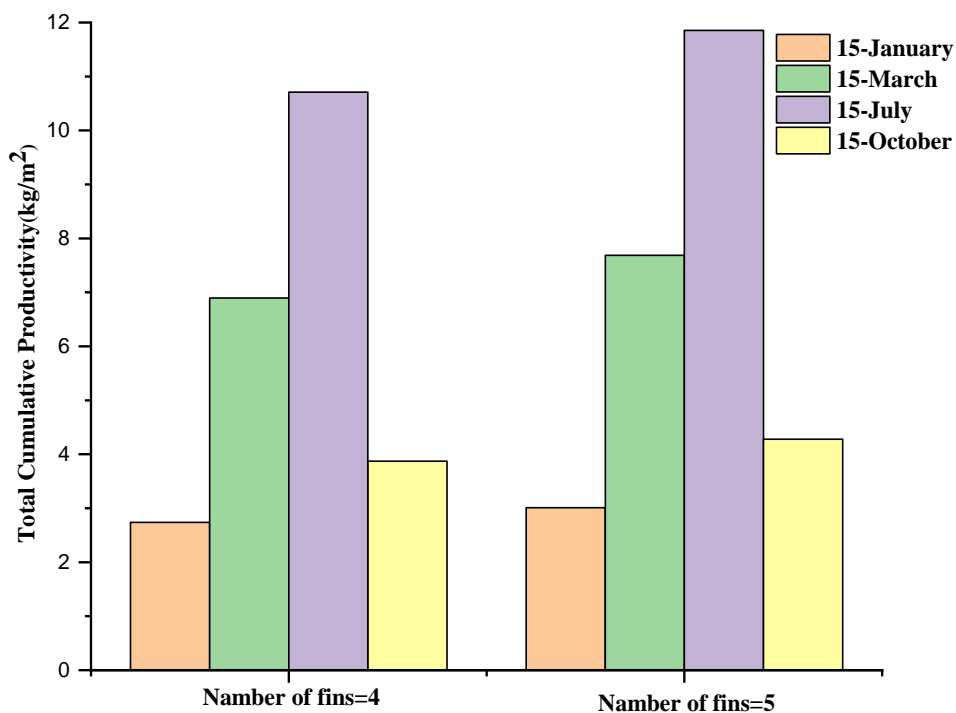


Figure (5.10): Total Cumulative Productivity for CSSHD at $H_f=8$ mm, $L_w=350$ mm

Figure (5.11) displays the thermal efficiency of the CSSHD enhanced with fins in two cases, one with 4 fins and the other with 5 fins. During the simulation spanning four months, we observed that increasing the number of fins led to a rise in efficiency. In the month of July, the efficiency reached its peak at 56.227%. In January, the rate reached its lowest point of 34.251%.

The heat accumulation in the still is directly correlated with the growth in the number of fins during a span of four months, as depicted in Figure

(5.12). The simulation was performed for four specific months: January, March, July, and October. For a 350 mm long cylinder with 4 and 5 fins, when the number of fins is increased to 5, the maximum heat gain is recorded. In March the heat volume is +1.1655W, although in July it reaches +1.071W. January and October have the minimum recorded quantities. When the reading approaches 0, it signifies a state of saturation caused by the rise in temperature at midday. After noon, when the temperature decreases, the distillery starts to emit the heat it accumulated over the day at a rate of -0.8316 W. In March, the highest temperature occurs in the afternoon as a result of a temperature differential, causing a fall in temperature. This is in contrast to July, where the high temperature persists both during the day and at night. There is no discernible disparity. At lower temperatures, the heat emission decreases to -0.60338 W.

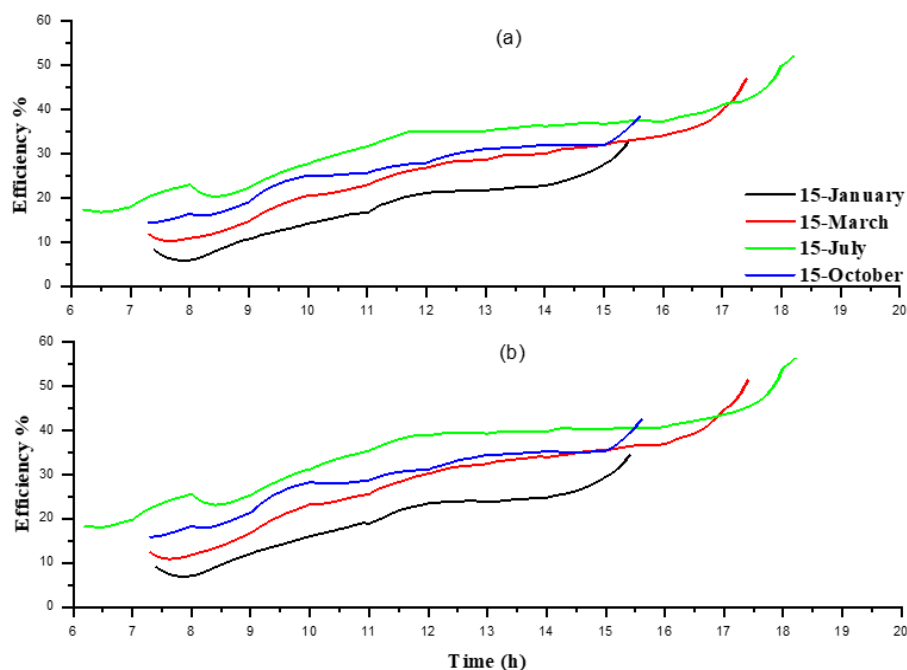


Figure (5.11): Variations of Efficiency for CSSHD at $H_f=8$ mm, $L_w=350$ mm (a) $N_f = 4$ (b) $N_f = 5$

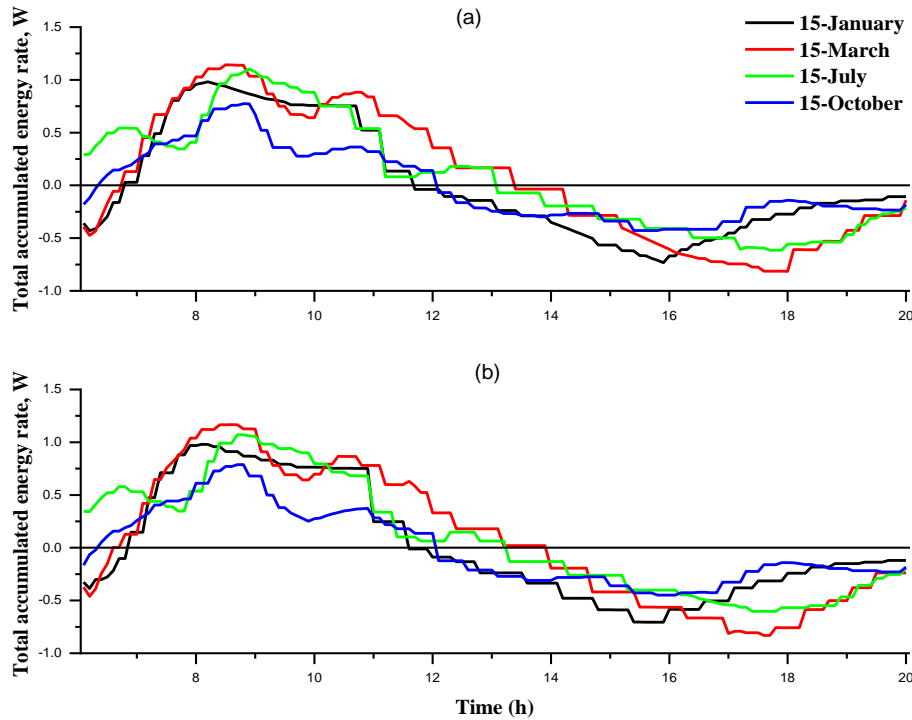


Figure (5.12): Variations of Total accumulated energy rate for CSSHD at $H_f = 8$ mm, $L_w = 350$ mm (a) $N_f = 4$ (b) $N_f = 5$

Figure (5.13) shows the average velocity of water vapor inside a solar module equipped with four or five fins. The simulation provides data for four specific months. Among these months, January recorded the highest average speed at 0.03099 m/s with five fins. Due to the cold weather in January, the temperature drops, resulting in minimal evaporation. The density of steam decreases and its velocity increases inside the still. Conversely, the velocity decreases in July due to higher temperatures, which leads to increased evaporation. As a result, the vapor density increases and its velocity decreases.

Figure (5.14) depicts the gradual increase in the size of fins on the distiller, as impacted by the monthly growth rate. During the month of July, determined that the most efficient production level was achieved when there were 5 fins, resulting in a production rate of 0.0408 kg/h. The intense sun radiation immediately causes the extensive condensation processes, which subsequently lead to a decrease in productivity in January. This

block exhibits an equal number of fins and has a productivity of 0.003672 kg/h.

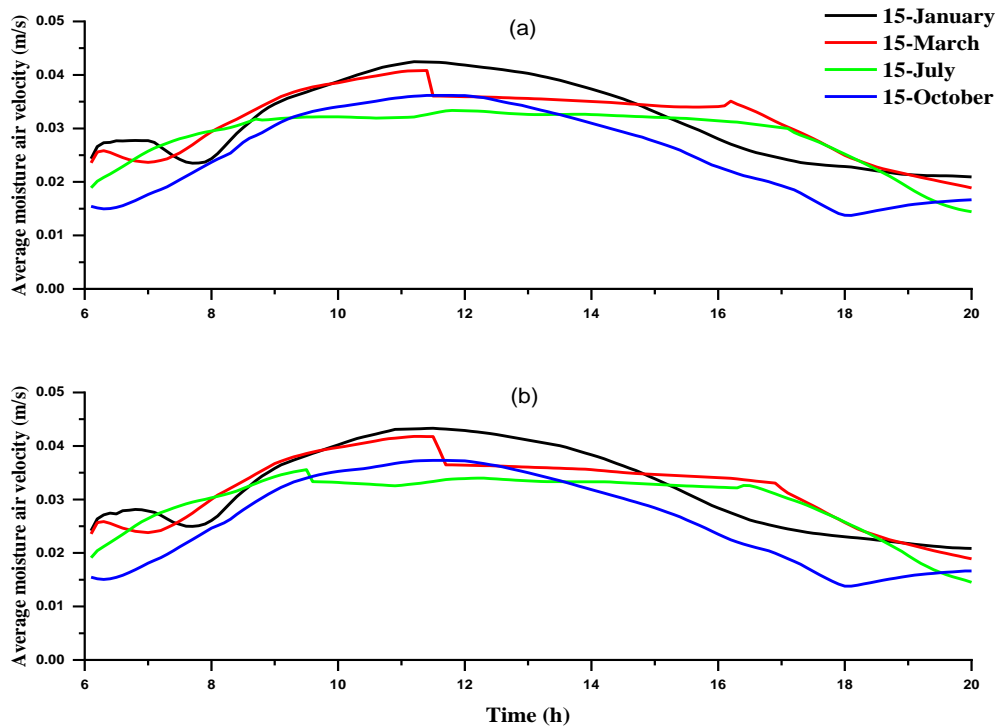


Figure (5.13): Variations of Average moisture air velocity for CSSHD at $H_f = 8$ mm, $L_w = 350$ mm (a) $N_f = 4$ (b) $N_f = 5$

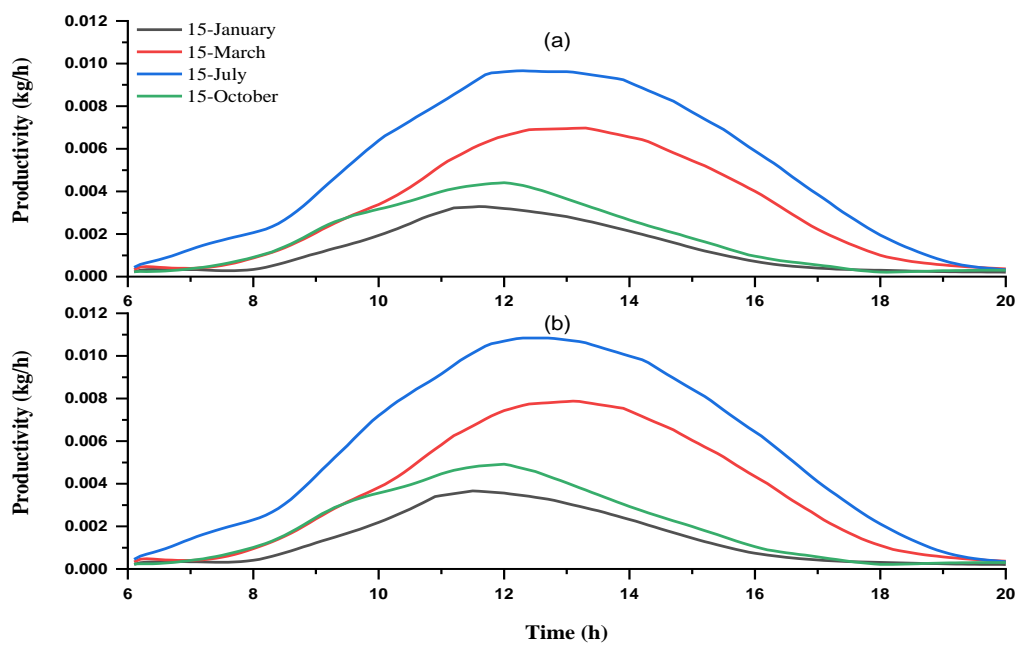
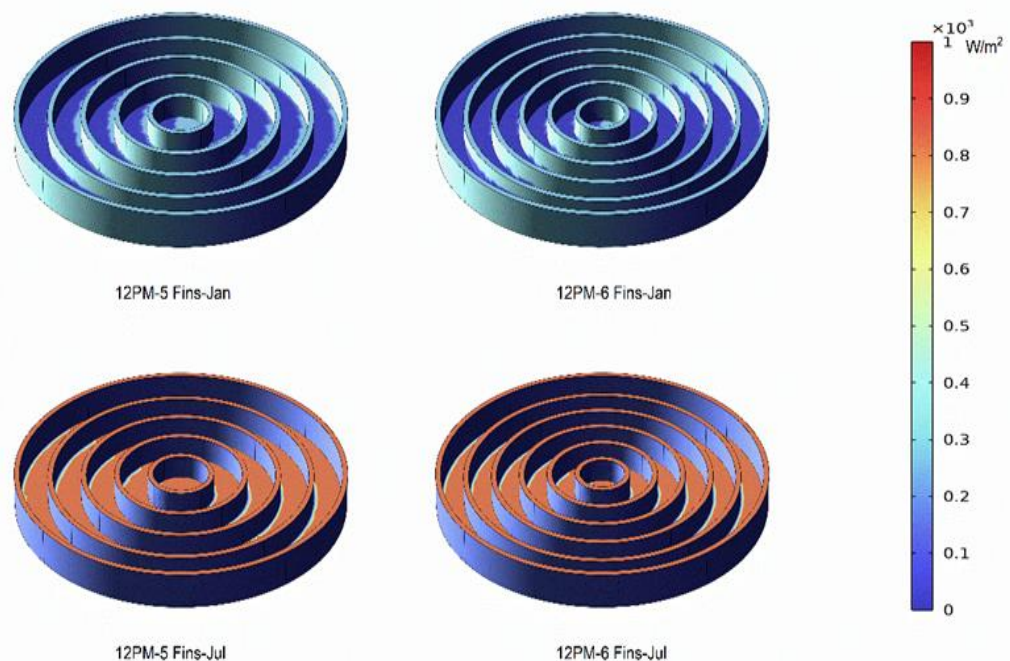


Figure (5.14): Change in Hourly Productivity for CSSHD at $H_f = 8$ mm, $L_w = 350$ mm (a) $N_f = 4$ (b) $N_f = 5$

Figure (5.15) illustrates the impact of fin quantity on the resultant shade. Numerical simulations were conducted from January to July. Increasing the number of fins correlates with a darker shade of the fins, resulting in diminished solar radiation absorption, which subsequently decreases the evaporation process and, thus, the daily productivity. The optimal solution was to add five fins in the solar still basin.

Figure (5.16) depicts the average source heat flux, demonstrating the influence of fin quantity on the average heat flux for January and July. The statistics indicate that an increase in the number of fins correlates with a reduction in the average source heat flux for January and July. The illustration indicates that the presence of five fins in the solar still significantly influences the source heat flux during both months. July attained its maximum value because to elevated sun radiation.



Figure(5.15): The effect of fin shadow during January and July

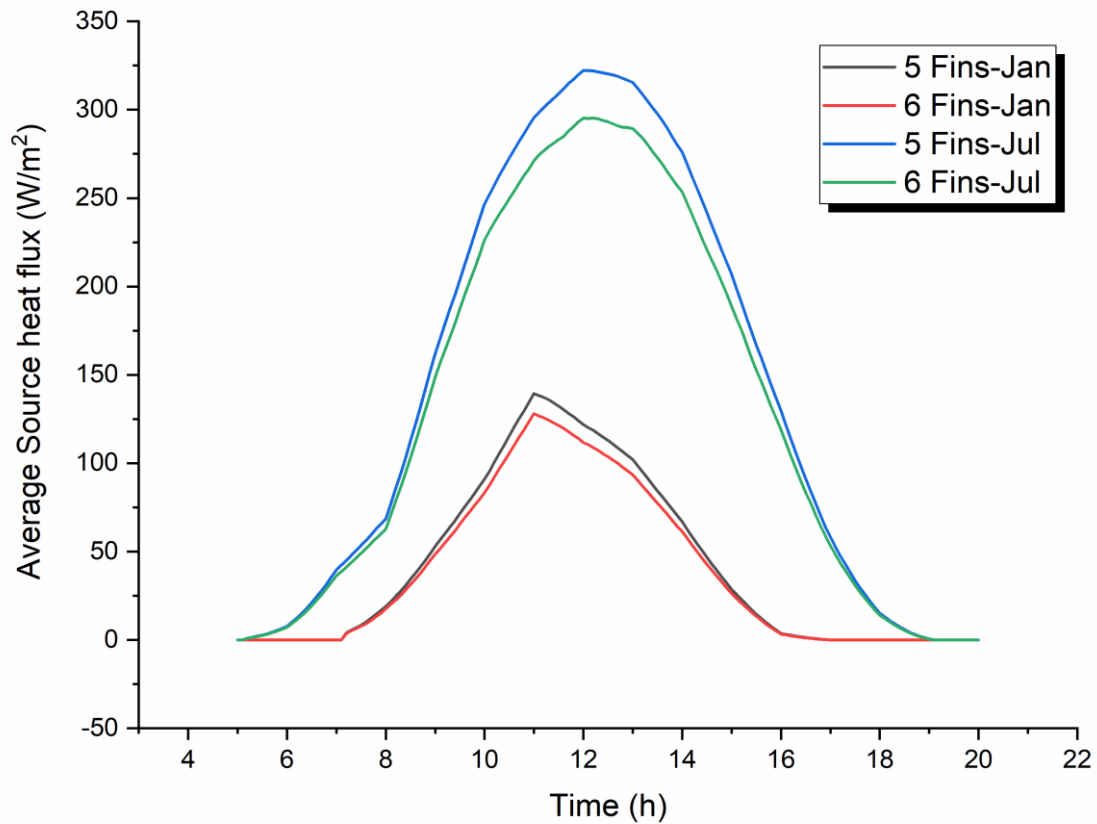


Figure (5.16): The effect of fin shadow during January and July

5.3.3. Study the Effect of Height of Fins

Figures (5.17 to 5.20) depict the temporal fluctuations in temperature over a span of four months. The temperatures being monitored include T_w , T_b , T_{g_in} , and T_{g_out} . Have observed an increase in the number of fins protruding from the water, accompanied by a rise in the temperature of both the water and the basin. Increasing the length of the fin improves its heat conduction. In July, the fin's surface recorded the highest temperatures, with noon water and basin temperatures reaching 63.146 C° and 63.868 C° , respectively.

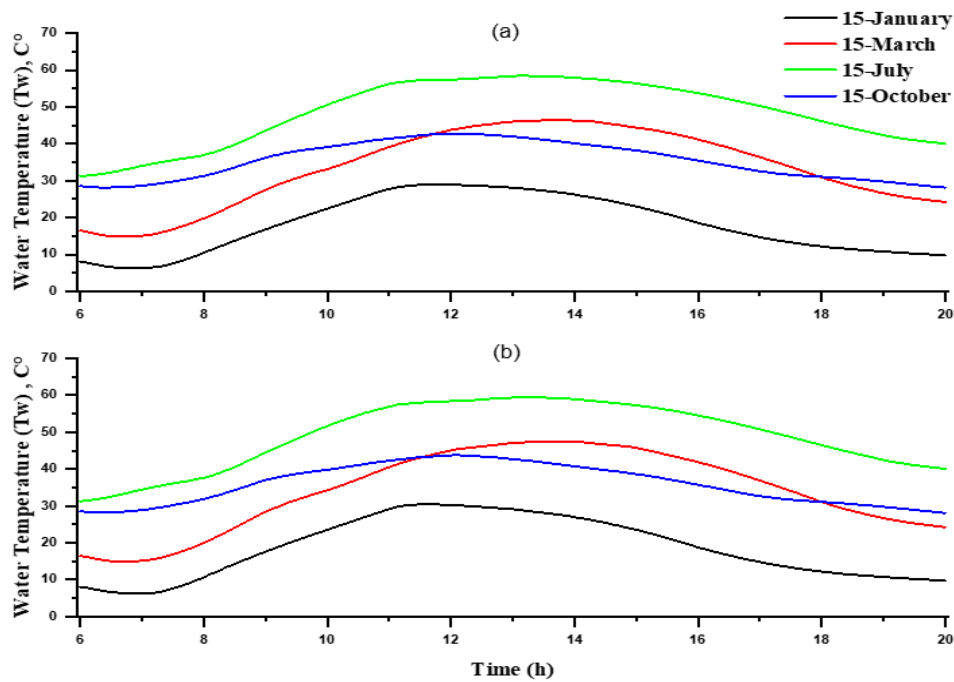


Figure (5.17): Variations of water temperature for CSSHD at $N_f=5$, $L_w=350$ mm
(a) $H_f = 4$ mm (b) $H_f = 6$ mm

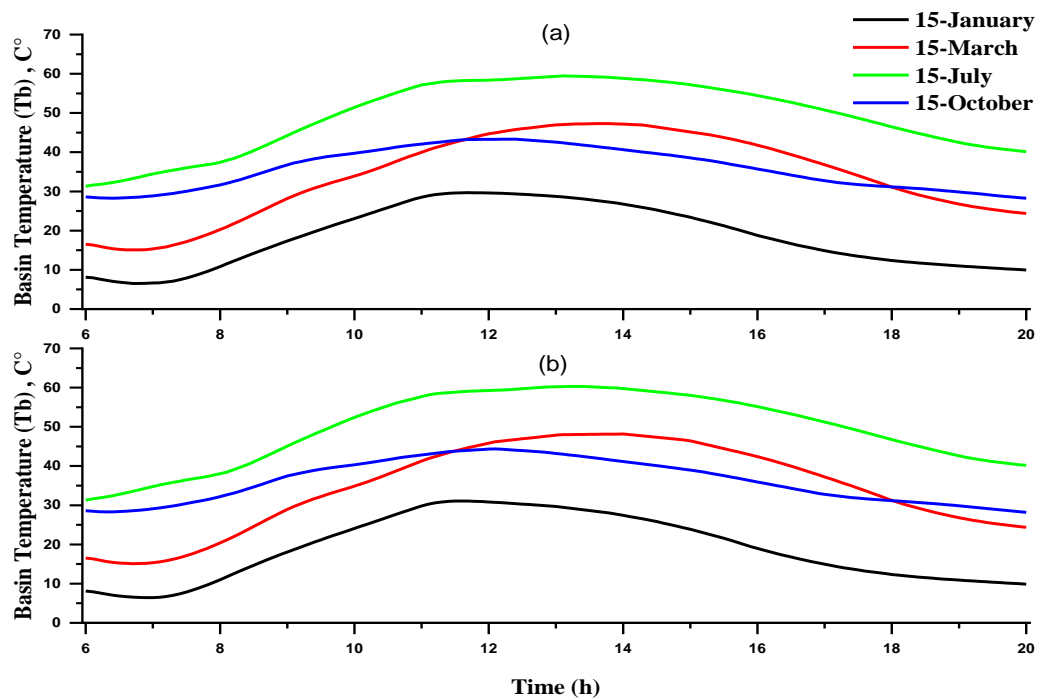


Figure (5.18) Variations of basin temperature for CSSHD at $N_f=5$, $L_w=350$ mm (a)
 $H_f = 4$ mm (b) $H_f = 6$ mm

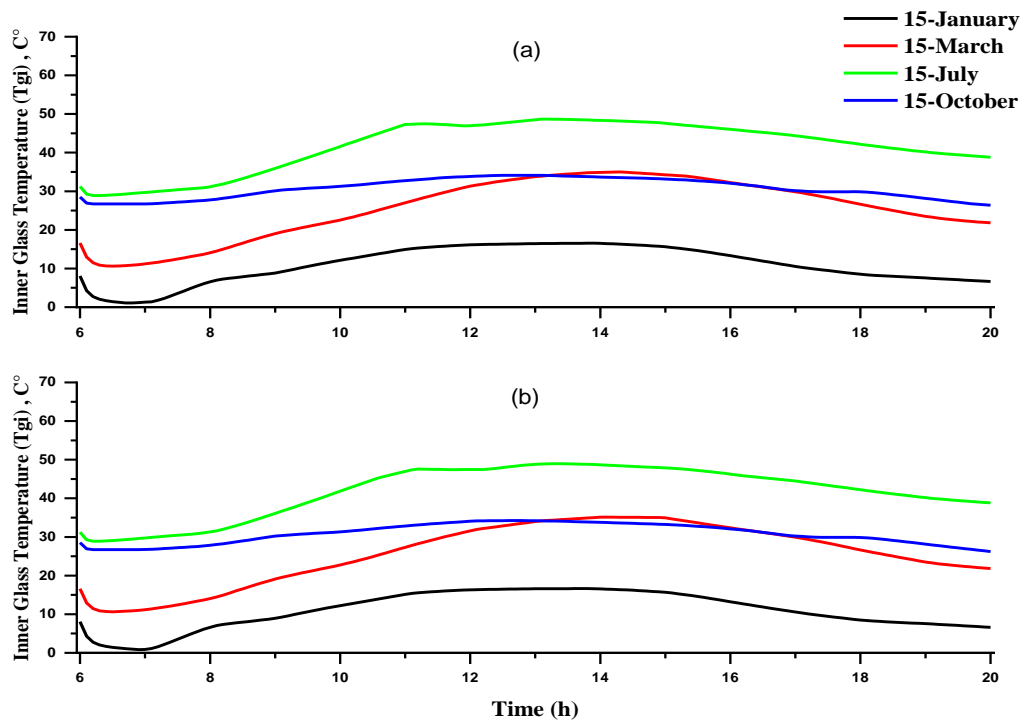


Figure (5.19): Variations of Inner Glass temperature for CSSHD at $N_f=5$, $L_w=350$ mm (a) $H_f = 4$ mm (b) $H_f = 6$ mm

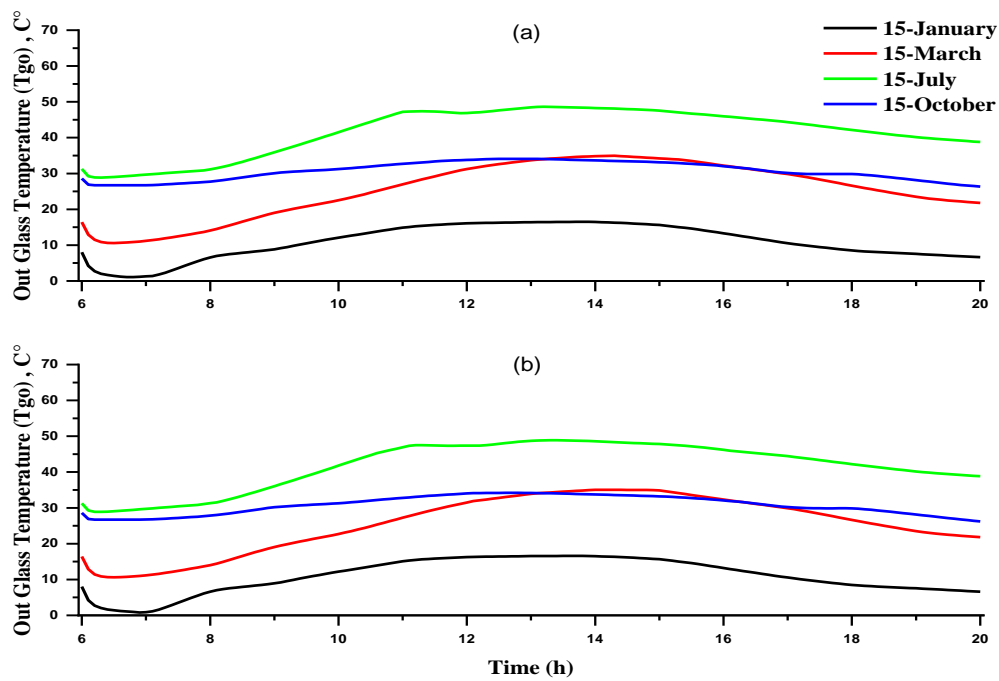


Figure (5.20): Variations of Out Glass temperature for CSSHD at $N_f=5$, $L_w=350$ mm (a) $H_f = 4$ mm (b) $H_f = 6$ mm

According to Figure (5.21), July had the highest cumulative productivity, while January had the lowest cumulative productivity. In July, the productivity reached 12.156 kg/m^2 , while in January it was 3.268 kg/m^2 . In addition, increasing the length of the fin by 8 mm led to a 24% boost in output. The remaining heights are all 4,6 mm.

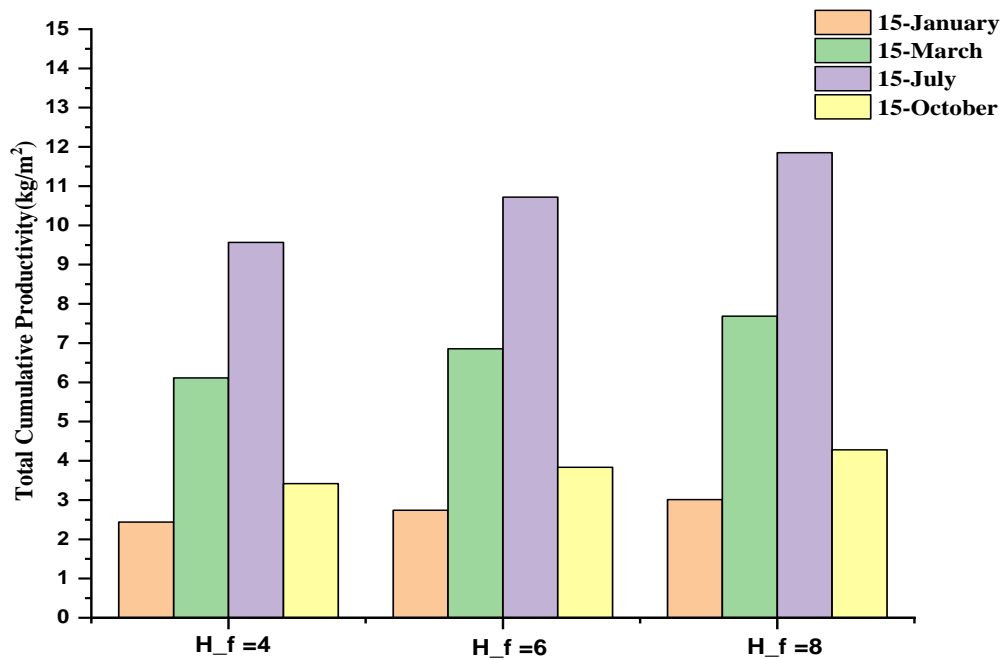


Figure (5.21): Total Cumulative Productivity for CSSHD at $N_f=5$, $L_w=350\text{mm}$

Figure (5.22) illustrates the correlation between the total cumulative productivity of a cylindrical solar still featuring a hemispherical dome and the fin length, with five fins and a cylinder height of 350 mm, for the month of January. It is shown that increased fin length correlates with enhanced productivity; nevertheless, at a fin length of 10 mm, a critical threshold is reached, beyond which cumulative output declines if the fin length beyond 10 mm.

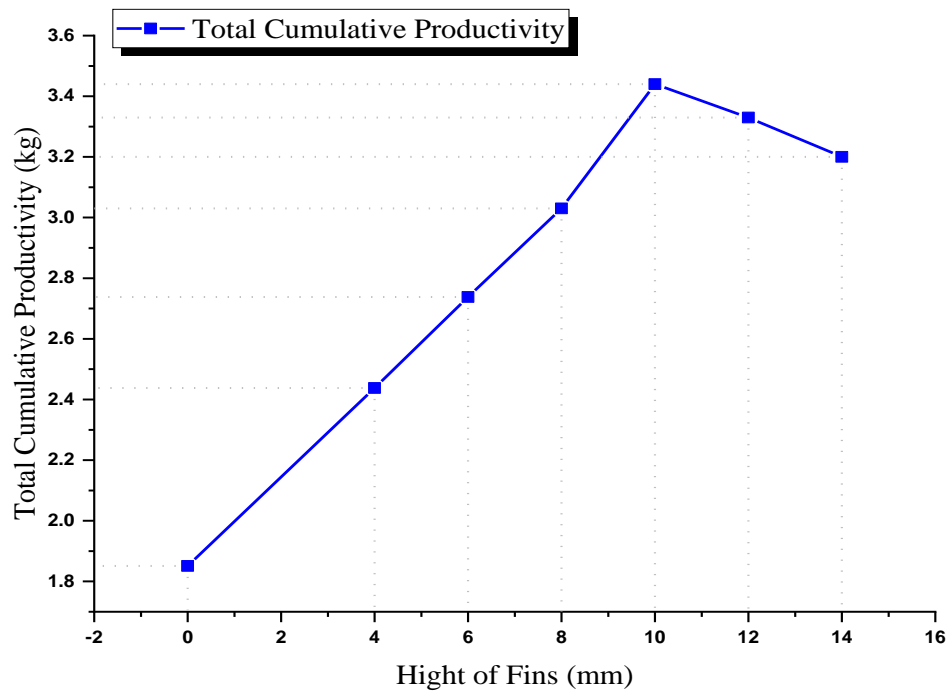


Figure (5.22): Total Cumulative Productivity for CSSHD during January at $N_f=5$, $L_w=350\text{mm}$

Figure (5.23) depicts the relationship between efficiency and Fin length for a span of four months. In July 2024, the highest recorded efficiency was 55.8% for a Fin length of 6mm, while a Fin length of 4mm had an efficiency of 48.8%. The heat buildup in the still is directly proportional to the increase in fin length as shown in Figure (5.24). The simulation was performed for four selected months, January, March, July and October. At a cylinder length of 350 mm and a fin number of 5, the maximum heat gain occurs at a fin length of 6 mm. The maximum heat gain is +1.1946 W at a fin height of 6 mm. As the reading approaches 0 at noon at 12:00 noon for July, this indicates a saturation state of heat gain. March takes longer to reach saturation state of heat gain as it approaches 0 at 1:00 P.M. In the afternoon, when the temperature drops, the solar still starts to emit the heat that has accumulated throughout the day. The maximum heat emitted at a fin height of 6 mm is -0.83599 W. In March, the maximum heat emitted occurs in the afternoon due to the temperature difference, i.e., the air

temperature decreases. This is in contrast to July, where high temperatures persist during the day and night. No noticeable variation. Heat emission is low, with the maximum heat emission reaching -0.54379 W.

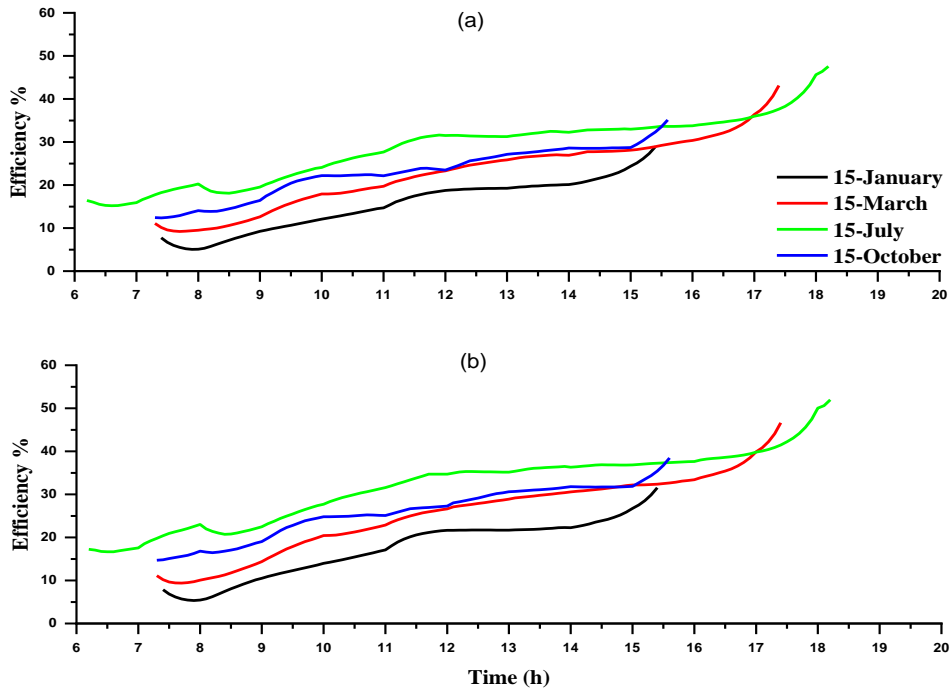


Figure (5.23): Variations of Efficiency for CSSHD at $N_f=5$, $L_w=350\text{mm}$ (a) $H_f = 4\text{mm}$ (b) $H_f = 6\text{mm}$

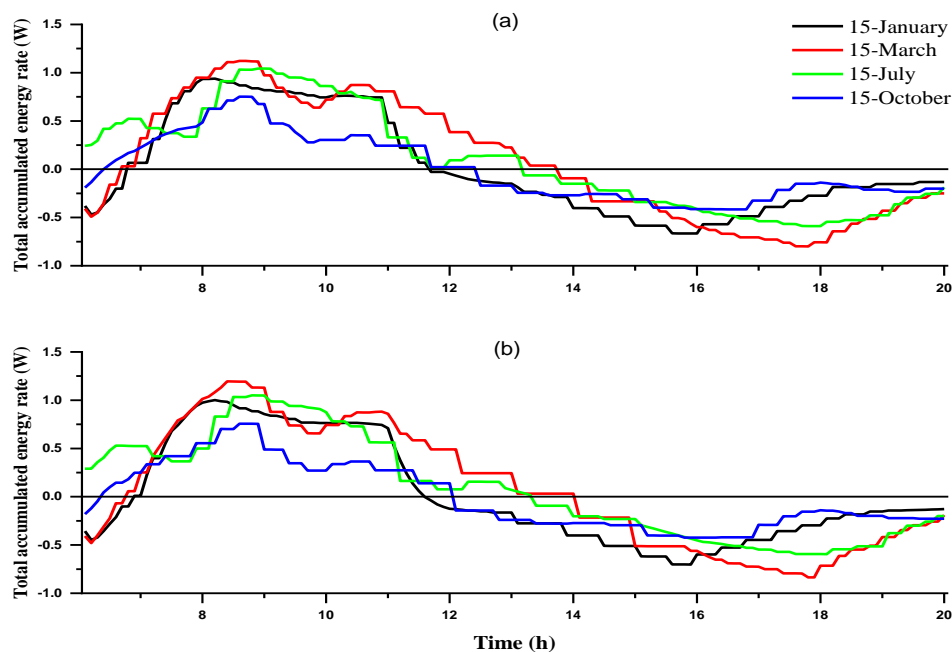


Figure (5.24): Variations of Total accumulated energy rate for CSSHD at $N_f=5$, $L_w=350\text{mm}$ (a) $H_f = 4\text{mm}$ (b) $H_f = 6\text{mm}$

Figure (5.25) displays the mean velocity of water vapor within a solar module that is fitted with five fins and has a cylinder length of 350 mm. The simulation yields data for four specific months: January, March, July, and October. Out of all the months, January had the highest average speed of 0.043357 m/s with a fin length of 6 mm. In January, the cold weather causes a decrease in temperature, leading to a minimum amount of evaporation. The steam's density falls while its velocity increases within the still. In contrast, the velocity diminishes in July as a result of elevated temperatures, hence causing augmented evaporation. Consequently, the steam becomes greater in density and its velocity drops, with an average evaporation rate of 0.034869 m/s in July.

Figure (5.26) shows a positive correlation between productivity and the length of the fin during the four-month simulation, it was seen that the month of July exhibited the highest hourly productivity of 0.00972kg/s. This may be attributed to the increase in temperature, which led to an enhancement in production. On the other hand, January recorded the lowest hourly productivity, amounting to 0.00325kg/s.

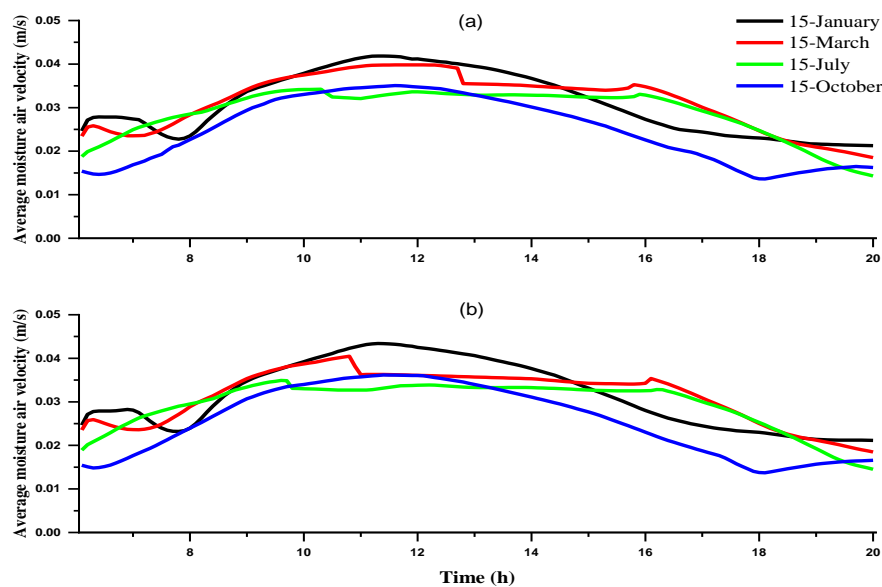


Figure (5.25): Variations Average moisture air velocity for CSSHD at $N_f=5$, $L_w=350\text{mm}$ (a) $H_f = 4\text{mm}$ (b) $H_f = 6\text{mm}$

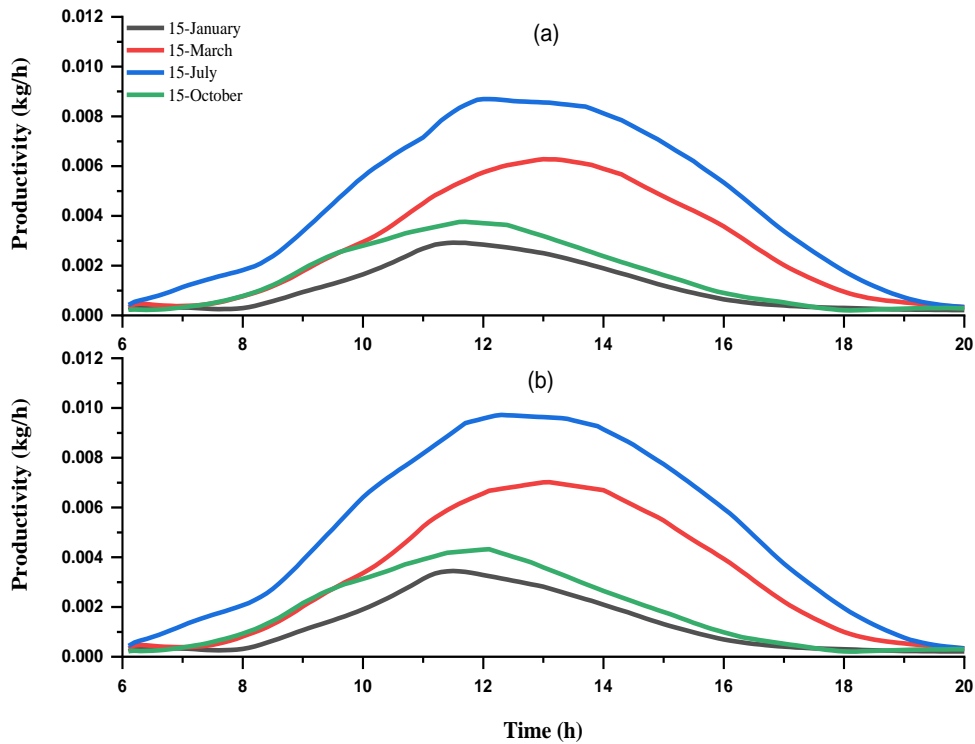


Figure (5.26): Change in Hourly Productivity for CSSHD at $H_f = 8$ mm, $L_w = 350$ mm

5.3.4. Study the Effect of Height of Cylinder

Figure (5.27 to 5.30) display the temperatures T_w , T_b , T_{g_in} , and T_{g_out} . It is observed that the cylinder with a height of 0 mm attained the maximum temperatures. In July, both the basin temperature and the water temperature peaked at 70.717°C and 70.236°C , respectively. During midday. As the height of the cylinder grows, there is a corresponding decrease in temperature. Consequently, the water temperature falls throughout the year. Additionally, as the height of the cylinder increases, the temperature of both the internal and external glass lowers.

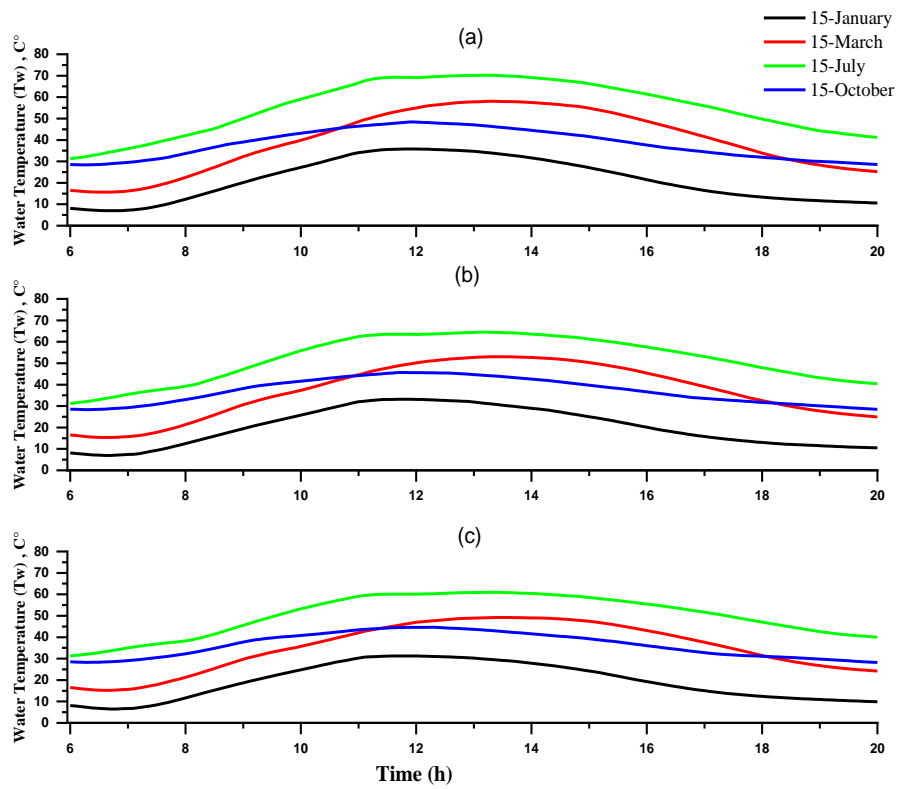


Figure (5.27): Variations of water temperature for CSSHD at N_f=5, H_f=8 mm (a) L_w =0mm b) L_w =50mm (c) L_w =200mm

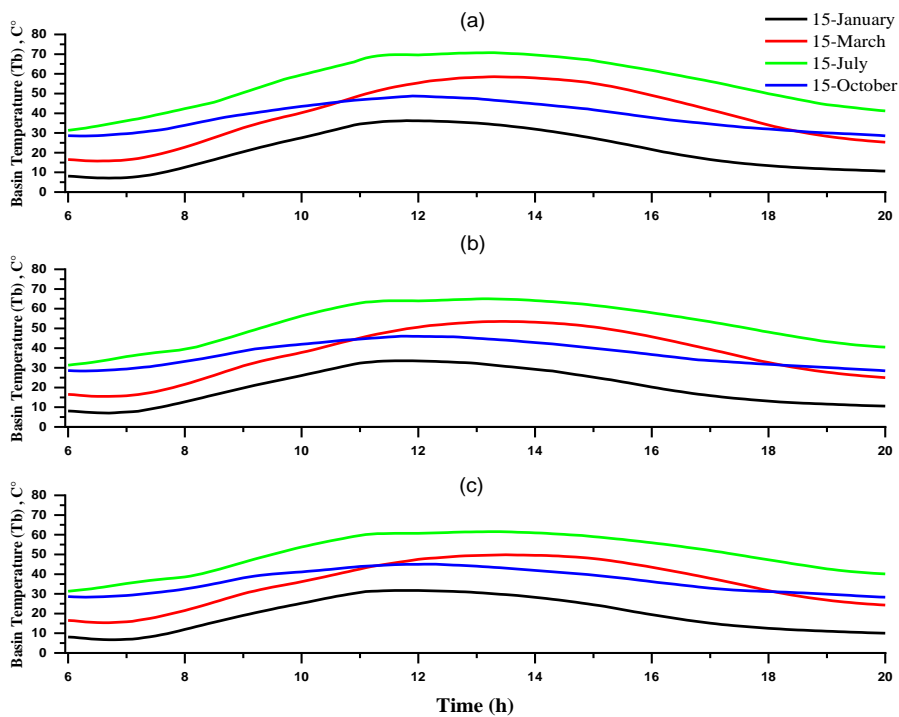


Figure (5.28): Variations of basin temperature for CSSHD at N_f=5, H_f=8 mm (a) L_w =0mm (b) L_w =50mm (c) L_w =200mm

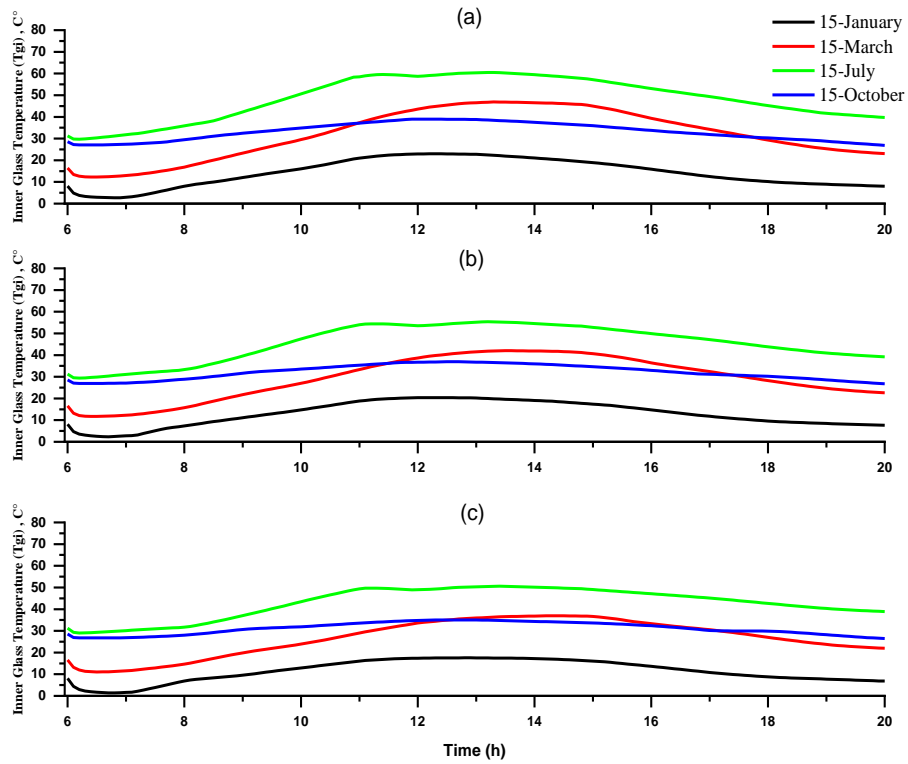


Figure (5.29): Variations of Inner Glass temperature for CSSHD at $N_f=5$, $H_f=8$ mm (a) $L_w=0$ mm (b) $L_w=50$ mm (c) $L_w=200$ mm

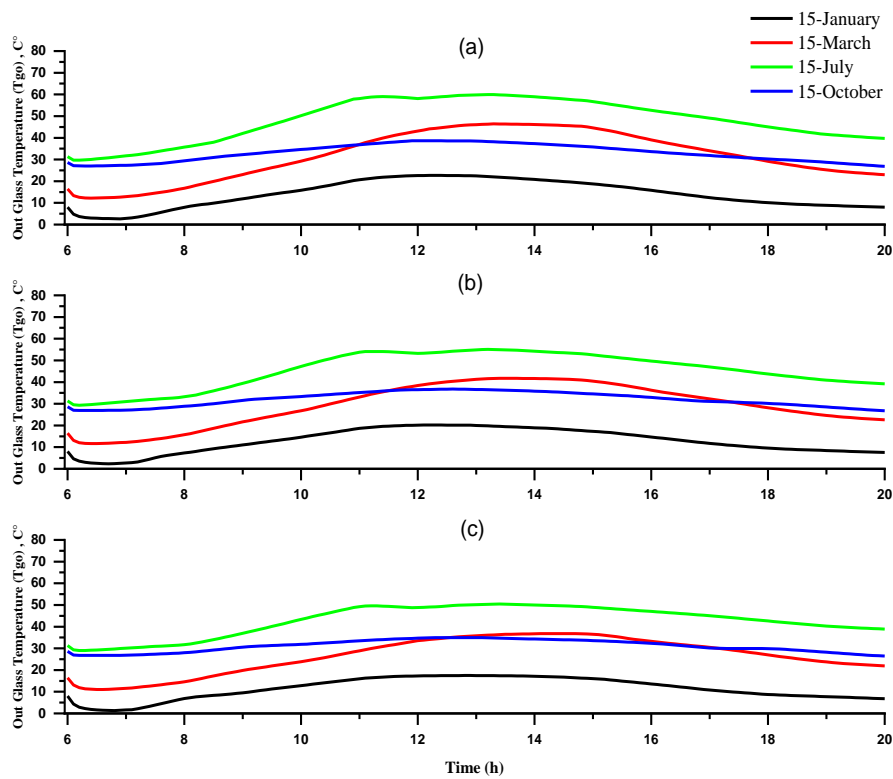


Figure (5.30): Variations of Out Glass temperature for CSSHD at $N_f=5$, $H_f=8$ mm (a) $L_w=0$ mm (b) $L_w=50$ mm (c) $L_w=200$ mm

Figure (5.31) demonstrates that a cylinder height of 50 mm is optimal, as it yields the maximum cumulative production across all months. In January, the total production was 3.268 kg/m^2 , and in March, it increased to 8.089 kg/m^2 . In July, it was 12.156 kg/m^2 , whereas in October it was 4.420 kg/m^2 . The cylinder achieved its peak efficiency of 60% in July at a height of 50mm.

Figure (5.32) displays the efficiency data for four months, specifically for cylinder heights of 0mm, 50mm, and 200mm. The month of July exhibited the best efficiency across all heights, mostly attributed to the surge in productivity resulting from the amplified solar radiation during this period. The cylinder with a height of 50 mm has the greatest height among all the cylinders, since it achieved an efficiency of 60%.

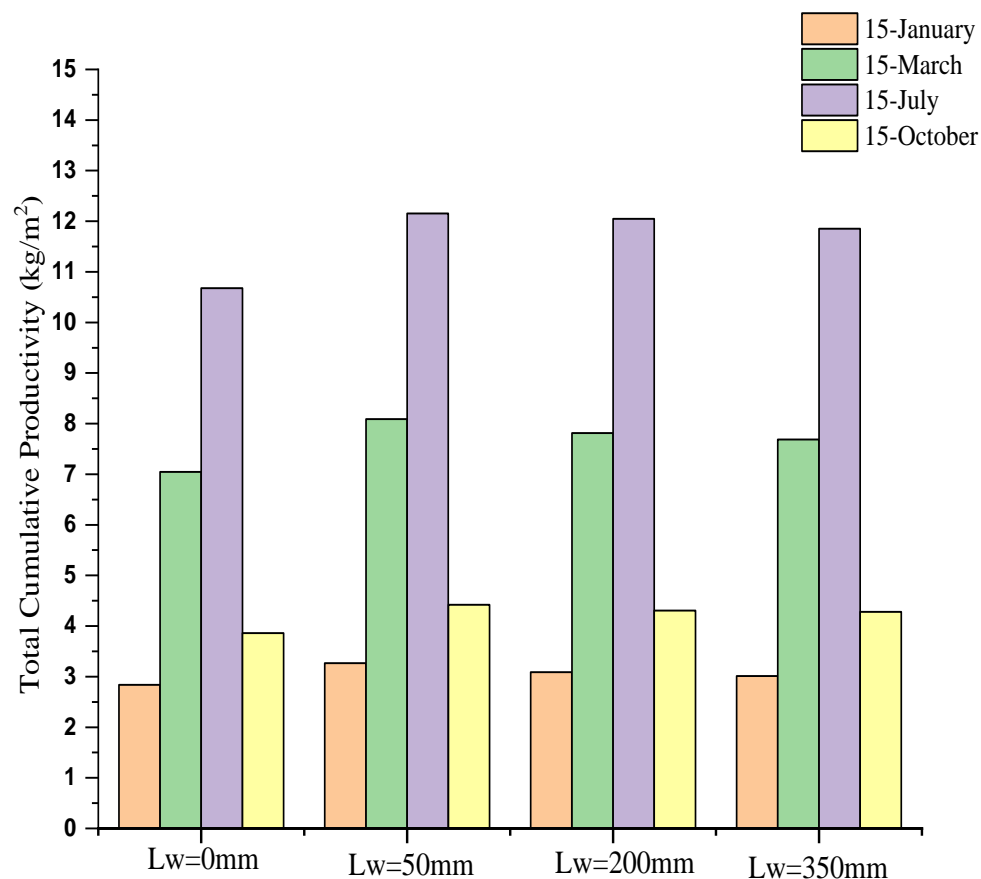


Figure (5.31): Total Cumulative Productivity for CSSHD at $N_f=5$, $H_f=8$ mm

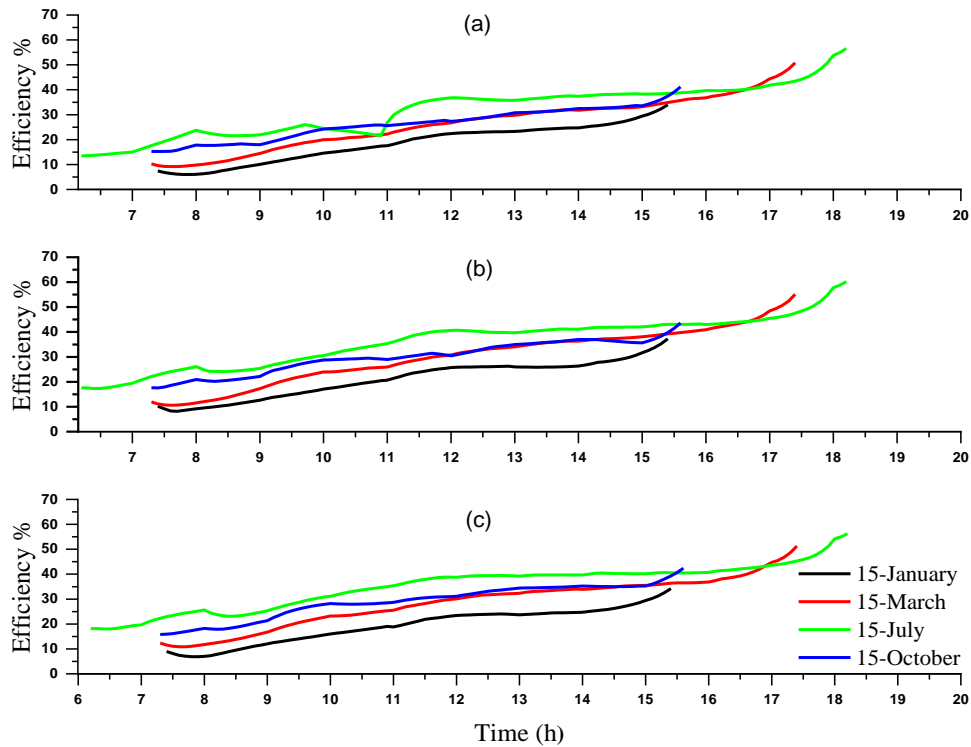


Figure (5.32): Variations of Efficiency for CSSHD at $N_f=5$, $H_f=8$ mm (a)

$L_w=0$ mm (b) $L_w=50$ mm (c) $L_w=200$ mm

Figure (5.33) displays the heat gained and emitted at various heights (0 mm, 50 mm, and 200 mm) of the cylindrical glass during four different seasons: January, March, July, and October. The behavior observed at the heights of the three cylinders is nearly identical. At the lowest point of the cylinder, it experienced the maximum increase in heat over the course of a month. The heat gain in March was $+1.3031$ W, whereas in July it was $+1.2257$ W. The maximum heat emitted, even after the reduction in solar energy, was -1.0151 W at 6:00 PM. At a height of 50 mm in the second scenario, it is also observed that the four months exhibiting similar behavior are in close proximity to each other. The month with the greatest heat accumulation is observed. On March 1st, the temperature reached a peak of 0.8678 W. At a distance of 200 mm, in the third scenario, the maximum temperature increase was 1.1545 W and the maximum heat emitted was 0.85845 W.

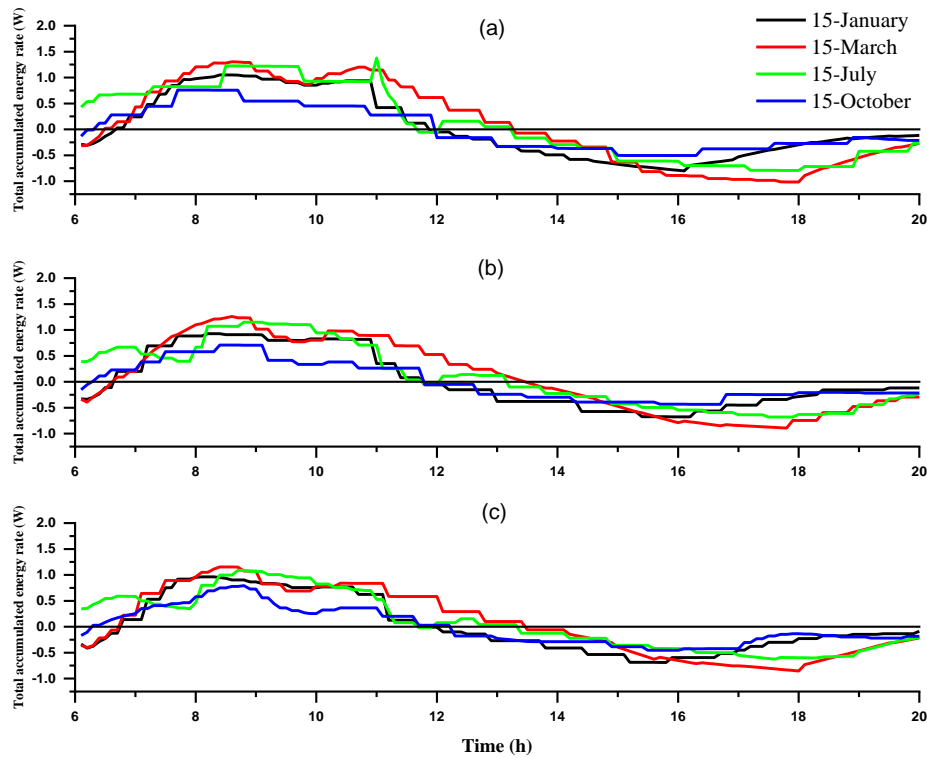


Figure (5.33): Variations of Total accumulated energy rate for CSSHD at $N_f=5$,
 H_f (a) $L_w = 0\text{mm}$ (b) $L_w = 50\text{ mm}$ (c) $L_w = 200\text{mm}$

Figure (5.34) displays the mean velocity of humid air within the confined area between the evaporating water surface and the condensing glass surface at various heights of the cylindrical glass. Figure A depicts the height of the zero-cylinder, which corresponds to a hemispherical dome distiller. The subsequent two cases illustrate cylinder heights of 50 and 200 mm, respectively. The simulation was conducted over various seasons, specifically in January, March, July, and October. At the hemispherical dome, the average velocity of water vapor reaches its peak in January during the middle of the day, slightly surpassing the values seen in other months. However, the highest values are recorded in July and March during the afternoon. This phenomenon occurs because there is an equilibrium between the evaporation caused by solar radiation and the condensation on the inner glass surface caused by its impact on the air temperature. In January, the evaporation rate is lower in the afternoon compared to noon, primarily because of the reduced solar radiation. In July,

the afternoon temperatures reach their peak due to the significant evaporation caused by the abundant sun radiation. In contrast, July values closely resemble values because of the low temperature of the condensation surface and the abundance of solar light. Upon further examination, it becomes evident that the month of July exhibits the minimum velocity of wet air. The rationale for this is that the maximum level of production will occur in this scenario due to the significant temperature disparity between the evaporation surface and the inner glass surface, resulting in a reduced velocity. In the third scenario, there was a proportional rise in the velocity of moist air throughout the month of July. However, the maximum velocity values were still seen in January. This can be attributed to the increase in the height of the cylinder.

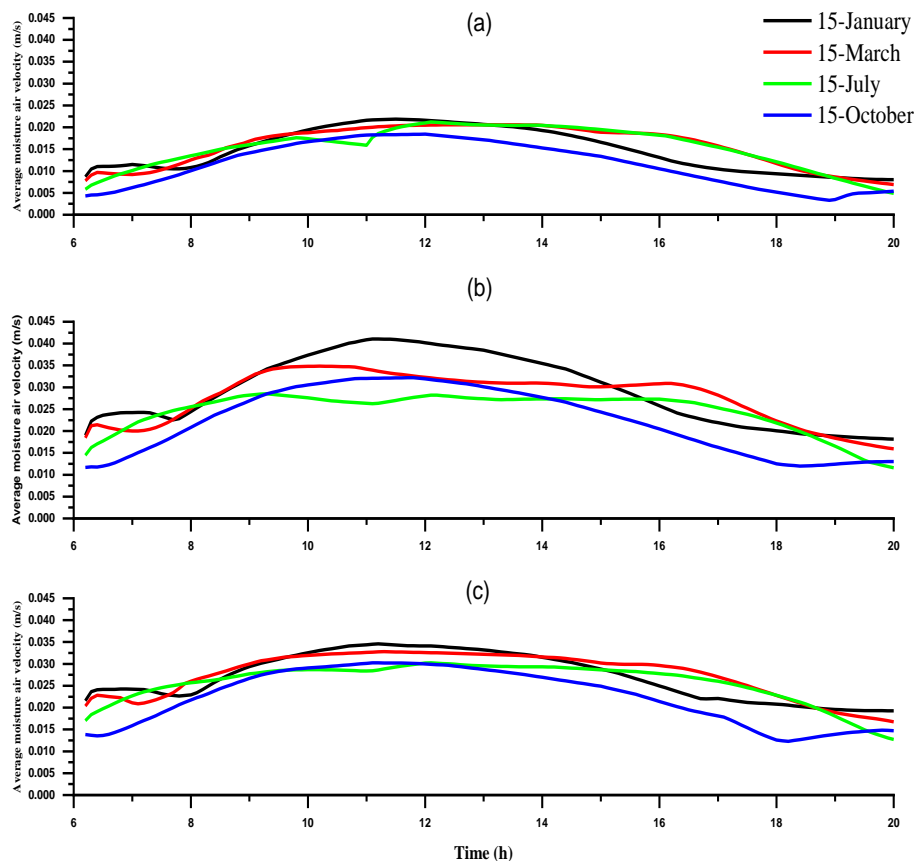


Figure (5.34): Variations of Average moisture air velocity for CSSHD at $N_f=5$, $H_f=8$ mm (a) $L_w=0$ mm (b) $L_w=50$ mm (c) $L_w=200$ mm

Figure 5.35 shows hourly productivity levels over the month of July. The production levels are indicated at three specific heights: 0 mm, 50 mm, and 200 mm. Observe the incremental rise in productivity until it attains a zenith at noon, thereafter commencing a decrease. The peak levels were attained in July. The maximum flow rates documented at elevations of 0, 50, and 200 were 0.005868 kg/h and 0.011232 kg/h, respectively.

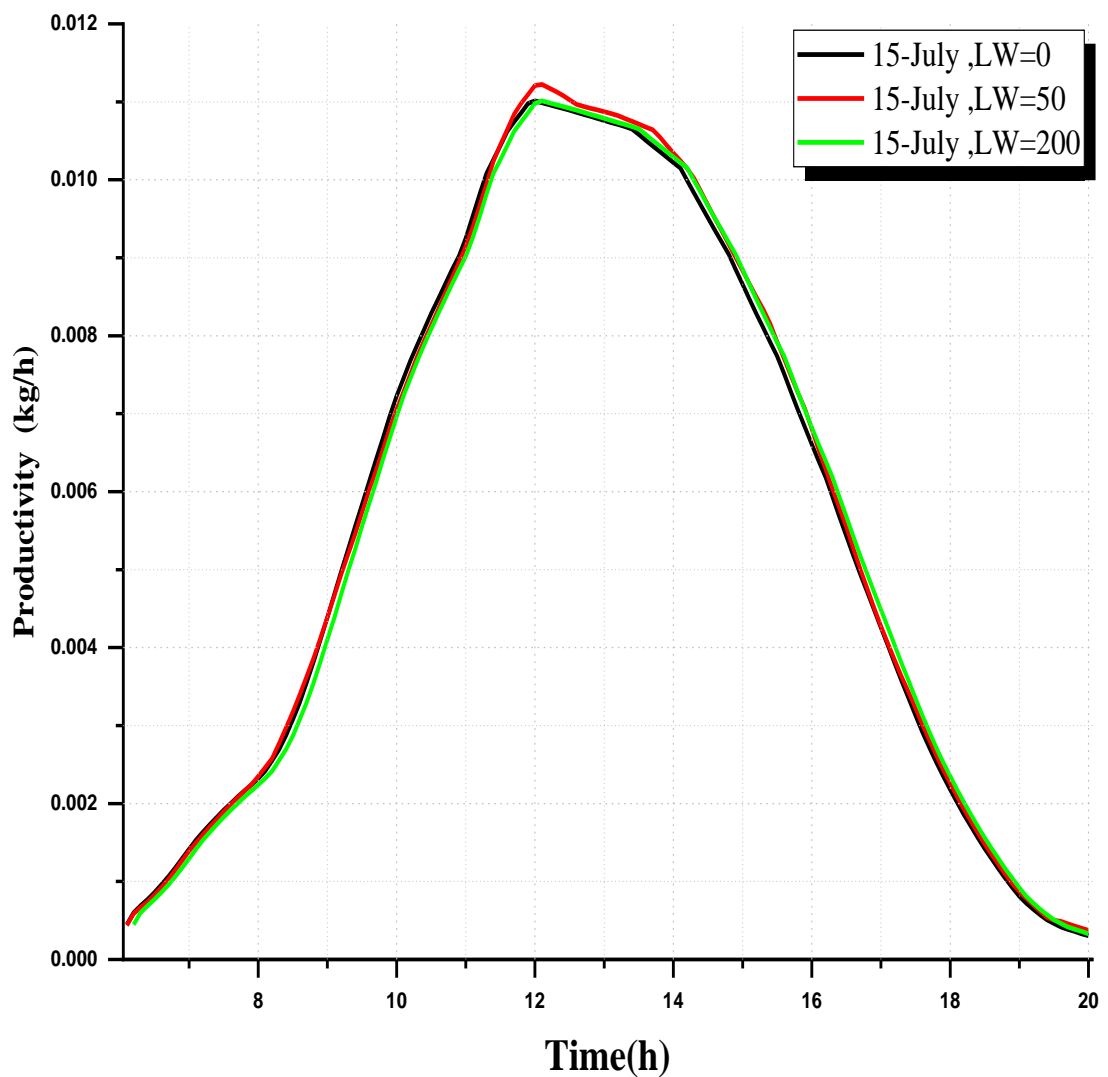


Figure (5.35): Change in Hourly Productivity for CSSHD at $N_f=5$, $H_f=8$ mm
 $L_w=0$ mm, $L_w=50$ mm, $L_w=200$ mm

5.4. Temperature, Concentration Contours and Streamlines

A simulation of the CSSHD design was carried out to demonstrate the impact of this innovative design on the efficiency of freshwater resources. A visual representation of the temperature distribution throughout different (hours of the day) across various months is depicted in Figure (5.36). The findings indicate that the highest temperature occurs in the month of July when compared to the other selected months. The peak temperature in July is attributed to the prevailing weather conditions, characterized by high “solar radiation” and “ambient temperature”. Additionally, Figure (5.37) presents the water vapor concentration in the CSSHD over different hours of the day for four distinct months. The results reveal that the concentration is directly proportional to the temperature, indicating that an increase in elevated temperature results in an increased rate of evaporation and subsequently, a rise in water vapor concentration in the air, as depicted in the graph. It is observed that water vapor concentration is “higher” at the water surface and lower near the interior surface of the glass.

Figure (5.38) displays the velocity lines in steam and inside of CSSHD at various times of the day during a span of four months. Within the context of CSSHD, there are no limitations. Consequently, the water that has turned into vapor ascends and adheres to the cooled glass surface before descending and exiting the CSSHD. The results indicate that the velocity of humid air in January is elevated as a result of minimal evaporation, leading to a fall in density and consequently an increase in velocity.

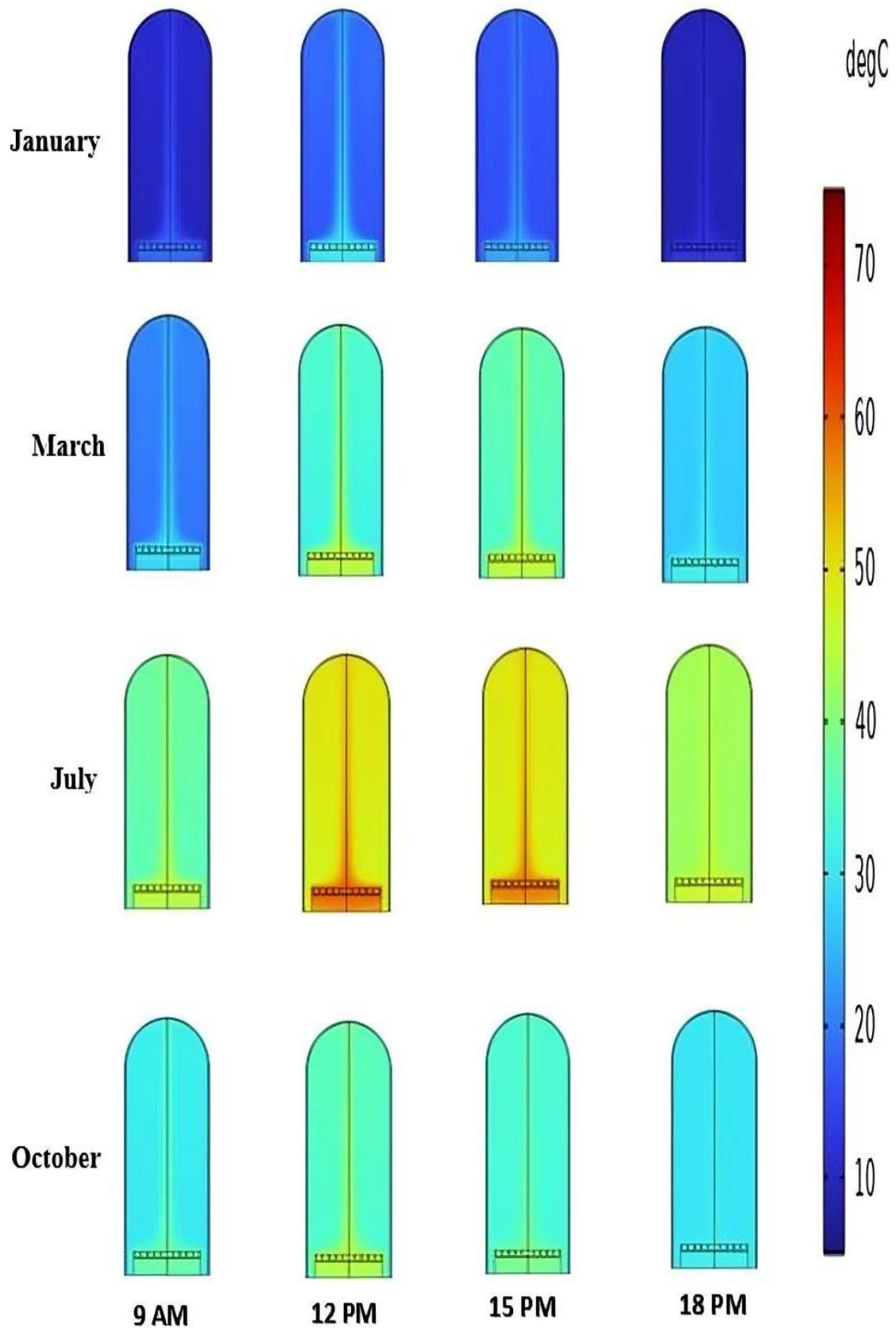


Figure (5.36): Variation of the temperature contours during a day 15-January, 15-March, 15-July, and 15-October.

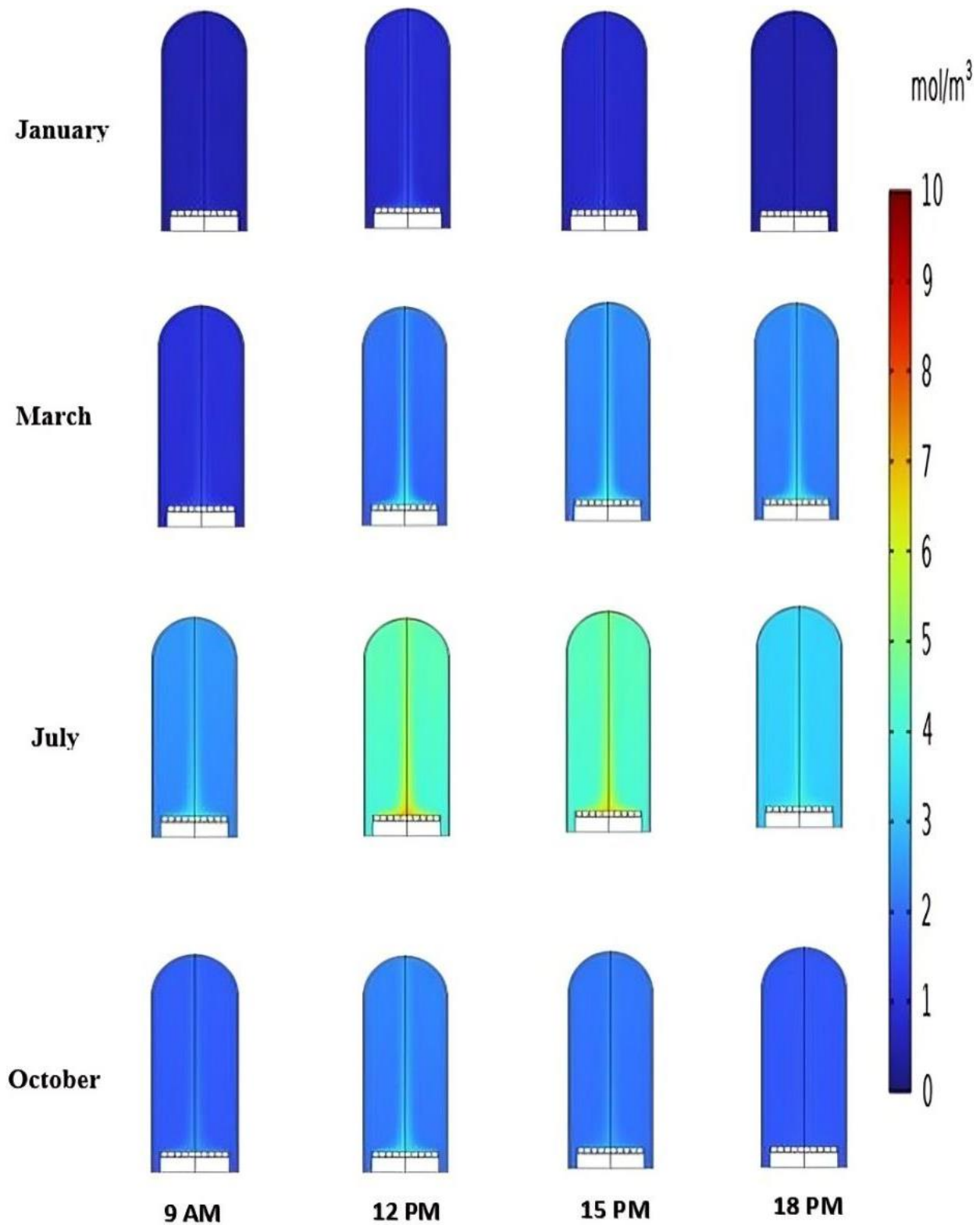


Figure (5.37): Presents the water vapor concentration during a day 15-January, 15-March, 15-July, and 15-October

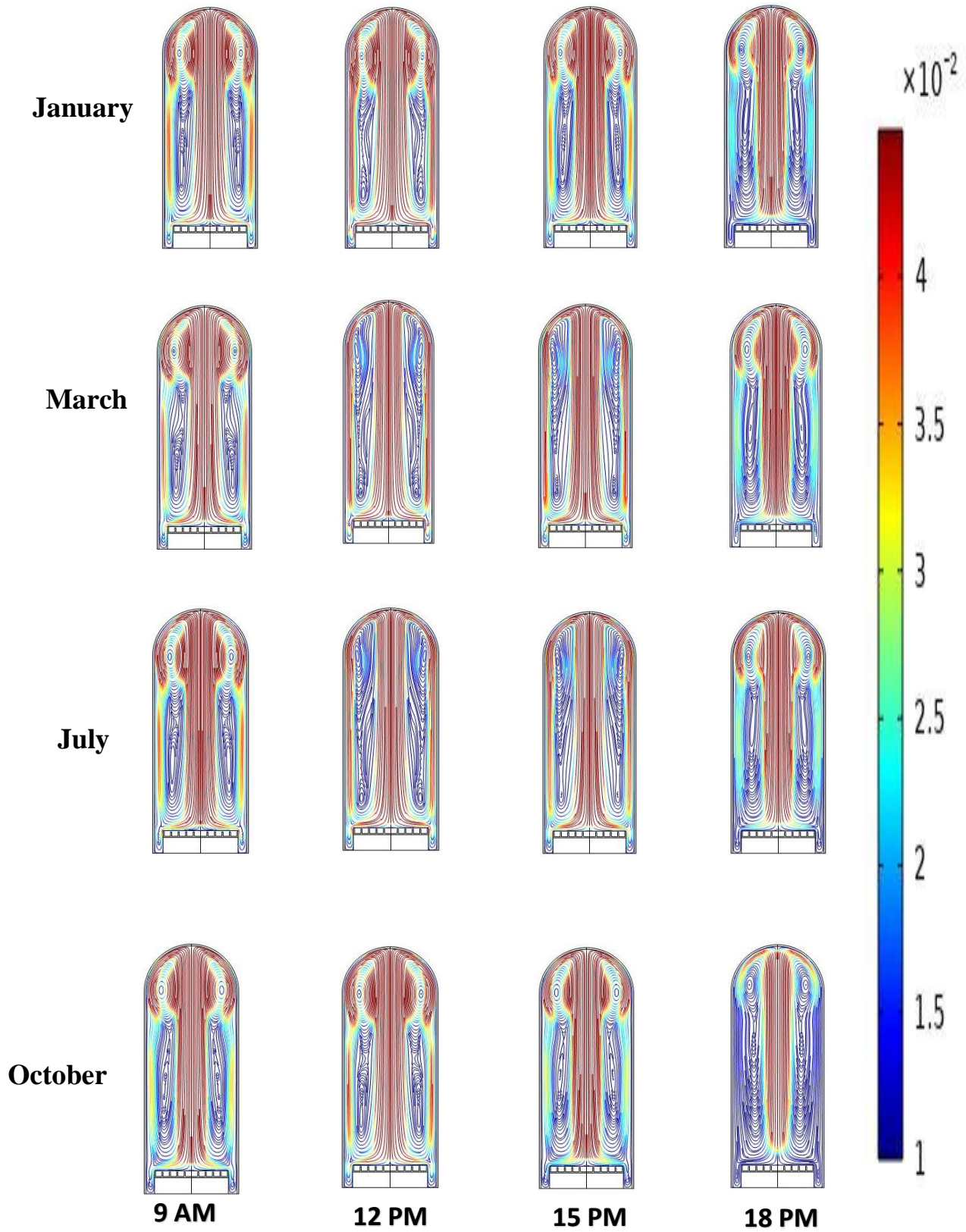


Figure (5.38): Streamlines and velocity field during a day 15-January, 15-March, 15- July, and 15-October.

5.2. Experimental Results

5.2.1. Weather Condition

The cylindrical solar still, with and without fins, was tested for eight hours per day in outdoor conditions. It is evident Figures (5.39 to 5.42) depict the variations in radiation intensity (W/m^2), ambient temperature ($^{\circ}\text{C}$), and wind speed (m/s) over time (h) on the dates 4,5,6,10 and March 11, 2024.

Solar radiation has a significant influence on the efficiency of solar distillation. In March 2024, note that an increase in the effectiveness of solar stills on hot days, which can be attributed to the significant absorption of solar energy on sunny days. Productivity is higher on clear days compared to cloudy days. Abundant sun radiation on a cloudless day result in the heating and evaporation of water. The solar radiation on March 10, 2024 exceeds the solar radiation on 4,5,6,10 and 11 March 2024. Furthermore, solar radiation reaches its maximum intensity during the period from 11:30 to 12:30, as a result of the substantial amount of solar energy present. The solar radiation reached its maximum intensity at $990 \text{ W}/\text{m}^2$. As a result, the daily readings were restricted. Achieve a solution by improving the solar diagnostic process.

The peak capacity is achieved between 11:30 and 14:00. Over time, the sun's heat accumulates, leading to an increased growth rate and improved output. Concerning the ambient temperature, it initially rises and continues to do so even after the radiation decreases, as a result of the earth's heat retention. As solar radiation decreases, the earth begins to emit thermal energy. As a result, the surrounding temperature stays high even after being subjected to different levels of sunlight.

The ambient temperature declines after 3:00 PM. The average ambient temperature on 4,5,6,10 and 11 March was recorded as 19.2, 19.21, 24.7, 26.9 and 21°C respectively. The findings indicate a direct

relationship between productivity and a reduction in ambient temperature. This occurs because a decrease in the surrounding temperature leads to a corresponding reduction in the temperature of the outer glass covering. Consequently, the vapor condensation process increases on the inner surface of the CSSHD, resulting in greater heat absorption by the glass cover and ultimately leading to increased productivity.

The fluctuations in wind velocity during defined time intervals on the designated dates. The wind speed measured on 4,5,6,10, and 11 March 2024 0.63 ,0.64 ,0.577 ,0.606 and 2.7 m/s respectively. The maximum wind velocity is recorded during the time interval from 14:00 to 15:00 on March 3, 2024. Productivity increases with increasing wind speeds due to enhanced cooling of the distillation process's outer covering, resulting in a larger temperature gradient between the covering and the water surface.

5.2.2. Comparison between CSSHD with fins and CSSHD without fins

The studies were carried out in March. Before commencing measurements, ensure that the basin is filled with brackish water, eliminate any dust particles from the glass cover, and set the temperature to a warm level between 8 A.M. and 5 P.M. Measurements of temperature, wind speed, and sun radiation are taken every 10 minutes, along with corresponding production numbers. Both possess a cylinder height of 350 mm. To evaluate the efficiency of the solar still in one hemisphere in relation to the proposed concept. The phrase denotes the ratio of solar energy utilized for the generation of fresh water in relation to the total solar energy obtained.

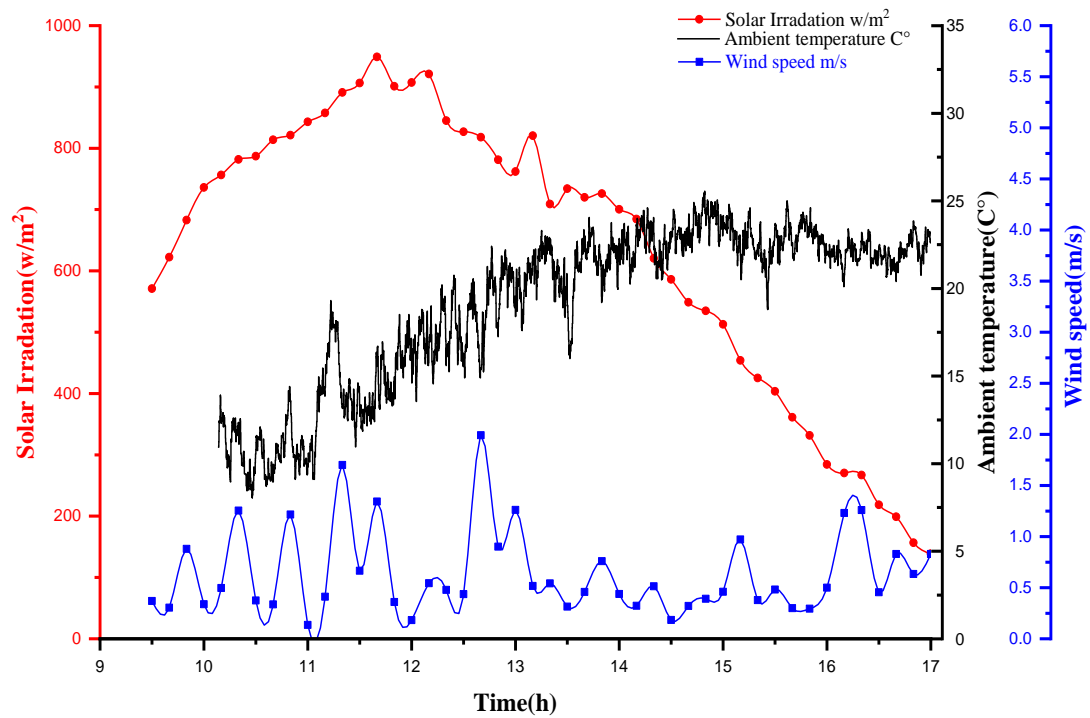


Figure (5.39): Variation of solar radiation, ambient temperature and wind speed with respect to time 4-3-2024.

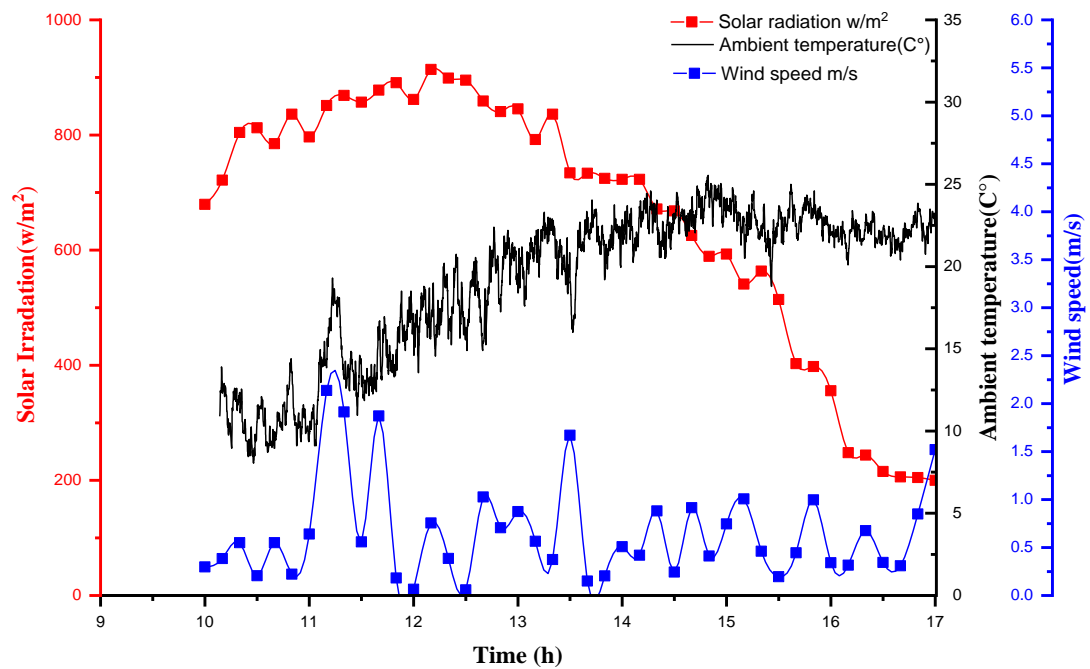


Figure (5.40) :Variation of solar radiation, ambient temperature and wind speed with respect to time 5-3-2024.

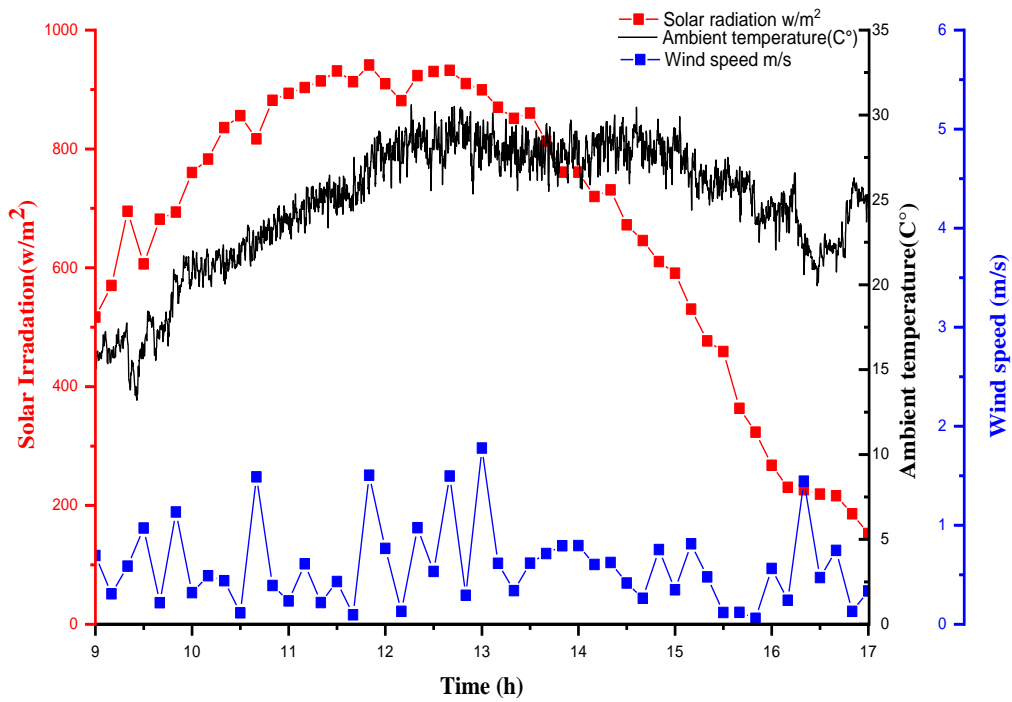


Figure (5.41):Variation of solar radiation, ambient temperature and wind speed with respect to time 6-3-2024.

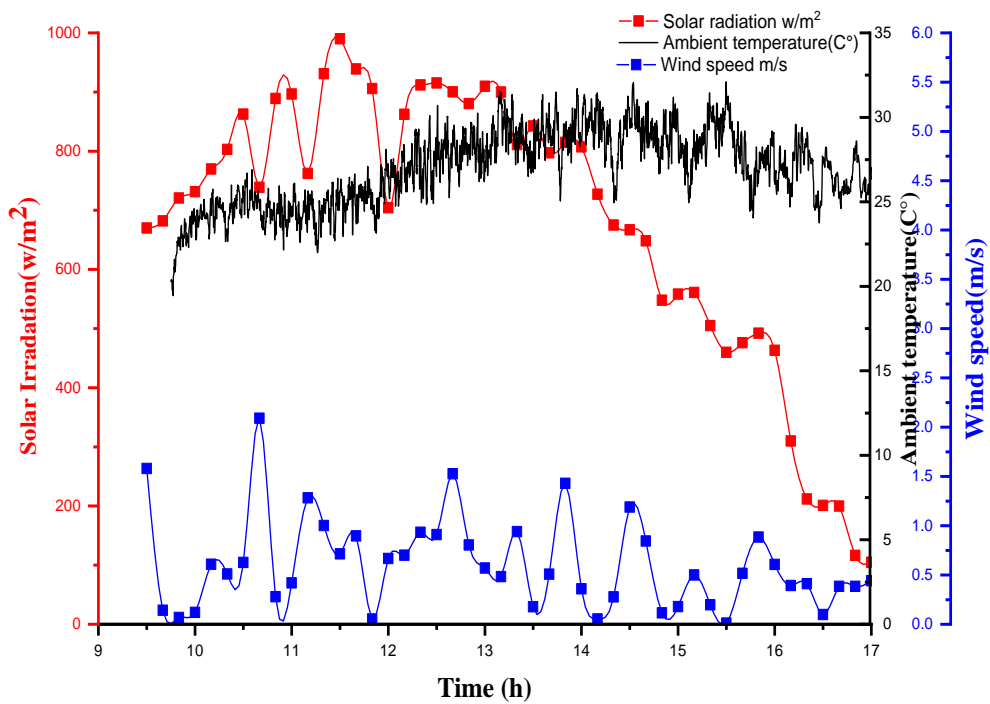


Figure (5.42): Variation of solar radiation, ambient temperature and wind speed with respect to time 10-3-2024.

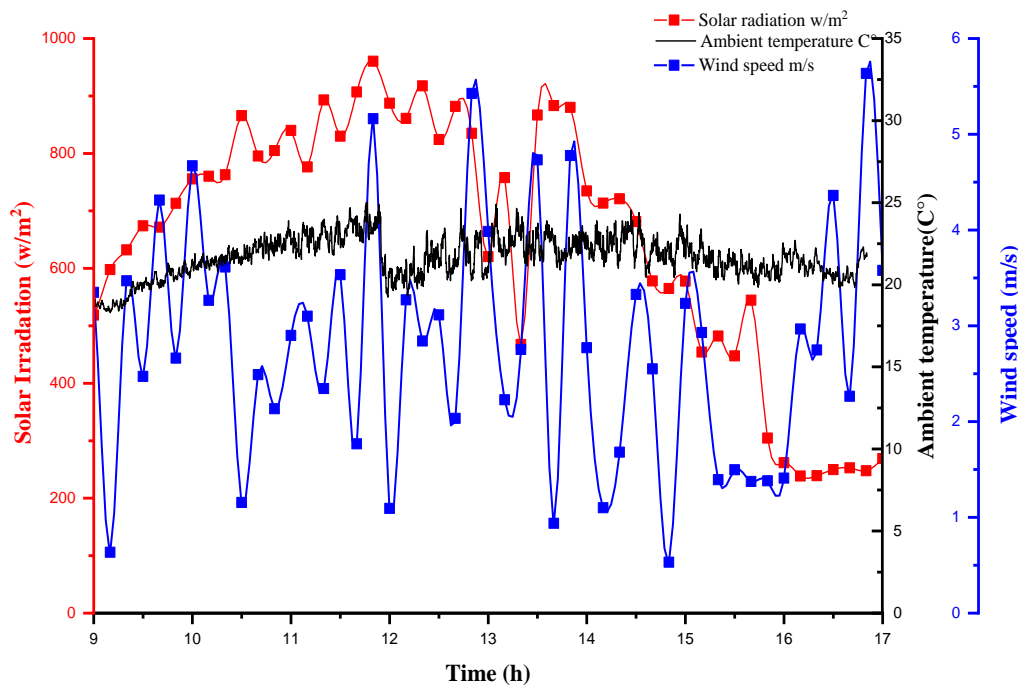


Figure (5.43): Variation of solar radiation, ambient temperature and wind speed with respect to time 11-3-2024.

Figures (5.44 to 5.48) depict the temperature changes at 10-second intervals in different regions of the snapshots for each of the fin-enhanced CSSHD systems. The data provided pertains to the month of March in the year 2024, specifically on the dates of March 4th, 5th, 6th, 10th, and 11th. The findings suggest that CSSHD systems equipped with fins have elevated tank liner and water temperatures in comparison to systems without fins. This illustrates the effectiveness of fin-enhanced CSSHD in absorbing and transferring energy by increasing the surface area for absorption and heat transfer, in contrast to solar systems that do not include fins. The external glass temperatures consistently display the lowest temperature values, with both thermometers indicating identical levels. Nevertheless, the CSSHD with fins regularly exhibits significantly lower values compared to the finless CSSHD. Interior glass values may display comparable characteristics to near-temperature values, but with somewhat lower CSSHD values. The results demonstrated that the solar still's (CSSHD) overall production was greater when it was equipped with fins, as opposed to when it did not have fins.

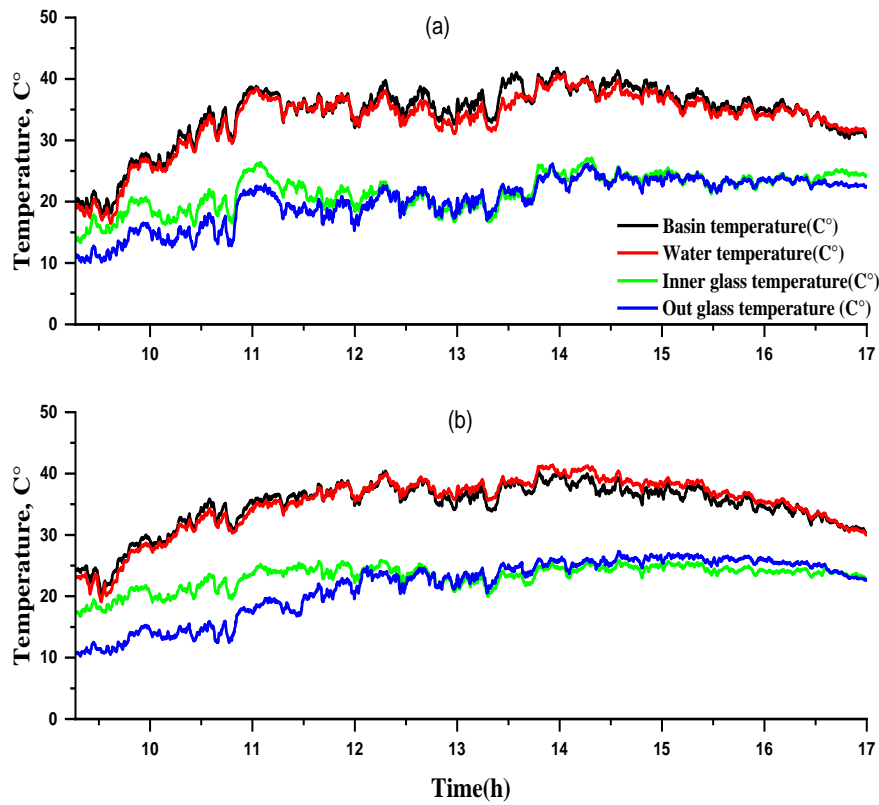


Figure (5.44): Variations of temperature for two solar still a-with fins b- without fins , at day 4-3-2024.

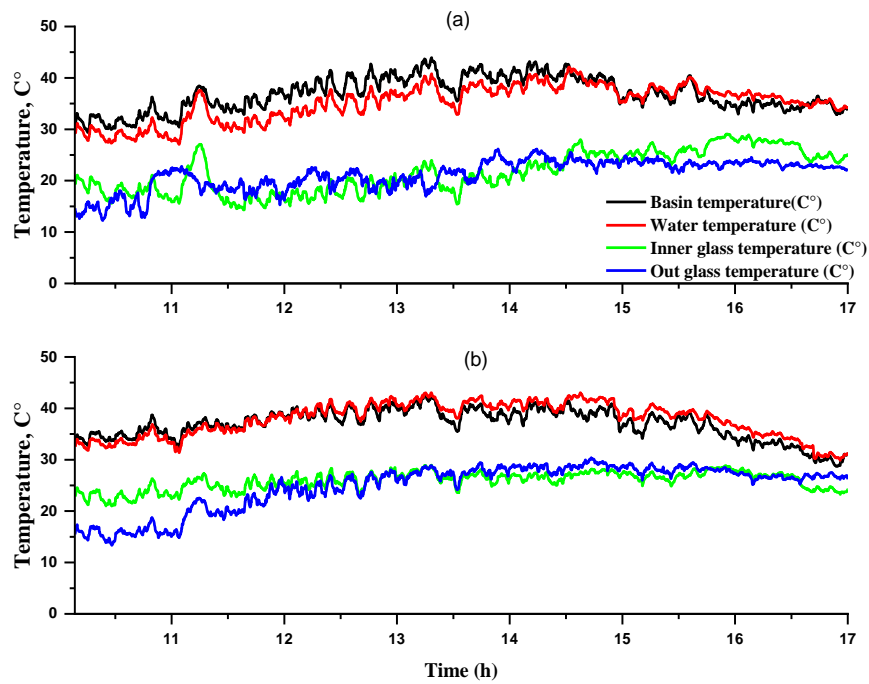


Figure (5.45): Variations of temperature for two solar still a-with fins b- without fins , at day 5-3-2024.

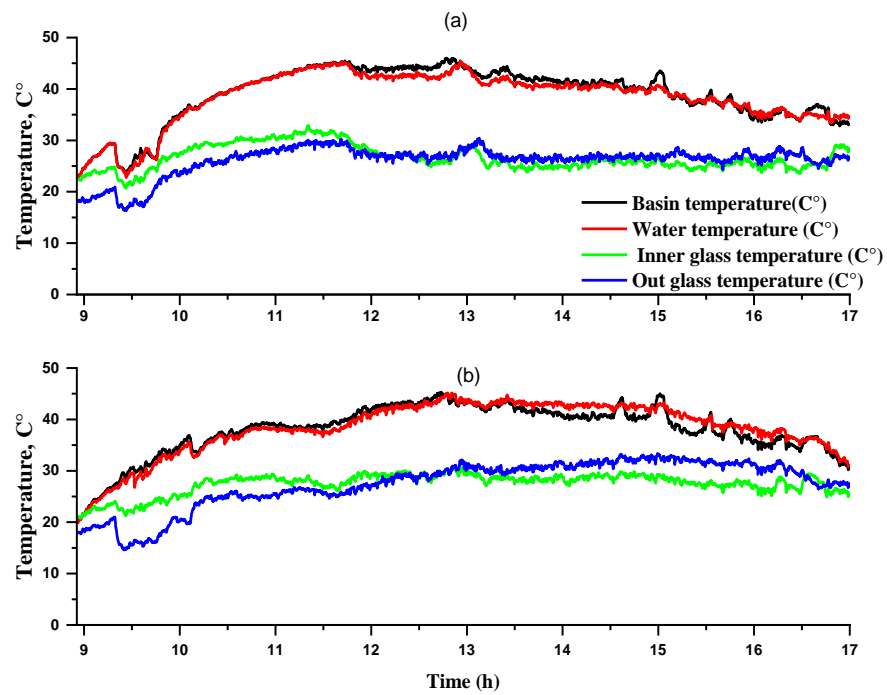


Figure (5.46): Variations of temperature for two solar still a-with fins b- without fins , at day 6-3-2024.

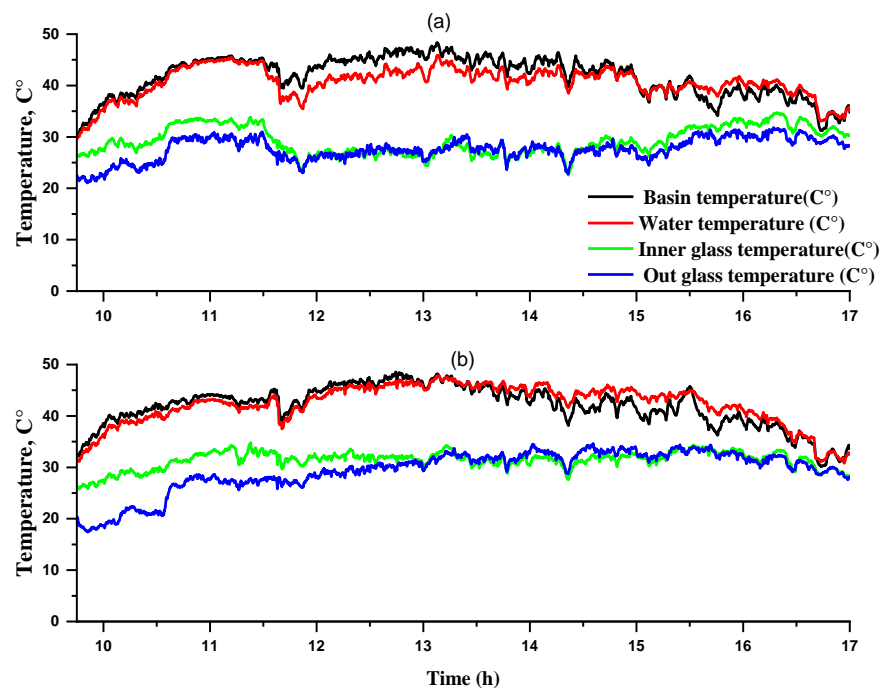


Figure (5.47): Variations of temperature for two solar still a-with fins b- without fins , at day 10-3-2024.

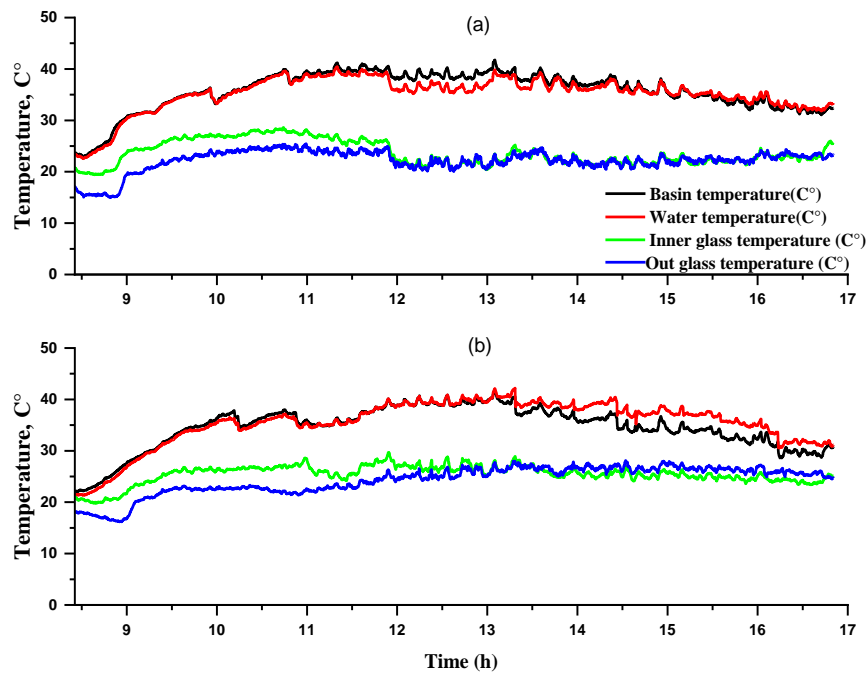


Figure (5.48): Variations of temperature for two solar still a-with fins b- without fins , at day 11-3-2024.

Figure (5.49) depicts the comparison of the cylindrical dome solar still on the following dates: 4,5,6,10 and 11March 2024. The productivity figures steadily rise from their original zero values at the beginning of the experiment, eventually reaching their maximum value, with the highest productivity being attained on 11-3-2024. The solar still equipped with a cylinder attains the utmost amount of output. The object has a hemispherical shape and its productivity is 3.710 kg/m^2 . The results demonstrate that including fins into the solar still (CSSHD) led to a greater overall output in comparison to the solar still without fins. Figure (5.50) depicts a comparative comparison of the overall production of two solar stills during multiple testing days. The addition of fins consistently enhances the generation of CSSHD compared to CSSHD without fins, irrespective of the day. The productivity is contingent upon the seasonal and meteorological circumstances that occur throughout the year.

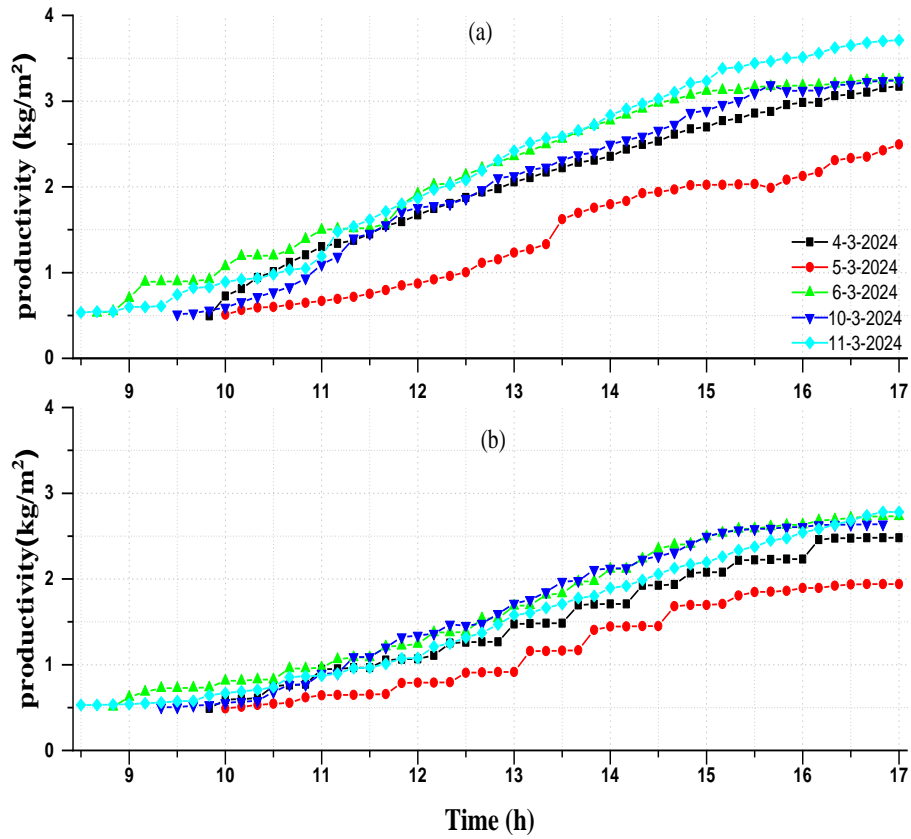


Figure (5.49): Comparison of experimental results between two solar stills at five days a-with fins b- without fins

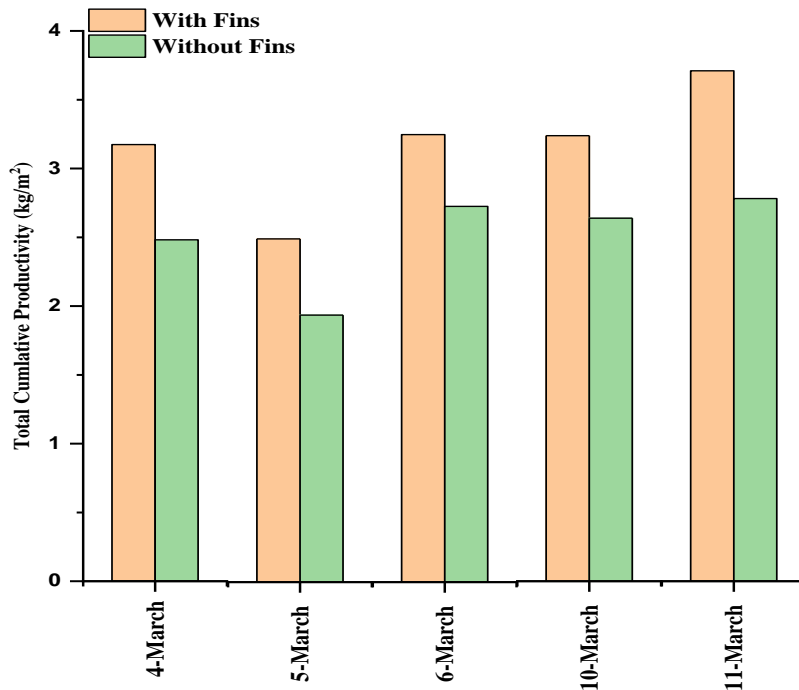


Figure (5.50): Displays the different levels of total productivity, comparing the use of fins and without fins

5.5. Comparing Numerical and experimental Results

An experimental productive was selected by comparing it with the numerical production. Regarding the productivity of distilled water, the simulation results and experimental results of the cylindrical solar distiller with a hemispherical dome, both with and without fins, show a convergence for the specified dates 6,10 March ,2024. Based on the findings of simulation programs, the productivity distilled water was approximately 3.565 kg/m². Regarding the experimental findings, the amount of distilled water obtained was approximately 3.252 kg/m². The highest error rate is 7% and the lowest error rate is 1.8%. Figure (5.51) illustrates the disparity in productivity.

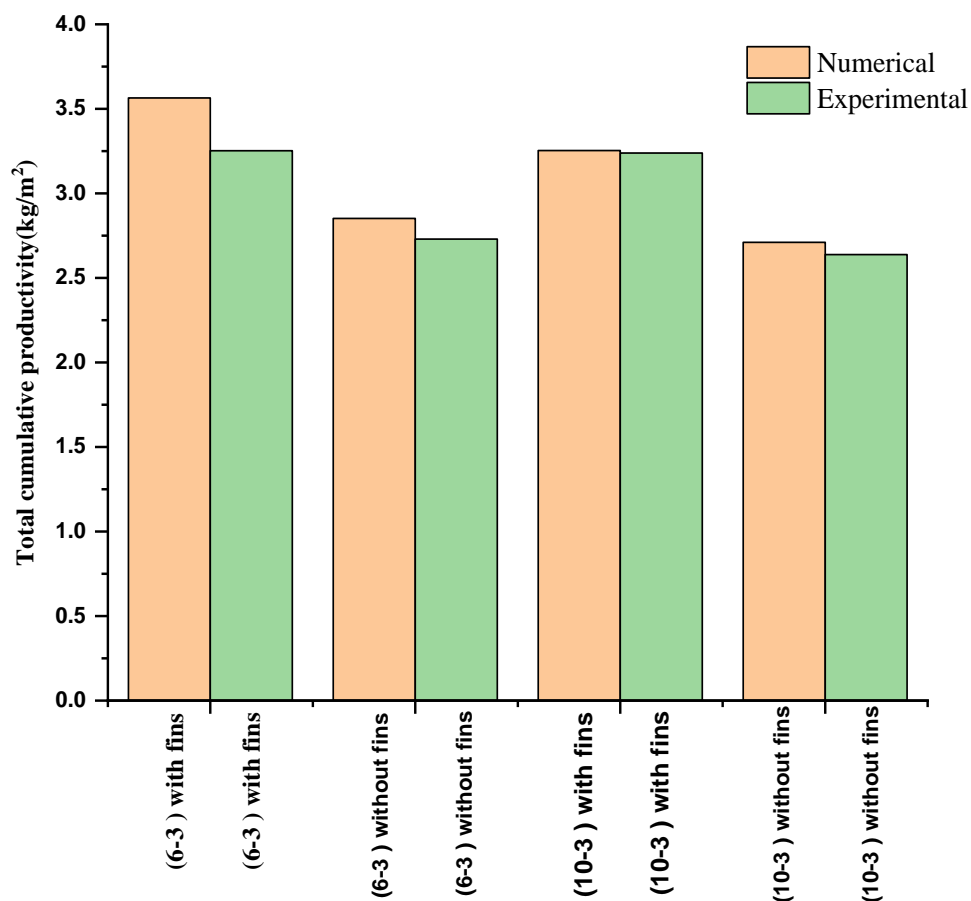


Figure (5.51): Validation Experimental Work with Numerical

5.6 Cost calculation:

Solar energy is the main source of input energy for solar stills. The primary advantage of solar energy is that it provides a free source of energy. The full cost of solar stills generally includes costs associated with installation, maintenance and operation. The cost can be calculated based on the accumulated daily production.[49]

$$C \text{ (the annual total cost)} = F \text{ (fixed cost)} + V \text{ (variable cost)} \quad (5-1)$$

In order to streamline and accomplish the cost calculation process for Models CHSSD with fins and CHSSD without fins, the following requirements can be considered. These requirements encompass the cost of each part and include the overall fixed cost Table (5.1).

The fixed cost (F) of a fixed-fin solar-powered CHSSD is about 45\$. The fixed cost (F) of a CHSSD without fins 35\$. Let the variable costs V be 0.3 times the fixed costs F per year. The total costs are denoted by C, where C is the sum of F and V. Assuming the estimated life of the machine is 10 years, we can calculate C as follows: $C = 45 + 0.3 \times 45 \times 10 = 180$ \$ for the first model and 140\$ for the second model. The average maximum output is determined using daily data from the study. To illustrate, let us determine the expenses incurred in July for both the initial and subsequent models. In July, the yield of the first model was 12.156 kg/m², while the yield of the second model was 6.565 kg/m². In Iraq, the sun is constantly active throughout the year, shining for about 360 days. The total yield for the static life period is calculated as follows: 12.156 multiplied by 10 and then multiplied by 360, which yields a value of 43761.6. The cost of wasting fresh water is calculated by dividing 180 by 43761.6, which yields \$0.004 for the first model. 6.565kg/m² multiplied by 10 and then multiplied by 360 yields a value of 23634kg. The cost of wasting fresh water is calculated by dividing 140 by 23634kg, which yields \$0.006 for the second model as shown in Table (5.2)

Table (5.1): Fixed Cost estimation for present still.

Model	Component	Price (\$)
CHSSD with fins	Basin with fins	20
	Cylinder with hemispherical dome	8
	Black paint	1
	Piping and fitting	16
	Total fixed cost	45
CHSSD without fins	Basin without fins	10
	Cylinder with hemispherical dome	8
	Black paint	1
	Piping and fitting	16
	Total fixed cost	35

Table (5.2): Type and the Total cost

Model	Fixed cost (\$)	Total cost (\$)	Daily Productivity January (kg/m ²)	Daily Productivity July (kg/m ²)	Cost/kg Productivity during January (\$)	Cost/kg Productivity during July (\$)
CHSSD with fins	45	180	3.268	12.156	0.015	0.004
CHSSD without fins	35	140	1.669	6.565	0.023	0.006

CHAPTER SIX

Conclusion and Recommendations

6.1. Introduction

The current work presented experimental and computational inquiries to obtain a new solar still with the highest possible productivity, extract pure water, and compare the resulting production with previous research studies in terms of productivity. Enhancing the performance of a cylindrical solar still with a hemispherical dome by adding fins in Najaf, Iraq.

6.2. The Conclusion

Conventional hemispherical solar stills have proven their usability due to their ability to operate without any specific orientation, resulting in higher productivity compared to sloped stills. From the results presented, the following conclusions were reached:

1. In the numerical simulation study where the results are shown, when the solar still is equipped with fins to increase the surface area of the tank, it achieves a peak throughput of 12.156 kg/m^2 .
2. The maximum cumulative productivity achieved for January, March, July and October is 3.268 kg/m^2 , 8.089 kg/m^2 , 12.156 kg/m^2 , 4.420 kg/m^2 respectively.
3. Numerical results showed that cumulative productivity increases or decreases depending on the month of the year with the area of condensation. When the condensate area is increased by 70%, 281% and 492% in July, at drum heights of 50, 200 and 350 mm, productivity increases by 14%, 12% and 10%, respectively.
4. By doing numerical simulations with four varying lengths of solar cylinders. According to the results, the greatest productivity was continuously recorded at a height of 50 mm during the entire year.

5. As the height of the cylinder increases at 50mm, the temperature of the glass covers decreases, causing increase productivity by 13.8%.
6. Use of fins improves distiller throughput by up to 64.7% compared to no fins with the best modified hemispherical cylindrical solar still configuration with a fin length of 8 mm N_f 5 and L_w 50 mm.
7. The maximum error between the simulation results with the results of previous studies is about (4.62%-11%)
8. The best Dimensions get from numerical simulation are height of fins ($h_f=8$ mm), number of fins ($N_f=5$ fins), and height of Cylinder ($L_w=50$ mm)
9. The experimental results show addition of fins to CSHHD in consistently higher productivity throughout the whole duration of the experiment. The highest daily productivity reached 3.7 kg/m² for March month.
10. The maximum error between the simulation results with the experimental results of present work is about (1.8%-7%)

6.3. Recommendation

Future suggestions for further improvements, the following suggestions can be taken into account:

1. Can used different ships of fins such as wavy fins.
2. Propose the construction of a solar still with a substantial surface area for the purpose of experimental evaluation under authentic atmospheric conditions.
3. Employing nanomaterials in conjunction with phase change materials PCM.
4. Use transparence cover absorb less heat having high thermal conductivity.
5. Build the structure of the CSSHD basin using various materials including Aluminum.

REFERENCES

- [1] W. W. A. P. (United Nations), *Water: A shared responsibility*, no. 2. UN-HABITAT, 2006.
- [2] M. S. Yousef, H. Hassan, S. Kodama, and H. Sekiguchi, “An experimental study on the performance of single slope solar still integrated with a PCM-based pin-finned heat sink,” *Energy Procedia*, vol. 156, pp. 100–104, 2019.
- [3] H. M. Qiblawey and F. Banat, “Solar thermal desalination technologies,” *Desalination*, vol. 220, no. 1–3, pp. 633–644, 2008.
- [4] F. C. Adams, “The birth environment of the solar system,” *Annu. Rev. Astron. Astrophys.*, vol. 48, pp. 47–85, 2010.
- [5] R. Dev and G. N. Tiwari, “Characteristic equation of a passive solar still,” *Desalination*, vol. 245, no. 1–3, pp. 246–265, 2009.
- [6] H. E. S. Fath, M. El-Samanoudy, K. Fahmy, and A. Hassabou, “Thermal-economic analysis and comparison between pyramid-shaped and single-slope solar still configurations,” *Desalination*, vol. 159, no. 1, pp. 69–79, 2003.
- [7] H. A. Jabar, “Experimental and theoretical study of performance of tubular solar still in Iraq,” *no. June*, 2016.
- [8] R. Sathyamurthy, H. J. Kennady, P. K. Nagarajan, and A. Ahsan, “Factors affecting the performance of triangular pyramid solar still,” *Desalination*, vol. 344, pp. 383–390, 2014.
- [9] T. Arunkumar *et al.*, “An experimental study on a hemispherical solar still,” *Desalination*, vol. 286, pp. 342–348, 2012.
- [10] M. E. H. Attia, A. E. Kabeel, M. Abdelgaied, and A. Abdullah, “A comparative study of the effect of internal reflectors on a performance of hemispherical solar distillers: Energy, exergy, and economic analysis,” *Sustain. Energy Technol. Assessments*, vol. 47, Oct. 2021, doi: 10.1016/j.seta.2021.101465.
- [11] M. E. H. Attia, A. E. Kabeel, and M. Abdelgaied, “Optimal concentration of El Oued sand grains as energy storage materials for enhancement of hemispherical distillers performance,” *J. Energy Storage*, vol. 36, Apr. 2021, doi: 10.1016/j.est.2021.102415.
- [12] W. A. Abd Al-wahid and Z. H. Hasan, “Experimental study to enhance the performance of cylindrical solar still with a hemispherical dome”.
- [13] M. E. H. Attia, A. E. Kabeel, M. Abdelgaied, M. M. Abdel-Aziz, A. Bellila, and A. Abdullah, “Optimal size of black gravel as energy storage materials for performance improvement of hemispherical distillers,” *J. Energy Storage*, vol. 43, Nov. 2021, doi: 10.1016/j.est.2021.103196.
- [14] M. E. H. Attia, W. M. El-Maghlany, M. Abdelgaied, and A. M. Elharidi, “Finest concentration of phosphate grains as energy storage medium to improve hemispherical solar distillate: An experimental study,” *Alexandria Eng. J.*, vol. 61, no. 7, pp. 5573–5583, 2022.
- [15] M. E. H. Attia, A. E. Kabeel, M. Abdelgaied, W. M. El-Maghlany, and A. Bellila, “Comparative study of hemispherical solar distillers iron-fins,” *J. Clean. Prod.*, vol. 292, p. 126071, 2021.

References

- [16] M. A. Al-Amir Khadim, W. A. A. Al-Wahid, D. M. Hachim, and K. Sopian, "Experimental study of the performance of cylindrical solar still with a hemispherical dome," *Smart Sci.*, vol. 9, no. 1, pp. 30–39, 2021.
- [17] M. E. H. Attia, A. E. Kabeel, M. Abdelgaied, W. M. El-Maghlany, and Z. Driss, "Enhancement of the performance of hemispherical distiller via phosphate pellets as energy storage medium," *Environ. Sci. Pollut. Res.*, vol. 28, no. 25, pp. 32386–32395, Jul. 2021, doi: 10.1007/s11356-021-12920-y.
- [18] M. E. H. Attia, A. E. Kabeel, S. A. El-Agouz, E. M. M. Lassaad, R. Sathyamurthy, and M. M. Abdel-Aziz, "Optimizing the performance of hemispheric solar still using nano-ZnO with cooling the glassy cover at a variable water flow rate," *Appl. Nanosci.*, vol. 11, no. 11, pp. 2727–2738, Nov. 2021, doi: 10.1007/s13204-021-02170-2.
- [19] M. E. H. Attia, A. R. Abd Elbar, and M. Abdelgaied, "Hemispherical Solar Distiller With Truncated Circular Cone-Shaped Reflector Mirrors (TCC-RM)," 2021.
- [20] M. E. H. Attia, M. Abdelgaied, A. S. Abdullah, A. Bellila, and M. M. Abdel-Aziz, "Performance assessment of the hemispherical solar distillers with the extended cylindrical iron fins: an experimental investigation," *Alexandria Eng. J.*, vol. 61, no. 12, pp. 11149–11157, 2022.
- [21] A. Bellila, M. E. H. Attia, A. E. Kabeel, M. Abdelgaied, K. Harby, and J. Soli, "Productivity enhancement of hemispherical solar still using Al₂O₃-water-based nanofluid and cooling the glass cover," *Appl. Nanosci.*, vol. 11, no. 4, pp. 1127–1139, 2021.
- [22] R. Sathyamurthy *et al.*, "Hemispherical Solar Distiller Performance Utilizing Hybrid Storage Media, Paraffin Wax with Nanoparticles: An Experimental Study," *Molecules*, vol. 27, no. 24, Dec. 2022, doi: 10.3390/molecules27248988.
- [23] M. E. H. Attia, A. E. Kabeel, M. E. Zayed, M. Abdelgaied, S. W. Sharshir, and A. S. Abdulla, "Experimental study of a hemispherical solar distillation system with and without rock salt balls as low-cost sensible storage: Performance optimization and comparative analysis," *Sol. Energy*, vol. 247, pp. 373–384, 2022.
- [24] M. Abdelgaied, M. E. H. Attia, M. Arıcı, and M. M. Abdel-Aziz, "Enhancing the productivity of hemispherical solar distillers using dyed flax fibers as natural inexpensive porous materials," *J. Clean. Prod.*, vol. 379, p. 134674, 2022.
- [25] M. E. H. Attia, A. R. Abd Elbar, M. Abdelgaied, A. S. Abdullah, M. M. K. Dawood, and A. Kabeel, "Improving the performance of a modified hemispherical solar distiller using a double-faces absorbing solar thermal receiver integrated with a solar concentrator," *Sol. Energy*, vol. 241, pp. 335–342, 2022.
- [26] M. E. H. Attia, A. E. Kabeel, A. Abdo, M. Abdelgaied, A. Bellila, and A. S. Abdullah, "Optimal configurations of hemispherical solar distillers using the higher conductivity extended hollow cylindrical fins filled with latent heat storage materials," *J. Energy Storage*, vol. 50, Jun. 2022, doi: 10.1016/j.est.2022.104706.

References

- [27] M. Mohsenzadeh, L. Aye, and P. Christopher, "Development and experimental analysis of an innovative self-cleaning low vacuum hemispherical floating solar still for low-cost desalination," *Energy Convers. Manag.*, vol. 251, p. 114902, 2022.
- [28] B. T. Kannan *et al.*, "Improved freshwater generation via hemispherical solar desalination unit using paraffin wax as phase change material encapsulated in waste aluminium cans," *Desalination*, vol. 538, p. 115907, 2022.
- [29] V. Savithiri, M. E. H. Attia, S. Vaithilingam, and G. Radhakrishnan, "Enhancing the productivity of hemispherical solar distillation by using energy storage (rubber) and wick materials at different thickness," *Sol. Energy Mater. Sol. Cells*, vol. 248, p. 112006, 2022.
- [30] M. E. H. Attia, A. E. Kabeel, M. Abdelgaied, and A. Bellila, "Optimization of the hemispherical solar distiller performance assisted by high thermal conductivity metal trays incorporated with reflective mirrors," *Environ. Sci. Pollut. Res.*, vol. 29, no. 25, pp. 38248–38257, 2022.
- [31] B. F. Felemban *et al.*, "Experimental investigation on dish solar distiller with modified absorber and phase change material under various operating conditions," *Environ. Sci. Pollut. Res.*, vol. 29, no. 42, pp. 63248–63259, 2022.
- [32] A. Al-wahid, A. Wisam, H. A. K. Saad, Z. H. Hasan, and K. Sopian, "Experimental study of the performance of hemispherical solar still with optimum value of rocks as heat transfer enhancers," *AIMS Energy*, vol. 10, no. 4, 2022.
- [33] A. E. Kabeel *et al.*, "The impact of the corrugated absorber shape on the performance of a hemispherical solar still for water desalination: an experimental study," *Appl. Water Sci.*, vol. 13, no. 4, p. 108, 2023.
- [34] I. M. Elsaywy, A. Hamoda, S. W. Sharshir, and A. Khalil, "Experimental study on optimized using activated agricultural wastes at hemispherical solar still for different types of water," *Process Saf. Environ. Prot.*, vol. 177, pp. 246–257, 2023.
- [35] M. E. H. Attia, A. K. Hussein, G. Radhakrishnan, S. Vaithilingam, O. Younis, and N. Akkurt, "Energy, exergy and cost analysis of different hemispherical solar distillers: A comparative study," *Sol. Energy Mater. Sol. Cells*, vol. 252, p. 112187, 2023.
- [36] A. Beggas, M. Abdelgaied, M. E. H. Attia, A. S. Abdulla, and M. M. Abdel-Aziz, "Improving the freshwater productivity of hemispherical solar distillers using waste aluminum as store materials," *J. Energy Storage*, vol. 60, p. 106692, 2023.
- [37] M. E. H. Attia, A. E. Kabeel, A. S. Abdullah, Y. Elmashad, R. Sathyamurthy, and M. Abdelgaied, "Optimized construction of marble pieces as thermal storage materials for performance improvement of hemispherical solar distiller," *J. Energy Storage*, vol. 68, Sep. 2023, doi: 10.1016/j.est.2023.107685.
- [38] M. E. H. Attia *et al.*, "Performance enhancement of hemispherical solar stills using different shapes of basin liners (sinusoidal and half-circle) incorporated with inverted solar collectors," *Environ. Dev. Sustain.*, pp. 1–19, 2023.

References

- [39] M. E. H. Attia, M. E. Zayed, A. E. Kabeel, A. S. Abdullah, and M. Abdelgaied, "Energy, exergy, and economic analyses of a modified hemispherical solar distiller augmented with convex absorber basin, wicks, and PCM," *Sol. Energy*, vol. 261, pp. 43–54, 2023.
- [40] M. E. H. Attia, M. Abdelgaied, A. S. Abdullah, and M. Arıcı, "Optimization configuration of scrubber steel wire coils as porous materials for augmenting the performance of hemispherical distillers," *J. Taiwan Inst. Chem. Eng.*, p. 104861, 2023.
- [41] M. A. Dahab, M. A. Omara, M. M. El-Dafrawy, G. B. Abdelaziz, and S. W. Sharshir, "Thermo-economic performance enhancement of the hemispherical solar still integrated with various numbers of evacuated tubes," *Therm. Sci. Eng. Prog.*, vol. 42, p. 101922, 2023.
- [42] S. W. Sharshir *et al.*, "Thermoenviroeconomic performance augmentation of solar desalination unit integrated with wick, nanofluid, and different nano-based energy storage materials," *Sol. Energy*, vol. 262, Sep. 2023, doi: 10.1016/j.solener.2023.111896.
- [43] Q. A. Abed, D. M. Hachim, and W. A. Abd Al-Wahid, "Performance of cylindrical solar still with hemispherical cover: CFD simulation study," in *E3S Web of Conferences*, EDP Sciences, Jul. 2021. doi: 10.1051/e3sconf/202128602005.
- [44] M. Z. Khan, I. Nawaz, G. N. Tiwari, and M. Meraj, "Effect of top cover cooling on the performance of hemispherical solar still," *Mater. Today Proc.*, vol. 38, pp. 384–390, 2021.
- [45] R. Fallahzadeh, N. Gholamiarjenaki, Z. Nonejad, M. Fallahzadeh, and M. Saghi, "Mathematical modeling and experimental study of a modified hemispherical solar still," *Fallahzadeh J. Eng. Res. Appl. www.ijera.com*, vol. 10, pp. 44–52, 2020, doi: 10.9790/9622-1002014452.
- [46] M. Abdelgaied, M. E. H. Attia, A. E. Kabeel, and M. E. Zayed, "Improving the thermo-economic performance of hemispherical solar distiller using copper oxide nanofluids and phase change materials: Experimental and theoretical investigation," *Sol. Energy Mater. Sol. Cells*, vol. 238, May 2022, doi: 10.1016/j.solmat.2022.111596.
- [47] H. N. Panchal and P. K. Shah, "Experimental and ANSYS CFD simulation analysis of hemispherical solar still," *J. Renew. Energy Smart Grid Technol.*, vol. 8, no. 1, pp. 1–14, 2013.
- [48] R. Taher Dang Koo, "Numerical modelling of single-and multi-phase flow and transport processes in porous media for assessing hydraulic fracturing impacts on groundwater resources." Dissertation, Göttingen, Georg-August Universität, 2020, 2020.
- [49] A. S. Joshi, A. Tiwari, G. N. Tiwari, I. Dincer, and B. V Reddy, "Performance evaluation of a hybrid photovoltaic thermal (PV/T)(glass-to-glass) system," *Int. J. Therm. Sci.*, vol. 48, no. 1, pp. 154–164, 2009.

Appendix

Appendix A: Thermocouples Calibration

The relationship between the results of the thermometer and the standard mercury thermometer (zero degree centigrade of ice and water mixture) is presented in the Figures A-1, A-2, A-3. The thermometer device is calibrated using these data Figure A-4 shows an illustration of the device calibration.

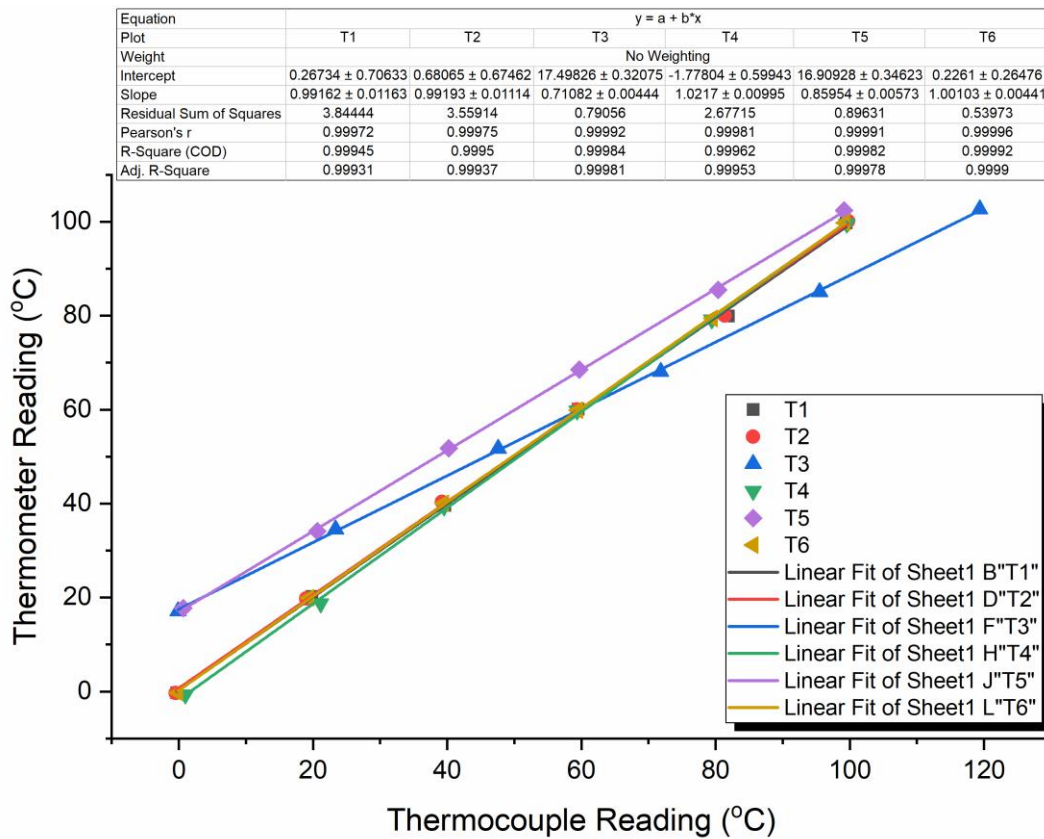


Figure A-1: Calibration of thermocouple (T1-T6).

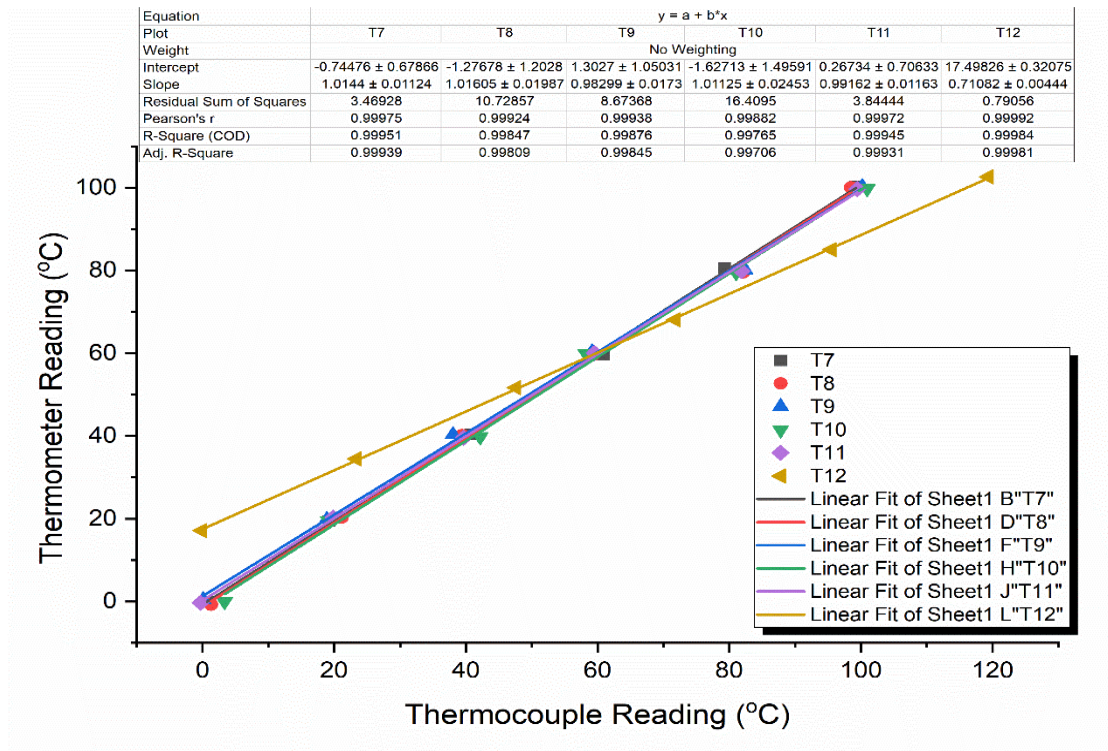


Figure A-2: Calibration of thermocouple (T7-T12).

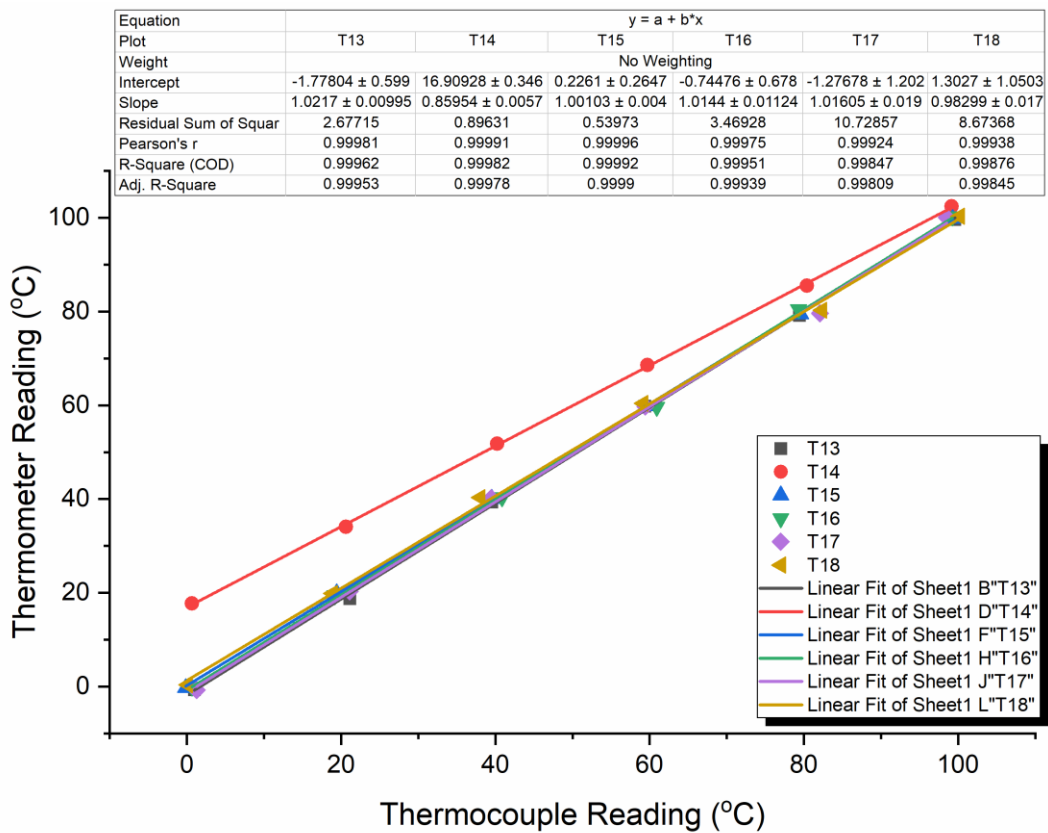


Figure A-3: Calibration of thermocouple (T13-T18).



Figure A-4: Photograph for the calibration of a device.

Appendix B: Calibration of Solar Intensity Sensor

In this work, The Pyrometer instrument was used to measure the intensity of direct sun radiation. The main advantages of this device are its ease of handling in all settings, generally acceptable accuracy, and the ability to calibrate it by comparing it to the suitable equipment under the same measurement conditions. The calibration equipment must be identical to the standards of measurement.

B.1 Solar Power Meter Calibration

The solar radiation measurement device (TENMARS SM-206) used in all experimental tests was calibrated with the standard Davis weather station built at Najaf Engineering Technical College/Iraq at 10 m above ground level. this station measures solar radiation in (W/m^2). The results of calibration appear in following chart (B-1).

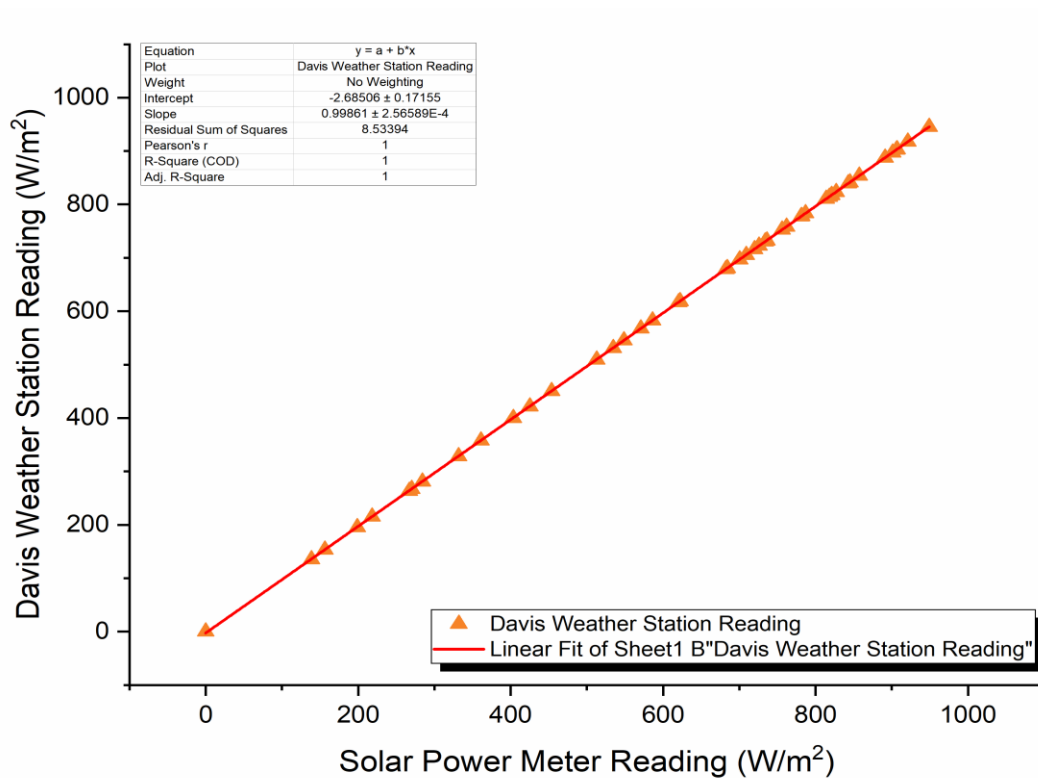


Figure B-1: Solar power meter calibration.

Appendix C: Wind Speed Sensor Calibration

The type of anemometer system (GM-8902), with a range (0.0 – 45.0 m/s) and an accuracy $\pm 3\%$ was used to measure wind speed in this work. This device is simple to manage under all conditions and can be adjusted by comparing it to the required equipment under the same measurement conditions, with generally acceptable precision. The calibration equipment must be similar to the proper level of measurement.

C.1 Anemometer Calibration

The type of wind speed measurement device (anemometer) (GM-8902) used in all experimental tests has been calibrated with the standard Davis weather station built at Najaf Engineering Technical College/Iraq at 10 m above ground level. The wind speed of this station is measured in (m/s) with a range of 0.1 to 89 m/s and $\pm 5\%$ accuracy. The results of the calibration appear in the following chart (C-1).

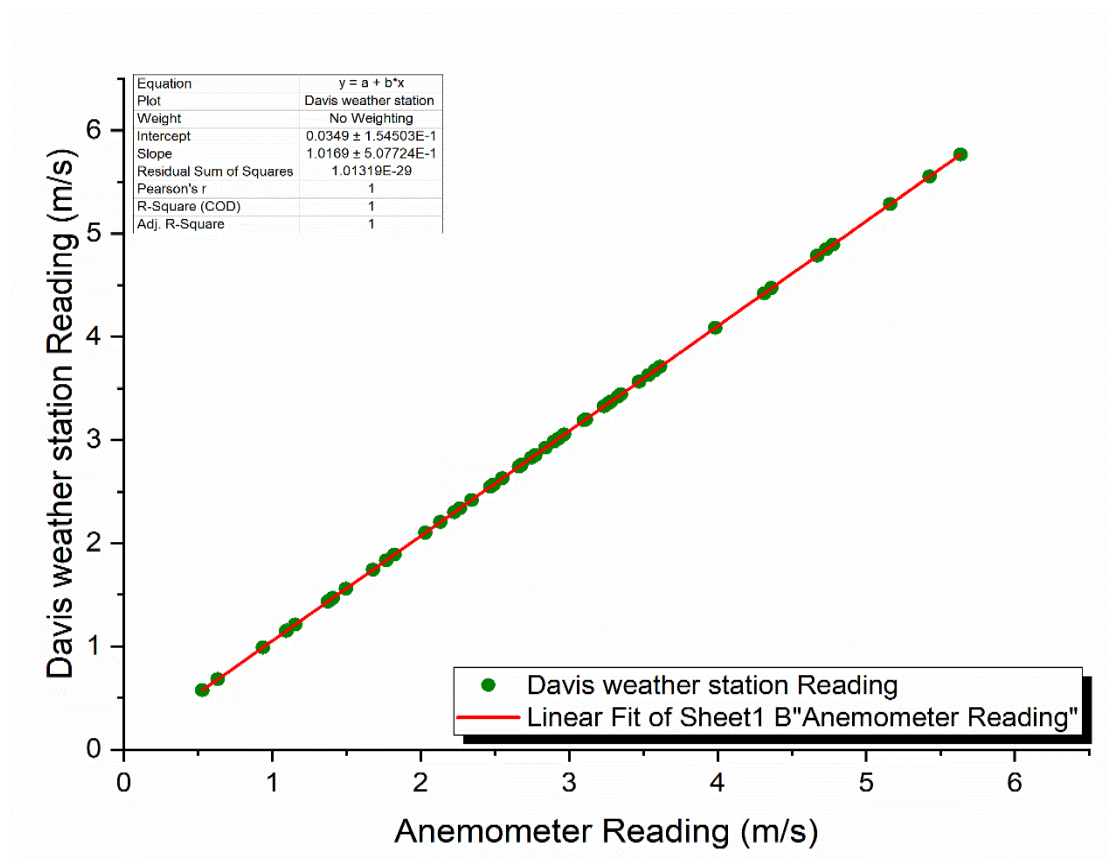


Figure C-1: Anemometer calibration.

Appendix D: Digital Scale Calibration

Figure D-1 shows the relationship between the measurements obtained from the digital scale and the standard weights. The weight is adjusted using this information. Figure D-2 depicts a picture illustrating the calibration process for the device.

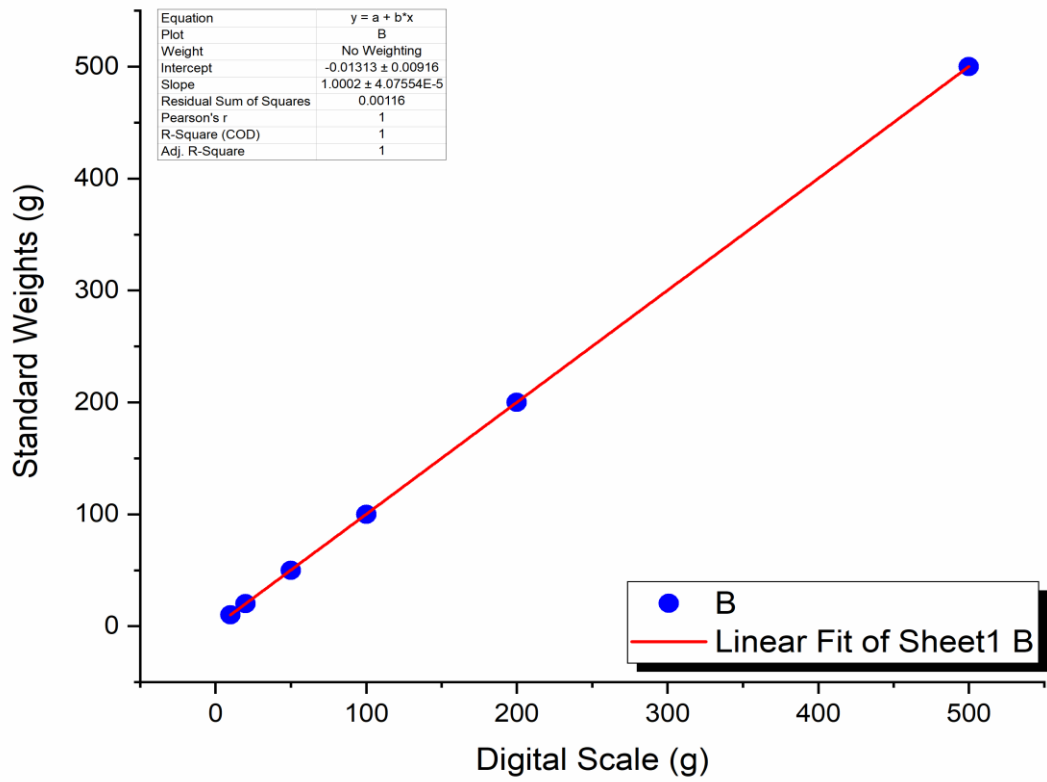


Figure D-1: Digital Scale calibration



Figure D-2: Photograph for the calibration of a device

Appendix E: Published Papers



ID.: 036 - ICASDG2024
Date of Issue: 26-7-2024

ACCEPTANCE LETTER

Dear Shahzanan Falah ,
Co-Authors : Dhafer Manea Hachim and Wisam A. Abd Al-wahid.

Congratulations!

It is with great pleasure that we inform you that, your manuscript
entitled:

*A Numerical Simulation Investigate the Effect of Basin and
Condensation Area on the Productivity of a Cylindrical Solar Still with
a Hemispherical Dome*

has been **ACCEPTED** for participation in the *3rd International
Conference on Engineering and Science to Achieve the
Sustainable Development Goals*, scheduled to be held on
September 25-26, 2024, Istanbul, Turkey and considered for
publication in **AIP Conference Proceedings**.

Thank you for your valuable participation in the 3rd ICASDG2024.

Prof. Dr. Ahmed Ghanim Wadday
The Head of Scientific Committee
Al-Furat Al-Awsat Technical University





ID.: 230 - ICASDG2024
Date of Issue: 27-9-2024

ACCEPTANCE LETTER

Dear Shahzanan Falah Nassif ,
Co-Authors : Dhafer Manea Hachim and Wisam A. Abd Al-wahid.

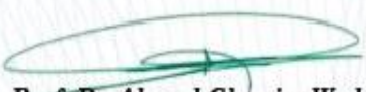
Congratulations!

It is with great pleasure that we inform you that, your manuscript
entitled:

*Recent Progress and Advancements Development of Hemispherical
Solar Stills a Review*

has been **ACCEPTED** for participation in the *3rd International
Conference on Engineering and Science to Achieve the
Sustainable Development Goals*, scheduled to be held on
September 25-26, 2024, Istanbul, Turkey and considered for
publication in **AIP Conference Proceedings**.

Thank you for your valuable participation in the 3rd ICASDG2024.


Prof. Dr. Ahmed Ghanim Wadday
The Head of Scientific Committee
Al-Furat Al-Awsat Technical University



← Revisions Being Processed for Author

Page: 1 of 1 (1 total revisions being processed)

Results per page 10

Action	Manuscript Number	Title	Date Submission Began	Status Date	Current Status
View Submission View Attachments Author Status Author Response Correspondence Publishing Options Send E-mail	IJTF-D-24-00717R1	Study the Performance of Cylindrical Solar still with Hemispherical Dome by Using Fins in Basin	Oct 04, 2024	Oct 04, 2024	Revised Manuscript Submitted

Page: 1 of 1 (1 total revisions being processed)

Results per page 10

الخلاصة

تُعتبر أنظمة التحلية بالطاقة الشمسية منهجيات مستدامة تُستخدم في عملية تحلية مصادر المياه غير الصالحة للشرب. يمكن ان تعزى الزيادة في الطلب على المياه الصالحة للشرب في السنوات الأخيرة إلى تعدد الملوثات التي تؤثر سلبيًا على المسطحات المائية الطبيعية. يشمل إطار هذا التحقيق عنصرين رئيسيين. يتضمن المكون الأول المحاكاة العددية للنموذج المقترح (الذي يتضمن استخدام الزعانف داخل المقطر الشمسي الأسطواني الذي يتميز بقبة نصف كروية)، مع التركيز على تحليل أطوال الزعانف المستخدمة (0 مم، 4 مم، 6 مم، و 8 مم)، إلى جانب تقييم عدد الزعانف المستخدمة (4 زعانف و 5 زعانف) الهدف من المكون الثاني هو تحديد الأبعاد المثلى للزعانف بناءً على النتائج المستمدة من المحاكاة العددية، تليها الاختبارات العملية في الظروف المناخية للعراق، وتحديدًا في مدينة النجف (31.590° شمالاً و 44.190° شرقاً). أشارت البيانات العددية إلى أن الإنتاجية التراكمية تتقلب وفقًا لشهر السنة بالنسبة لمنطقة التكثف. وتؤدي زيادة مساحة المكثف بنسبة 70%، و 281%، و 492% في يوليو، عند ارتفاعات الأسطوانة 50، 200، و 350 مم على التوالي، تؤدي إلى تحسينات في الإنتاجية بنسبة 14%، و 12%، و 10%. إدخال الزعانف يعزز بشكل كبير من إنتاجية المكثف بنسبة تصل إلى 64.7% مقارنةً بالتكوين الخالي من الزعانف، حيث يظهر التكوين المثالي المعدل للمقطر الشمسي الأسطواني نصف الكروي طول زعنف يبلغ 8 ملم، وعدد زعانف 5، وطول اسطوانة 50 ملم، حيث ان أقصى تباين بين نتائج المحاكاة والدراسات السابقة يتراوح بين حوالي 4.62% إلى 11%. تُظهر النتائج التجريبية أن دمج الزعانف في المقطر الشمسي الاسطواني ذو القبة النصف كروية يؤدي باستمرار إلى إنتاجية متفوقة طوال فترة التجربة بأكملها. بلغت ذروة الإنتاجية اليومية 3.7 كجم/م² خلال شهر مارس.



جمهورية العراق

وزارة التعليم العالي والبحث العلمي

جامعة الفرات الاوسط التقنية

الكلية التقنية الهندسية – نجف

دراسة تجريبية وعددية لتحسين أداء جهاز التقطير الشمسي الأسطواني
ذو القبة النصف كروية باستخدام الزعانف

رسالة مقدمة الى

قسم هندسة تقنيات ميكانيك القوى

كجزء من متطلبات نيل درجة الماجستير تقني في الهندسة الميكانيكية
(حراريات)

تقدم بها الطالبة

شهزنان فلاح نصيف

(بكالوريوس هندسة ميكانيك القوى)

اشراف

الأستاذ الدكتور ظافر مانع حاجم

الأستاذ المساعد الدكتور وسام احمد عبد الواحد

2024 م